ABSTRACT

Title of Document: COMPUTATIONAL FLUID DYNAMICS ANALYSIS OF SPATIALLY-RESOLVED SPRAY SCANNING SYSTEM (4S) SPRAY PATTERNS

Jeffrey Sean Bors
Master of Science, 2023

Directed by: Professor Arnaud Trouvé
Department of Fire Protection Engineering

In computational fluid dynamics (CFD) fire models, sprinkler sprays are represented in complex numerical simulations using Lagrangian particles. These CFD sprays are typically characterized using a combination of experimental data, literature correlations, and estimation. The Spatially-Resolved Spray Scanning System (4S) machine provides high resolution data to characterize sprays for use in CFD analysis, however a quantitative analysis on the effect of this high resolution data with FDS in realistic fire scenarios has not been completed before.

4S spray data is analyzed and compared to a basic spray estimated from literature correlations with and without the presence of fire to analyze trends. In all environments, the basic nozzle overestimated water flux closer to the center of the nozzle and underestimated water flux farther from the center. Differences between the basic and 4S nozzle ranged from 1% to 240% in the enclosure fire scenario. Investigation into the differences showed the polar water distribution to be the most impactful parameter provided by the 4S. Local azimuthal trends were shown to be significant, but non-impactful in the enclosure fire simulation. Global azimuthal trends were apparent but not significant.

COMPUTATIONAL FLUID DYNAMICS ANALYSIS OF SPATIALLY-RESOLVED SPRAY SCANNING SYSTEM (4S) SPRAY PATTERNS

By

Jeffrey Sean Bors

Theses submitted to the Faculty of the Graduate School of the
University of Maryland, College Park, in partial fulfillment
Of the requirements for the degree of
Master of Science
2023

Advisory Committee:
Professor Arnaud Trouvé
Professor James Milke
Professor Fernando Raffan-Montoya

Dedicated to my mom,
Shirley Bors
1959-2010

Acknowledgments

I would like to thank Dr. Milke, Dr. Trouvé, Dr. Raffan-Montoya for the guidance during my time in this program. I would like to thank Kelliann, Sofia, & Zishan for making the program fun. Finally, I would like to thank my wife, Julia, for her continued and unwavering support.

Table of Contents

List of Tables

List of Figures

Chapter 1 : Introduction

1.1 Background

Water is the most commonly used firefighting agent in the world for its wide availability, cost, and performance. With a high specific heat and heat of vaporization, water can absorb up to 2500 kJ of heat per gallon [1]. The earliest automatic sprinkler head was patented in 1874 by Henry Parmelee that contained a valve held closed by a spring attached with low fusing material [2]. In 1884, the first extensive testing report was published by Factory Mutual evaluating the response times of fifteen different types of sprinklers [2].

It was not until the mid-20th century that attempts to characterize aspects of the sprinkler spray itself, such as droplet size distributions, began [3]. Some of the first attempts to analyze spray involved capturing water droplets in oil or freezing them to determine droplet sizes [4]. In the 1980s, with the increasing commonality of video cameras and image analysis, shadowgraph and Particle Tracking Velocimetry (PTV) techniques were implemented to improve droplet characterization [3]. Since then, there have been numerous studies in measuring water flux distributions and droplet velocities.

With the introduction of computational fluid dynamics (CFD) fire models, sprinkler sprays are now represented in complex numerical simulations. The standard approach to modeling sprinkler sprays uses a Lagrangian model that simulates the spray as a small population of water droplets injected after atomization of the sprinkler water jet has occurred. Some of the many studies that utilize CFD simulation of water sprays include: interaction of water spray and fire plumes, suppression of liquid pool fire using fine water sprays, a numerical study of high-pressure water-mist nozzle sprays, and a CFD Investigation of large-scale pallet stack fires [5], [6], [7], [8]. All these studies require the characterization of the spray to be represented by prescribing parameters in the CFD software based on experimental data available or estimations based on previous research.

The Spatially-Resolved Spray Scanning System (4S) machine, developed by the University of Maryland around 2017 and is currently licensed and operated by Fire Risk Alliance LLC, provides high resolution data to characterize sprays for use in CFD analysis [4]. The 4S provides a robust measurement system for the spray droplet diameter distribution, velocity, and water flux from 0 to 100 degrees of elevation in 10-degree increments and 0 to 360 degrees of azimuth in 1-degree increments. The data is processed to recreate the three-dimensional spray with 3600 segments.

While the increased fidelity of spray data is clear, the quantitative effect of this within FDS is largely unknown when compared to lower fidelity sprays. This study attempts to quantify the differences of the higher resolution characterization of the 4S to understand the value of this detailed spray characterization with and without the presence of a fire.

1.2 Computational Modeling

In this study, the computational fluid dynamics (CFD) software Fire Dynamics Simulator (FDS) version 6.7.9 and Smokeview version 6.7.21, both developed by the National Institute of Standards and Technology (NIST), are used [9], [10]. These programs are readily available, free, and widely utilized within the fire protection engineering community. Simulations were run on the University of Maryland's Linux-based high performance computing cluster 'Zaratan' which employs 360 nodes each with dual 64-core CPUs with a theoretical peak processing power of 3.5 peta floating point operations per second (PFLOPS) [11].

FDS was developed to model fire driven fluid flow by numerically solving a form of the Navier-Stokes equations for low speed, thermally driven flows with emphasis on smoke and heat transport from fires [12]. Details about the model and governing equations can be found in the FDS User Guide and FDS Technical Reference Guide [12], [13]. Validation of the models is found in the FDS Validation Guide [14]. Further details of the specific sub-models and inputs are included in the applicable sections of this study.

Post processing of water flux data was done in MathWorks MATLAB version R2022a using the program slread.m by Simo Hostikka to read slice files and the program radial_profile.m by Randy McDermott to calculate average radial particle flux [15], [16], [17]. An example script can be seen in Appendix E. The slice files used measure the water flux at a plane of interest through time. The program reads each cell in the plane at each time step in the plane of interest creating a three-dimensional matrix. The resulting matrix can then average in time and graphed as is, or data can be manipulated and combined with other data sets to create some of the plots seen later.

1.3 4S Description

The 4S provides high-fidelity spray characteristics for sprinklers. Figure 1-1 depicts the operational diagram of the machine consisting of a rotating sprinkler assembly, (1), with mechanical (2) and optical (3) measuring systems. The mechanical measuring system consists of 11 funnels that capture the water sprayed to obtain volume flux data. The optical measurement

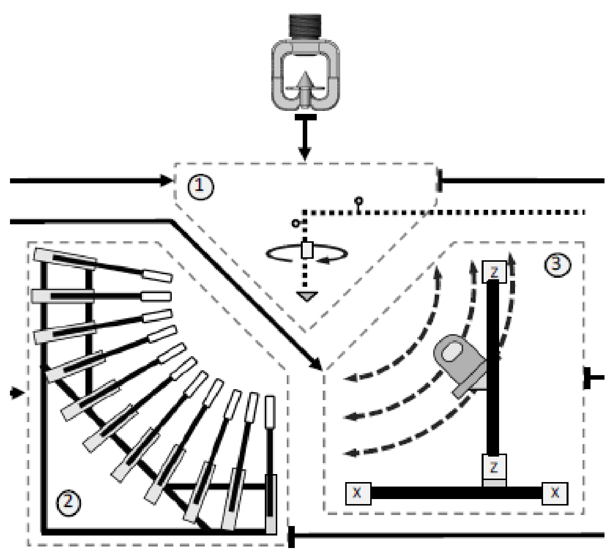

Figure 1-1: 4S Operational Diagram [4]

system uses cameras and lasers, employing shadowgraph and Particle Tracking Velocimetry (PTV) techniques to obtain droplet diameter and velocity data [4]. The 4S measurements are discussed in Section 2-2.

1.4 Objective and Approach

A sprinkler spray has several purposes: it delivers water to the burning material to reduce the burning rate, wets surrounding material to reduce flame spread, cools surrounding air and displaces oxygen through evaporation, and cools structural members [3]. The main factor in the spray's ability to perform these functions is the mass of water delivered to the area of interest. This study seeks to compare, using FDS modeling of realistic scenarios, the effects the increased spray resolution that the 4S provides versus a more basic spray pattern through analyzing water flux ($kg/m^2 s$) at locations and planes of interest.

In Chapter 2, studies of existing correlations for spray parameters are presented along with the basics of what parameters are needed to define a spray in FDS. Next, in Chapter 3, FDS simulations for a K5.6 nozzle using the spray characteristics from the 4S are compared to a basic nozzle in an open, quiescent environment. After the differences are analyzed in quiescent air, a crossflow of air is applied in Chapter 4 to see how the sprays are affected. In Chapter 5, a small enclosure fire experiment is modeled with both the 4S and basic nozzle to analyze quantitative results. Chapter 6 explores what parameters were most impactful in the enclosure fire scenario results. Conclusions and recommendations are presented in Chapter 7.

Chapter 2 : Literature Review

2.1 Lagrangian Particle Model

Liquid water droplets in FDS are modeled as Lagrangian Particles as they cannot be resolved on the numerical grid. FDS has default values for liquid and water vapor built into the software including density, specific heat, and heat of vaporization. The particle transport through the numerical grid is calculated with the following equations for acceleration and position,

$$\frac{du_p}{dt} = g - \frac{1}{2}\frac{\rho C_d A_{p,c}}{m_p}(u_p - u)\left|u_p - u\right| \qquad \text{(Eq. 1)}$$

$$\frac{dx_p}{dt} = u_p \qquad \text{(Eq. 2)}$$

where u_p is the particle velocity, m_p is the particle mass, $A_{p,c}$ is the particle cross-sectional area, C_d is the drag coefficient, u is the gas velocity, and ρ is the gas density. Momentum transfer between the gas phase and particles is governed by the following equation.

$$f_b = \frac{1}{V}\sum \frac{\rho}{2} C_d A_{p,c}\left(u_p - u\right)\left|u_p - u\right| - \frac{dm_p}{dt}(u_p - u) \qquad \text{(Eq. 3)}$$

In reality, a water spray is made up of millions of particles that are not feasible to individually track in simulation. Instead, a lesser number of particles are injected by each nozzle through the PARTICLES_PER_SECOND (PPS) parameter. This means that each simulated particle represents a much larger number of realistic droplets. The FDS default is 5,000 PPS, however, an analysis of this parameter should be conducted for each simulated spray as there is limited guidance on the “right” number of particles for a CFD spray.

To ensure that the total flow rate of water is modeled, each simulated particle has a weighting factor which describes how many real drops each computational particle represents. This weighting factor then impacts the effect of that particle evaporating or hitting a burning surface in the model. For example, if a single particle represents 15 real water droplets and evaporates fully, the time to evaporation and trajectory will be that of a single droplet, but the mass of gaseous water vapor produced, and cooling effect of that droplet evaporating will be 15 times that of the single droplet.

2.1.1 Particle Diameter and Distribution

Water drops within a spray are not uniform in size. The droplets are inserted based on a prescribed probability distribution such as the default Rosin-Rammler-Lognormal distribution established by Yu [18]:

$$CVF(D) = \begin{cases} \frac{1}{\sqrt{2\pi}} \int_0^D \frac{\gamma}{1.15D'} exp\left(-\frac{\left[ln\left(D'/D_{v,0.5}\right)\right]^2}{2(1.15/\gamma)^2}\right) & \left(D > D_{v,0.5}\right) \\ 1 - exp\left(-.693\left(\frac{D}{D_{v,0.5}}\right)^\gamma\right) & \left(D > D_{v,0.5}\right) \end{cases} \quad \text{(Eq. 4)}$$

where γ is the distribution parameter and $D_{v,0.5}$, is the median droplet size by volume.

The probability distribution function defines the Cumulative Number Fraction (CNF) and Cumulative Volume Fraction (CVF) curves in Figure 2-1. The CNF expresses the fraction of the total number of droplets in the spray that are at a given diameter or smaller. The CVF expresses the fraction of the total volume of water characterized by droplets at or below a given diameter.

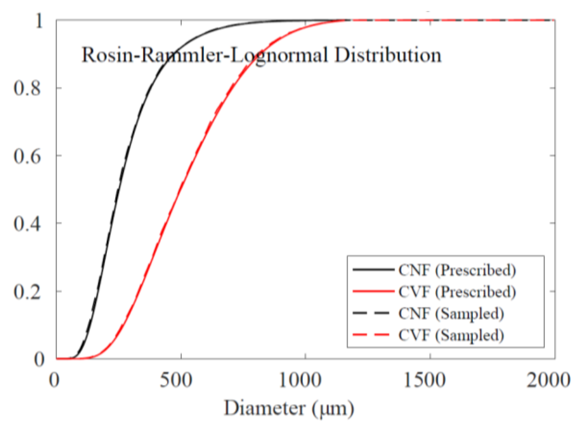

Figure 2-1: Rosin-Rammler-Lognormal Distribution [12]

The distribution is described by its center that corresponds to the diameter at 0.5 probability and the width of the distribution about that center. In FDS, the DIAMETER input prescribes the median droplet size by volume (CVF), or $D_{v,0.5}$. On the distribution given in Figure 2-1, the FDS input would be DIAMETER=500 (μm) and means that half of the volume of water is contained in droplets over 500 μm in diameter and half under 500 μm. The CNF curve at the same diameter prescribes a probability of 0.9, meaning that the larger droplets (greater than 500 μm) carry 50% of the total volume but only make up about 10% of the total spray by number of droplets. Typical values for $D_{v,0.5}$ range from 500 μm to 3500 μm depending on the type of sprinkler [3].

The width of the distribution is effected by the parameter γ (Γ in some literature), specified as GAMMA_D in FDS. Larger values correlate to a narrower distribution around the median diameter and smaller values correlate to a wider distribution. The FDS default of 2.4 appears to be based on Chan's experiment of two ESFR sprinklers at two pressures [12], [19]. Shepard reports values for γ ranging from 1.85 to 2.57 with an average of 2.19 and standard deviation of 0.186 while Jordan reports common values ranging between 2 and 4 [3], [4].

Currently the only way to determine droplet distributions is through experimentation, measuring distributions at a variety of locations and multiple pressures [3]. It has been found in those experiments that the median droplet diameter increases with elevation angle which was confirmed by Jordan and can be visualized in Figure 2-2 [4].

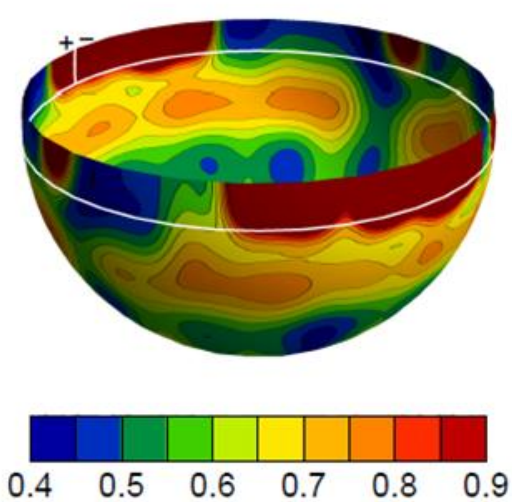

Figure 2-2: Volume Median Diameter (mm) [4]

2.1.1.1 Effect of Water pressure on Particle Diameter

Several studies have confirmed that as water pressure increases, the median droplet diameter decreases [12]. This increase is proportional to the weber number (*We*), a dimensionless number that relates inertia to surface tension:

$$\frac{D_{v,0.5}}{d} = C_w \, (We)^{-\frac{1}{3}} \tag{Eq. 5}$$

$$We = \frac{\rho_p {u_p}^2 d}{\sigma} \tag{Eq. 6}$$

where ρ_p is liquid density, σ is liquid surface tension, u_p is discharge velocity, and d is the oriface diameter. The proportionality constant, C_w, varies with location in a spray and across sprinklers [3]. Table 1 shows ranges of proportionality constants and corresponding orifice diameters that were measured across three different studies.

Table 1: Values for Proportionality Constants

Proportionality Constants	Number of Sprinklers	Range of Orifice Diameters	Source
Average 2.7	3	13 to 16 mm	Lawson J.R
Range 0.72 to 2.48 Average 1.53	12	9.5 to 25.4 mm	Sheppard
4.3, 2.9, 2.3	3	16.3, 13.5. 12.7 mm	Yu, H.Z.

To illustrate the effect of this parameter, Sheppard's range of 0.72 to 2.48 was used to calculate droplet diameter for three common k-factor sprinklers at two reasonable operating pressures as seen in Table 2. The

Table 2: Calculated Droplet Diameters

K-Factor	Pressure (psi)	Proportionality constant 0.72	Proportionality constant 2.48
		Diameter (μm)	
K5.6	20	445	1533
	40	353	1217
K11.2	20	516	1779
	40	410	1412
K14	20	583	2009
	40	463	1595

largest range is the K14 sprinkler at 20 psi with a diameter range of 583 μm to 2009 μm.

2.1.2 Flow Rate and Water Flux

The total flow rate from a nozzle can be specified in two ways within FDS. Either the FLOW_RATE (q) in L/min is specified directly, or the K_FACTOR (k) and OPERATING_PRESSURE (P) are specified and FDS will solve for flow rate using Equation 7.

$$q = k\sqrt{P} \qquad \text{(Eq. 7)}$$

With the latter method, the operating pressure can vary throughout the simulation using the command PRESSURE_RAMP and specifying the pressures at a corresponding number of activated sprinklers. This ability to manipulate pressures can be helpful as sprinklers open at different times in a realistic scenario.

2.1.3 Particle Velocity

Particle velocity can be specified with the line PARTICLE_VELOCITY (m/s). If no particle velocity is known, FDS will calculate the velocity using the FLOW_RATE, q, and ORIFACE_DIAMETER, d, using the following equation:

$$u_p = \frac{q}{A} = \frac{q}{\pi d^2/4} \qquad \text{(Eq. 8)}$$

Conceptually, this is the velocity of the stream of water immediately after exiting the orifice. This is an ideal maximum velocity as momentum is lost when the stream strikes the deflector plate and as the droplets interact with the surrounding air and break up. While FDS uses Eq. 8 as a default, it is noted that "quite often you must fine-tune the PARTICLE_VELOCITY in order to reproduce a particular spray profile" [12].

Another estimation of velocity can be obtained from a study by Shepard that measured and mapped the radial velocity of droplets from 15 different sprinkler tests. The sprinklers varied in K factor and pressure as seen in Figure 2-3. Shepard developed a velocity coefficient, C, that relates the particle velocity to a nondimensionalized Bernoulli-type velocity:

$$u_{ave} \approx C \sqrt{\frac{P}{\rho}} \qquad \text{(Eq. 9)}$$

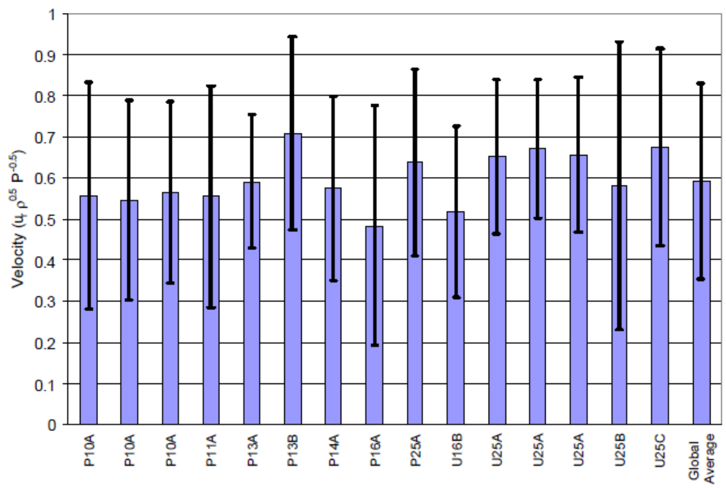

Figure 2-3: Average Nondimensionalized Velocities [3]

The average coefficient of the sprays examined was 0.59 and the range between 0.5 and 1.0. This provides another method to estimate the particle velocity input in the absence of experimental data.

Although an average velocity can be calculated, there are local variations within the spray pattern of any sprinkler. The variations also differ from sprinkler to sprinkler. Two sprinklers with the same K factor or the same nozzle at different pressures could have different velocity profiles [3]. Figure 2-4 shows the radial velocity of 4 sprinklers, one of which is tested at three pressures. Sprinkler U25A has a maximum velocity at 75 degrees of elevation when operating at 48 kPa whereas the maximum velocity occurs at 65 degrees when operating at 103 kPa. Additionally, three sprinklers of the same K factor, U25A, U25B, and U25C, have maximum velocities at 65, 55, and 60 degrees respectively at the same pressure.

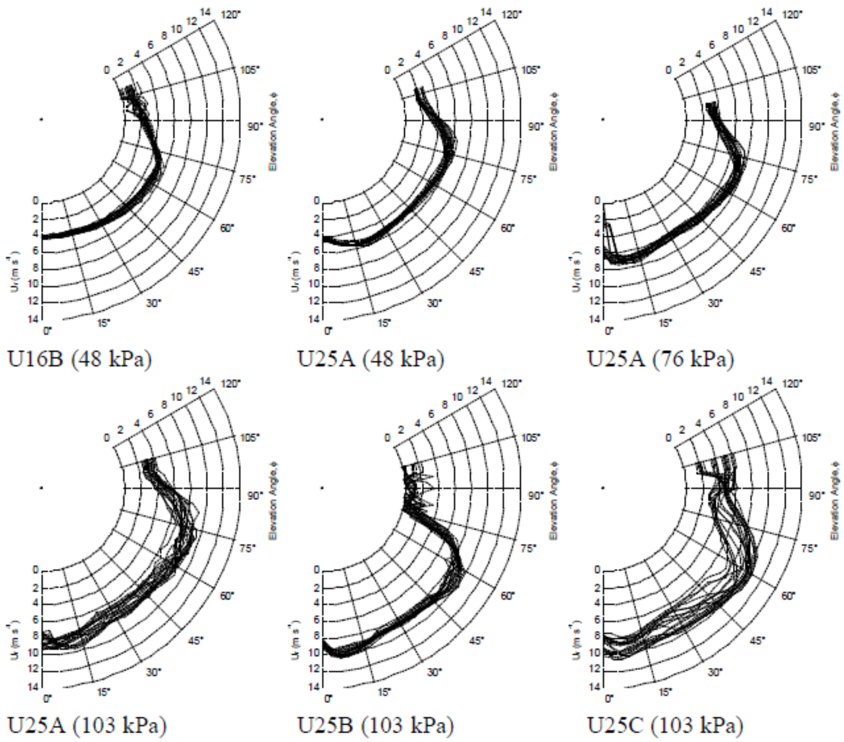

Figure 2-4: Radial Velocities of Upright Sprinklers [3]

2.1.4 Nozzle Characteristics

The following is a brief overview of the inputs required in FDS to define a nozzle spray pattern. OFFSET is the radial distance from the nozzle at which the particles are inserted into the domain. FDS default is 0.05 m however many of the literature correlations are measured at farther distances such as 0.2 m or 0.3 m.

SPRAY_ANGLE defines the elevation angles through which the particles are sprayed. Within these angles, the density of spray varies according to a Gaussian distribution, defined by μ and β seen in Figure 2-5. Alternatively, a uniform distribution can be specified where there is no variation with polar angle which corresponds to a β value of 0.

SPRAY_PATTERN_MU, μ, determines at which latitude the maximum density of droplets occurs. If no value is given, the latitude of the maximum density occurs halfway between the two spray angles.

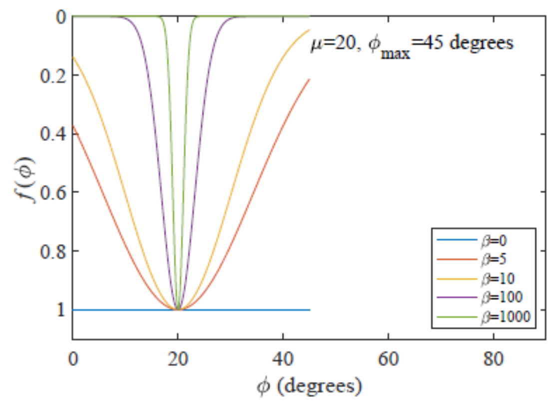

Figure 2-5: Spray Pattern μ and β [12]

SPRAY_PATTERN_BETA, β, determines the width of the distribution of the spray. A zero value results in a uniform distribution, whereas a higher value of 1000 results in a very narrow band. The FDS default is a relatively dispersed value of 5.

To show the impact of β, four simulations of a basic nozzle were run with the same spray angles 10º - 80º and μ of 45. This simulation was run with the particle drag model disabled, in quiescent air, to isolate the effect of β from the impacts of particle drag discussed in Section 2.1.5. Figure 2-6 shows β = 0 created a wide, dispersed spray whereas β=1000 created a very concentrated spray. Particle flux data is measured by a slice file and represents the pattern of water on the floor, averaged over 60 seconds of the simulation.

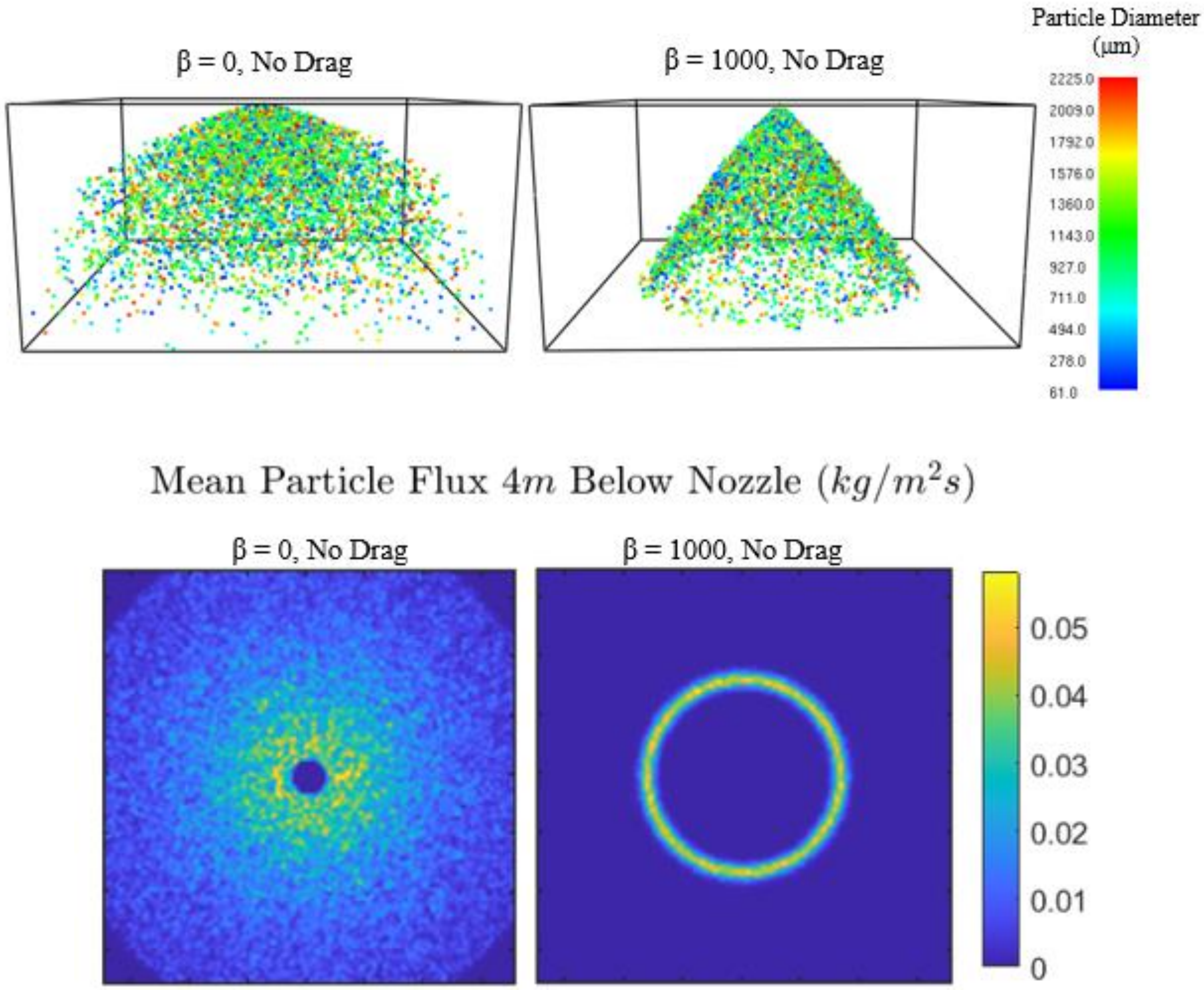

Figure 2-6: Simple Spray with Large and Small β Values, No Drag

2.1.5 Particle Drag

Particle drag (C_d) in FDS is calculated using Eq. 10 and is based on the Reynolds (Re_D) number for a spherical particle.

$$C_d = \begin{cases} 24/Re_D & Re_D < 1 \\ 24(0.85 + 0.15Re_D^{0.687})/Re_D & 1 < Re_D < 1000 \\ 0.44 & 1000 < Re_D \end{cases} \qquad \text{(Eq. 10)}$$

Table 3: Calculated Terminal Velocity

Diameter (μm)	Calculated Terminal Velocity (m/s)
50	0.074
300	1.24
500	2.1
1000	3.81
1500	5.36
2000	6.8

Calculated terminal velocity of various particle diameters is shown in Table 3. The smaller particles have a smaller Reynolds number resulting in a higher drag coefficient and lower terminal velocity. It is important to note that these are single particle velocities in static fluid and do not account for effects of air entrainment or the wake effect. An experiment by Chan found "the average droplet velocity for each drop size was found to be very close to the experimental terminal velocity for a single water droplet traveling through air" [19].

To visualize the effects of drag on particles in a spray, two tests in FDS were run. First, droplets of 50, 300, 500, 1000, 1500, and 2000 μm were injected with a horizontal velocity of 10 m/s with the default particle drag model shown in Figure 2-7. An additional droplet (farthest blue) was introduced as a 50 μm droplet without drag. We see that the smallest droplet 50 μm (close blue) quickly reaches terminal velocity, the largest particle (red) travels the furthest among particles with drag, and the particle without drag (far blue) travels even farther than the largest particle.

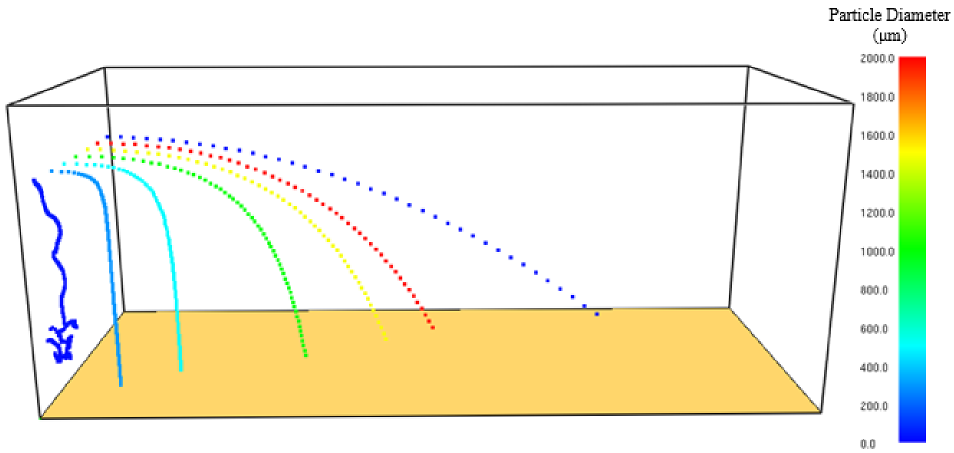

Figure 2-7: Terminal Velocity FDS Simulation

The second test to visualize particle drag effects in a spray is the same simulation as Section 2.1.4 with β = 0 and β = 1000, this time with the default particle drag model enabled, as seen in Figure 2-8. The spray does not travel as far horizontally, and the smallest particles (blue) are concentrated more towards the center. The larger particles (orange/red) have a higher terminal velocity and higher momentum and remain on the outsides of the spray.

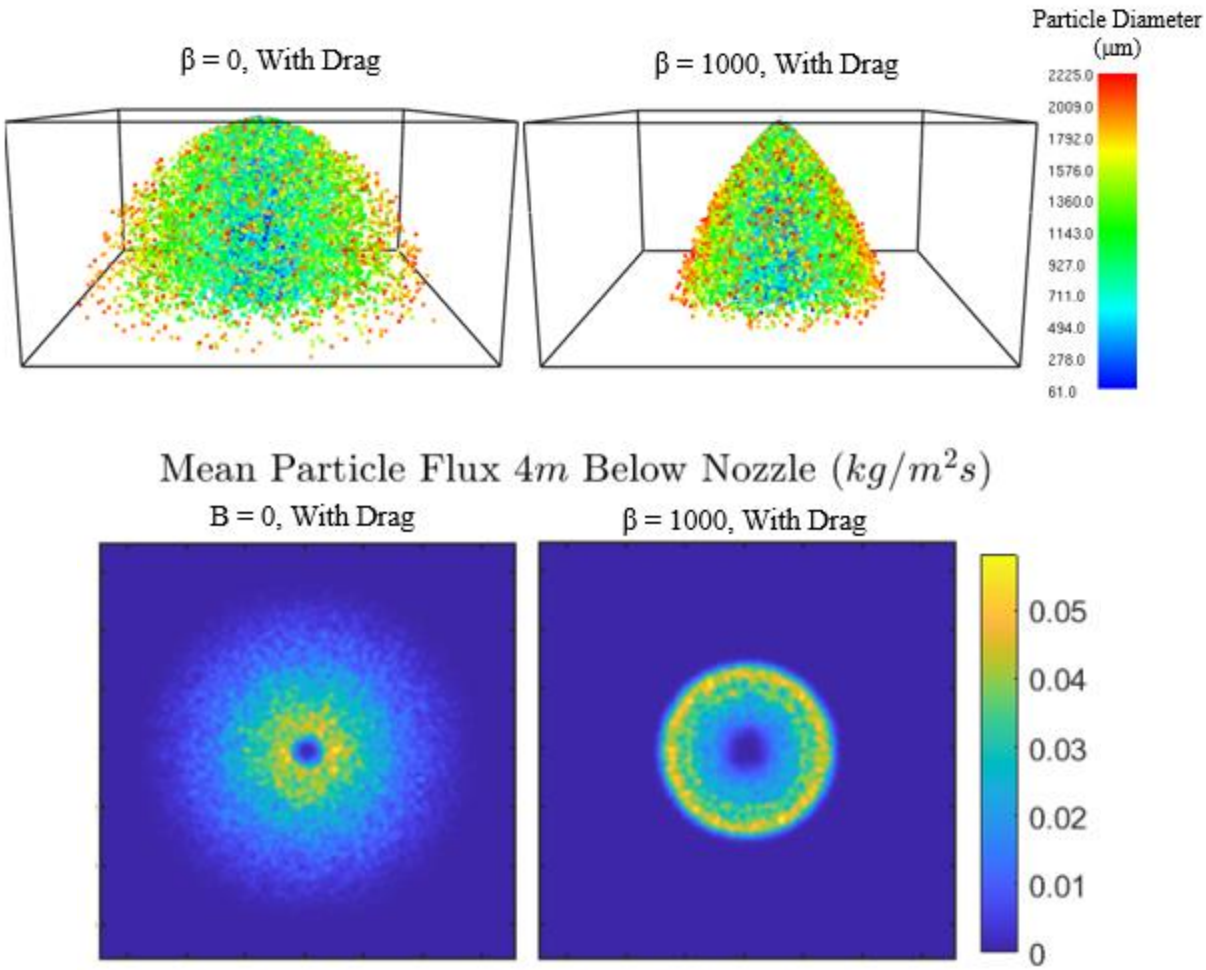

Figure 2-8: Simple Spray with Large and Small β Values, With Drag

It's important to know that this is in quiescent air. In Figure 2-9 a crossflow of 1 m/s air is introduced. The smaller particles are pushed out of the center of the spray due to the higher drag forces resulting from lower Reynolds Numbers. The effect of crossflow of air on the spray pattern is examined in detail in Chapter 4.

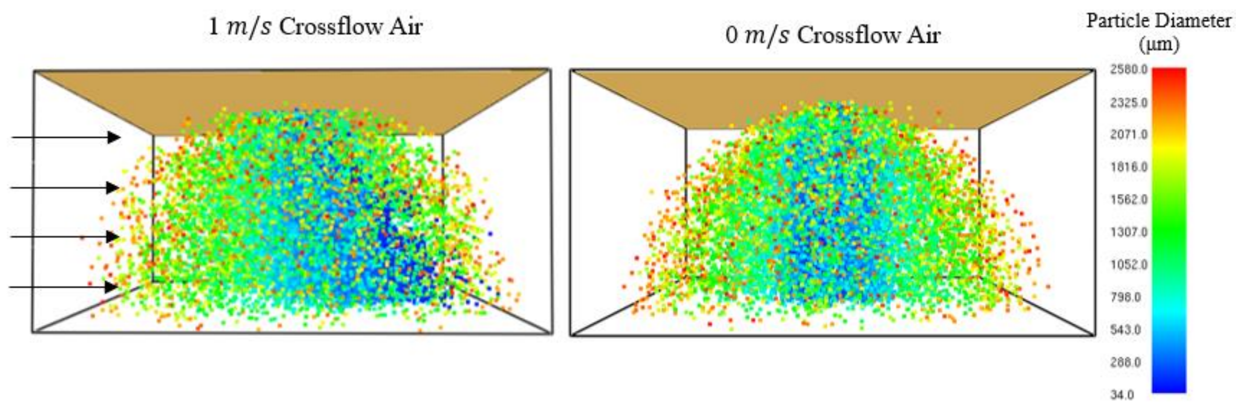

Figure 2-9: Bucket Test 4S Nozzle w/ 1 m/s Crossflow

2.2 4S Measurements

The 4S provides spatially resolved measurements 0.3 m from the nozzle of spray characteristics of volume flux, volume median diameter, volume weighted velocity, and distribution parameter, γ or Γ, seen in Figure 2-10 [4].

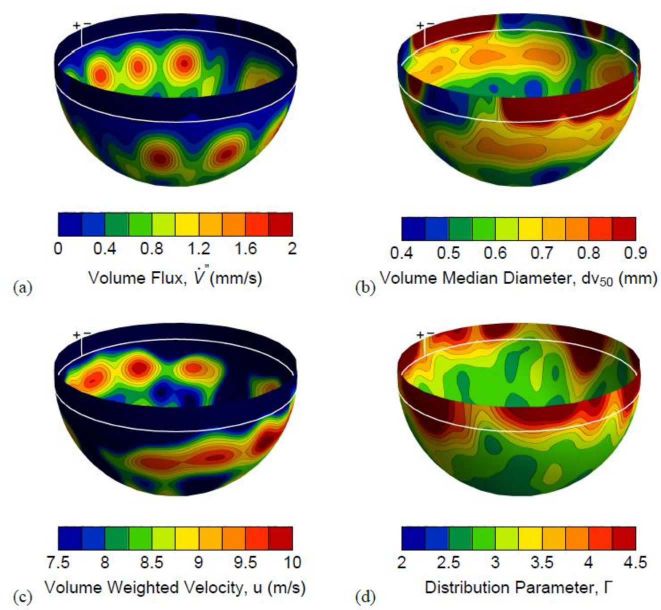

Figure 2-10: 4S Spatially Resolved Measurements [4]

These measurements are taken at 10 degree latitude (elevation) increments with 1 degree longitude (azimuth) resolution. In FDS, a complex spray pattern is specified by table with the following line of code.

```
&TABL ID='table_id', TABLE_DATA=LAT1,LAT2,LON1,LON2,VELO,FRAC /
```

An example is provided in Appendix A. The first four inputs, LAT1, LAT2, LON1, and LON2 define the latitude and longitude of the angular region. The next two inputs, VELO and FRAC, define the velocity and water flux which are two of the four spatially resolved measurements the 4S provides. The other two spatially resolved parameters of the median diameter and the distribution parameter, Γ (GAMMA_D), are only specified for the entire spray in the &PART line. The spatial resolution of these two inputs is lost within FDS.

2.3 Radial Water Flux

In addition to measuring the different aspects of the spray though with the 4S, another common approach is to measure the distribution of water at a horizontal plane below the sprinklers [3]. One common way to obtain this data is through a bucket test in which a series of buckets are set up beneath the sprinkler in a line and weighed before and after a period of activation to determine water flux. Below Figure 2-11 shows the results of a ten pan bucket test 10 feet below the sprinklers [3]. The Y-axis is the water density (flux) normalized by the total flow rate of the sprinkler for comparison. The graph shows that the water distribution is very dependent on the type of sprinkler. Additionally, the same sprinkler tested at two different pressures can exhibit similar spray characteristics, as is the case with model 6, or very different spray characteristics, as the case with model 3.

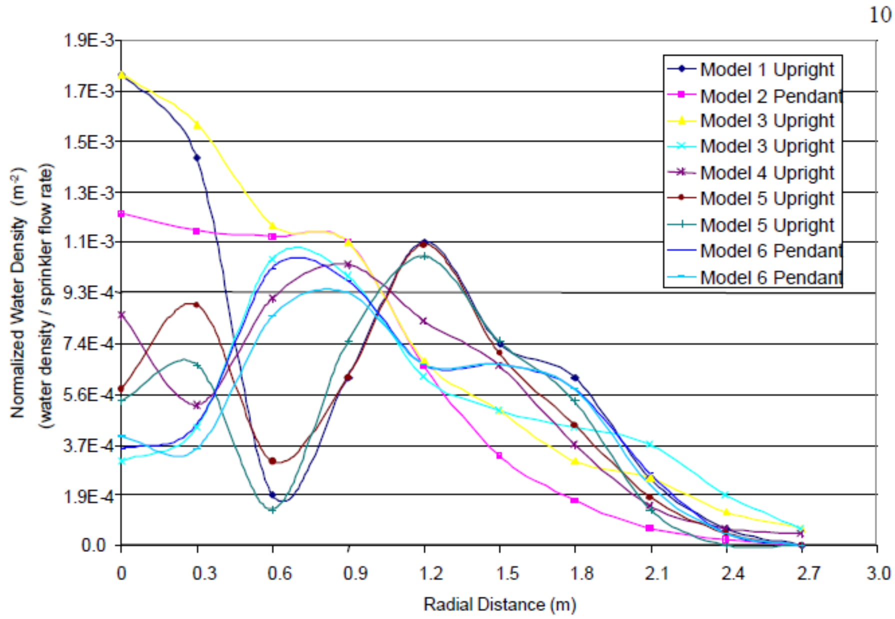

Figure 2-11: Normalized Water Density (Water Flux/ Sprinkler Flow Rate) as a Function of Radial Distance of Various Sprinklers [3]

Chapter 3 : Bucket Test Comparison Quiescent

3.1 4S Nozzle Set Up

For the quiescent bucket test analysis of spray patterns, a K 5.6 pendent sprinkler was analyzed in a 14 m x 14 m x 7.6 m domain. The pendant sprinkler was placed 0.6 m below the ceiling. All boundaries except for the ceiling were set to OPEN boundaries. A grid size of 10 cm was selected based on an FDS study discussed in Chapter 5. Humidity was set to 100% to eliminate evaporation. 4S nozzle characteristics for a K 5.6 sprinkler at 14 psi were provided by Fire Risk Alliance LLC. Full simulation code is included in Appendix C. The sprinkler activates at 0 s and remains on for 70 s. A Smokeview representation of this simulation can be seen in Figure 3-1. Visual observation concludes that the smaller particles remain at the center of the spray because those particles have less momentum and higher drag coefficients. This agrees with the results from the terminal velocity tests in Section 2.1.5.

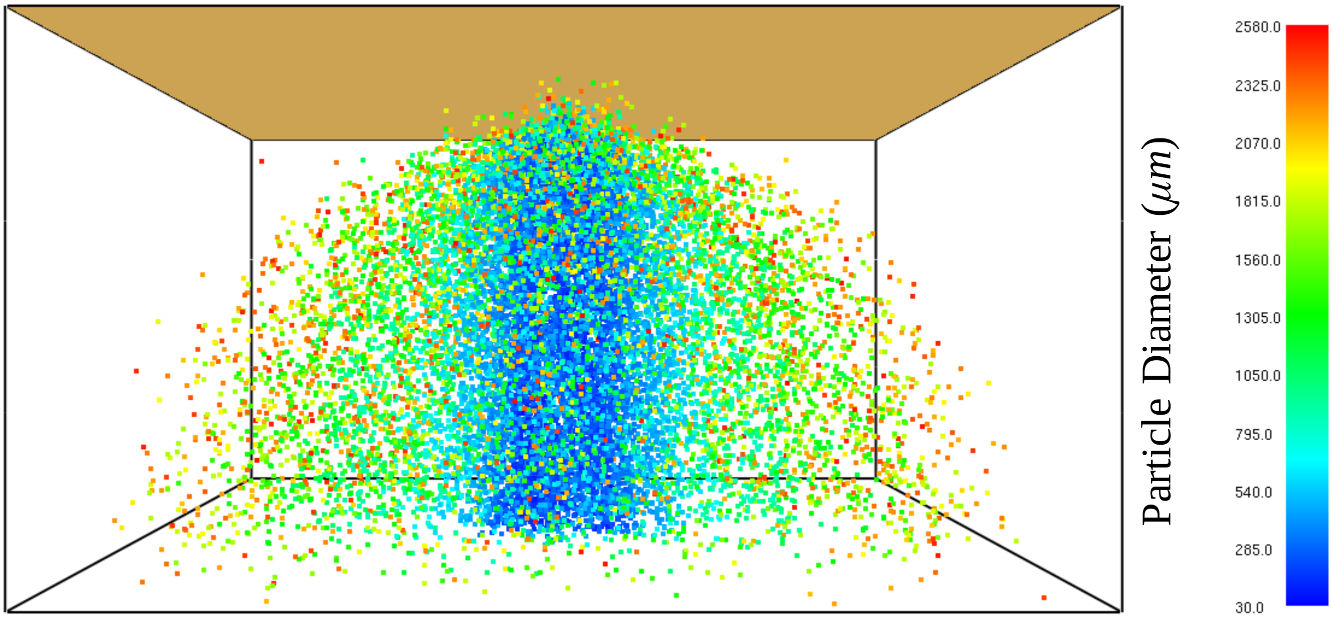

Figure 3-1: 4S Nozzle Bucket Test Simulation in Quiescent Air

3.1.1 Particles Per Second Analysis

For the bucket test simulation, particles per second were varied at 2500, 5000, 10000, 20000, and 30000. This particle per second analysis looks at the mean particle fluxes at different elevations below the nozzle. In Figure 3-3, results are presented at 1, 4, and 7 m below the nozzle along the Y = 1 m and Y = 3 m axis. The axes Y = 1 m and Y = 3 m at 7 m below the nozzle are shown in Figure 3-2 for reference.

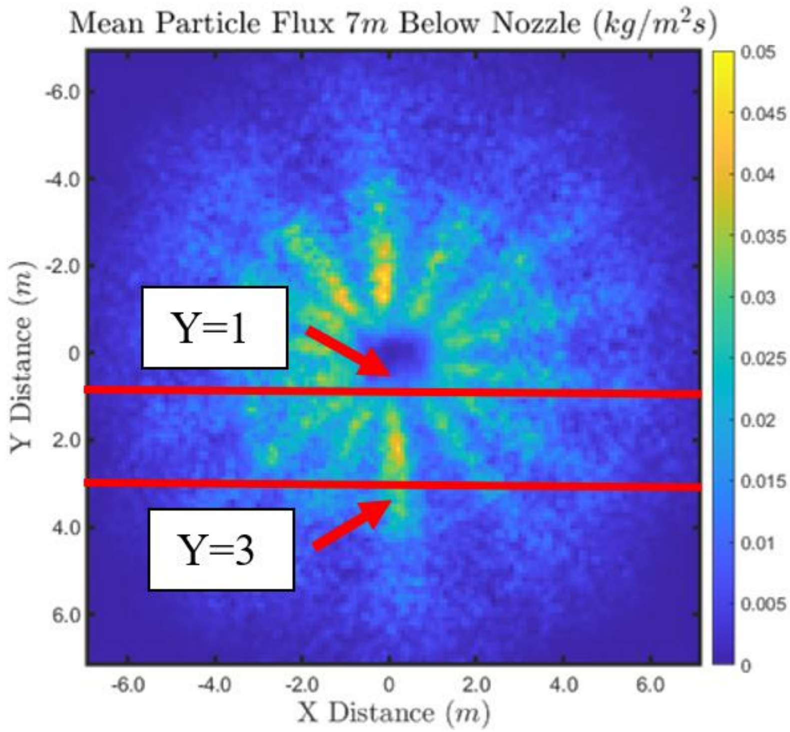

Figure 3-2: 4S Nozzle, 7m Below Nozzle, Y = 1 m and Y = 3 m

Overall, the water flux distributions for 5000, 10000, 20000, and 30000 particles per second all follow the same shape and magnitude, as seen in Figure 3-3. 2500 PPS at 1 m below the nozzle, in the Y=1 m and Y= 3 m planes, exhibits higher maximums and lower minimums than the higher PPS values so it should not be used to characterize this spray. The main difference between the remaining PPS choices is the magnitude of the oscillations. This magnitude of oscillations will have an effect during a fire scenario as large oscillations can lead to non-physical evaporation patterns and numerical instabilities. The largest decrease in oscillations happens when transitioning from 5000 to 10000 PPS as seen in 7 m below the nozzle at Y =3 m. There is a slight decrease from 10000 to 20000 and 20000 to 30000; however, 10000 provides a good balance between computational demands and benefits so 10000 PPS will be used in subsequent tests with the 4S nozzle.

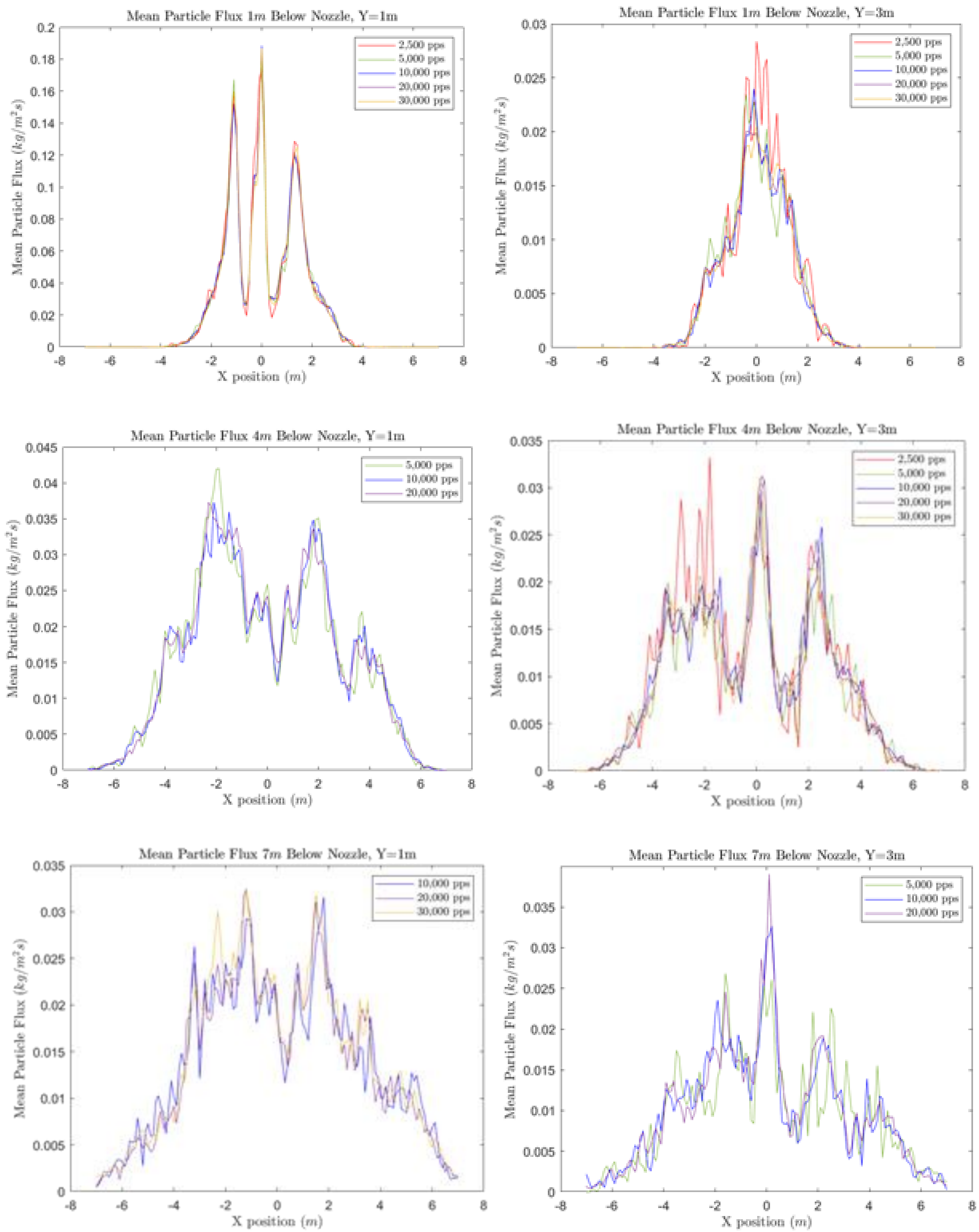

Figure 3-3: 4S PPS Analysis Y Slices

3.1.2 4S Nozzle Results

Following the particle per second analysis, the flow rate through various elevations was measured as seen in Figure 3-4 to ensure the correct flowrate from the nozzle. The prescribed flow rate of the simulation was 94.8 liters per minute. As the spray reaches 5 m below the nozzle, some of the particles visibly exit the domain (Figure 3-1) which corresponds to the drop in flow rate. The minimum of 93.9 liters per min equates to a 1% error from 94.8 liters per minute and the maximum value of 95.2 liters/min corresponds to < 0.5% error which are acceptable fluctuations.

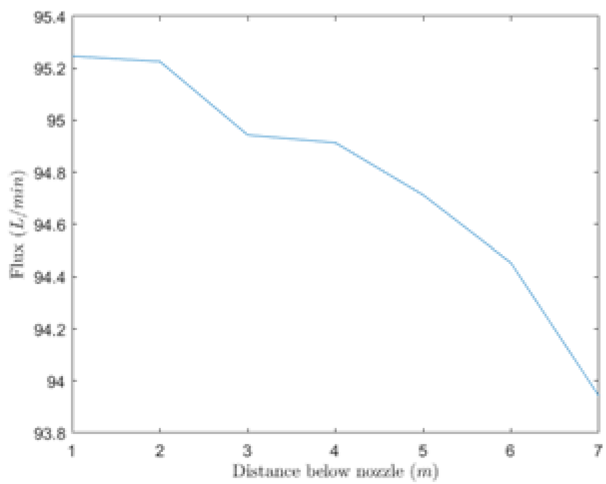

Figure 3-4: 4S Nozzle Flux Check

In Figure 3-5, the particle flux at all elevations show consistent azimuth variations in the spray. The radial variation of the spray is most prominent 1 m below the spray with a clear ring of reduced water flux. This ring is still visible at 4 m but disappears 7 m below the nozzle. This visual observation suggests strong azimuth resolution through all distances and radial resolution through 4 m.

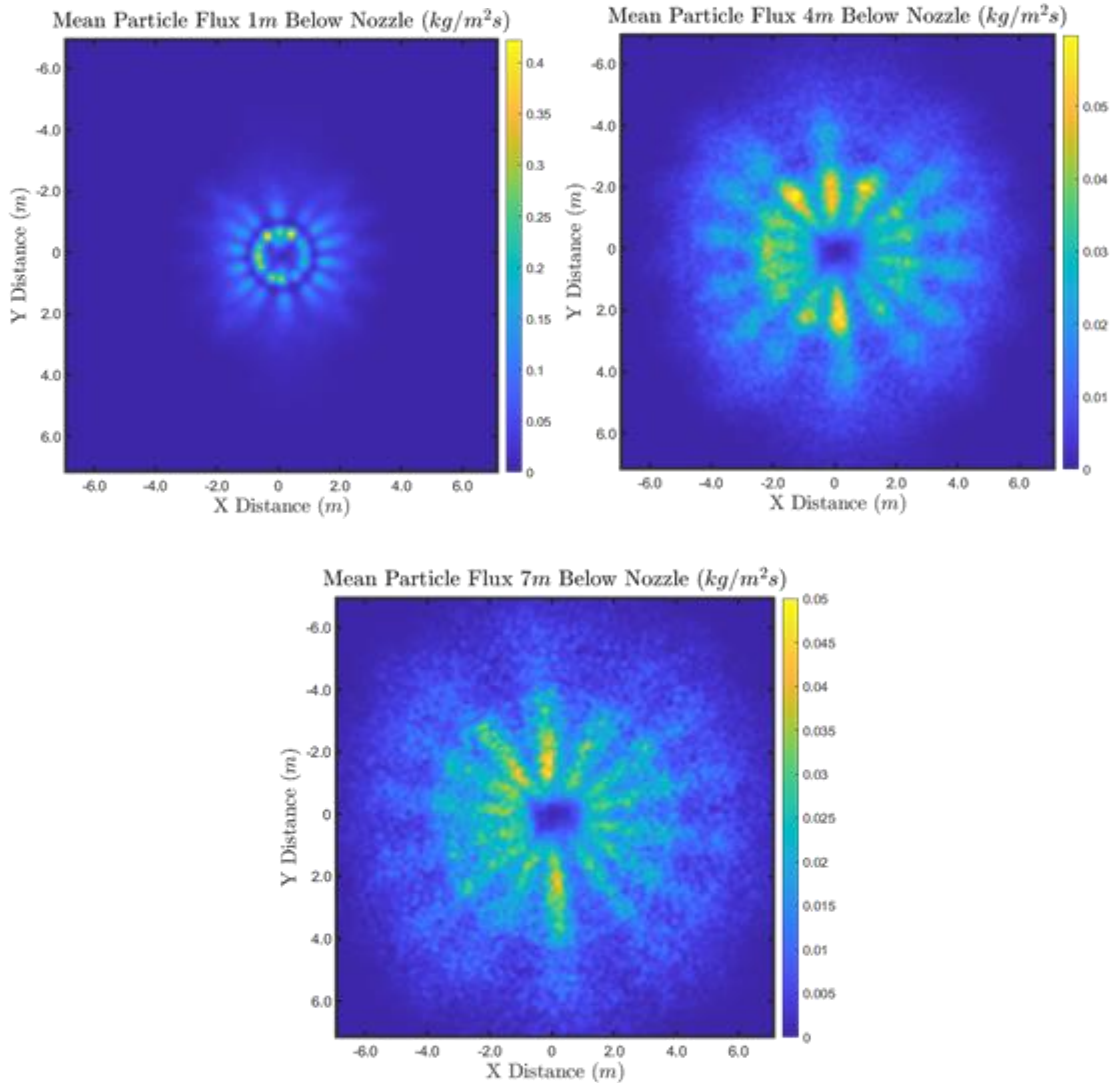

Figure 3-5: Mean Particle Flux 4S Nozzle at 1, 4, 7 m Below Nozzle

In Figure 3-6, the radial profiles of the spray at 1 m, 4 m, and 7 m are presented and confirm the trends discussed previously. The variation in particle flux at the lower elevations flattens with decreasing elevation. At 1 m below the nozzle, there are two well defined peaks with a trough that was visible in Figure 3-5 as well. These smooth out to a slight dip 4 m below the nozzle and the radial profile of 7 m below the nozzle is the smoothest. Also of note, the location of the highest water density at 4 m is around 2.3 m from the center where at 7 m it’s around 1.4 m from the sprinkler.

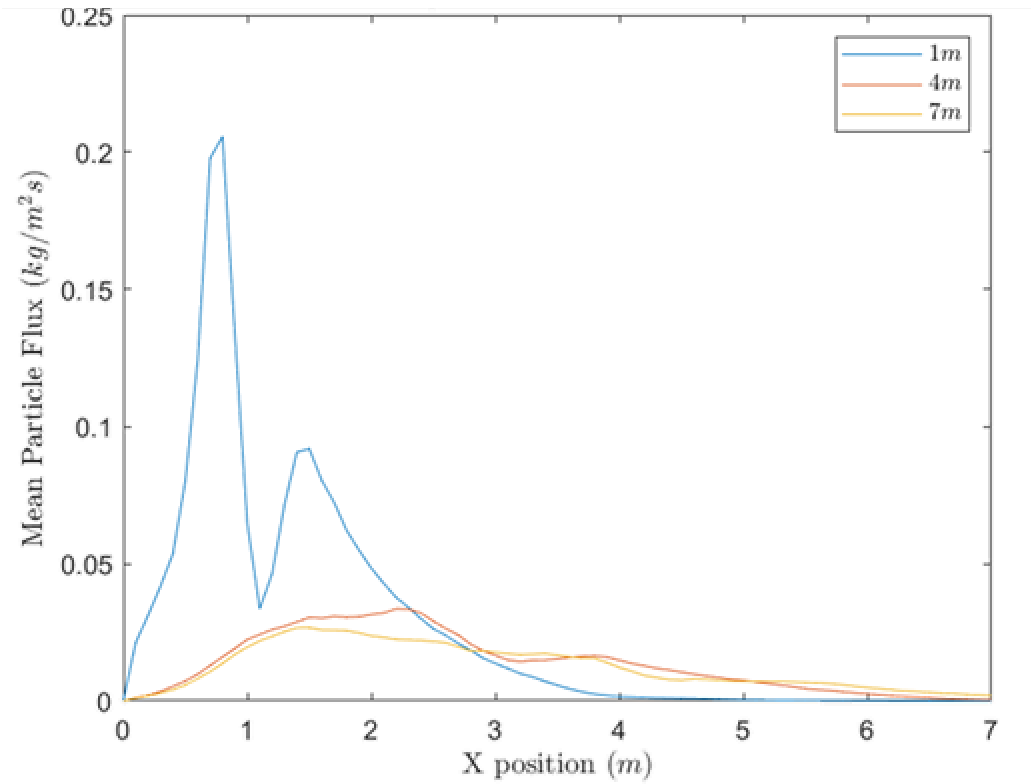

Figure 3-6: 4S Average Radial Particle Flux

3.2 Basic Nozzle Set Up

Having analyzed the 4S nozzle for a K5.6 nozzle, next a basic version of the K5.6 nozzle was estimated using a combination of FDS default parameters and previously discussed correlations taken from the literature. A summary of these parameters and their compared values to 4S can be seen in Table 4. The full basic nozzle code can be found in Appendix B.

Table 4: 4S vs Basic Nozzle Parameters

Parameter	4S Nozzle	Basic Nozzle	
	Value	Value	Correlation
DIAMETER	967 µm	954 µm	Eq. 5
GAMMA_D	2.07	2.4	FDS Default
OFFSET	0.3 m	0.05 m	FDS Default
FLOW_RATE	94.8 L/min	94.79 L/min	Eq. 7
SPRAY_ANGLE		10-80	Visual Estimation
ORIFACE_DIAMETER		0.127 m	Standard K-Factor Size
PARTICLE VELOCITY	13.32 m/s (max)	12.47 m/s	Eq. 8

The flow rate of the sprinklers is almost the same. The median diameter is also very similar but the 4S nozzle has a wider distribution, meaning its largest particles will be larger than the basic nozzle and the smallest particles will be smaller. In the simulation, the largest 4S particle is 2580 µm while the largest basic nozzle particle is 2225 µm. The maximum velocity for the 4S spray is 13.32 m/s while the velocity for the basic nozzle is 12.47 m/s.

3.2.1 Basic Nozzle Particle Per Second Analysis.

The basic nozzle follows the same trends in the PPS analysis as the 4S nozzle, which can be seen in Figure 3-7. Similarly, to the 4S PPS analysis, 2500 and 5000 PPS curves were eliminated in these tests due to variation from the curves with higher PPS. The use of 10000 PPS and greater show convergence so 10000 PPS was used moving forward.

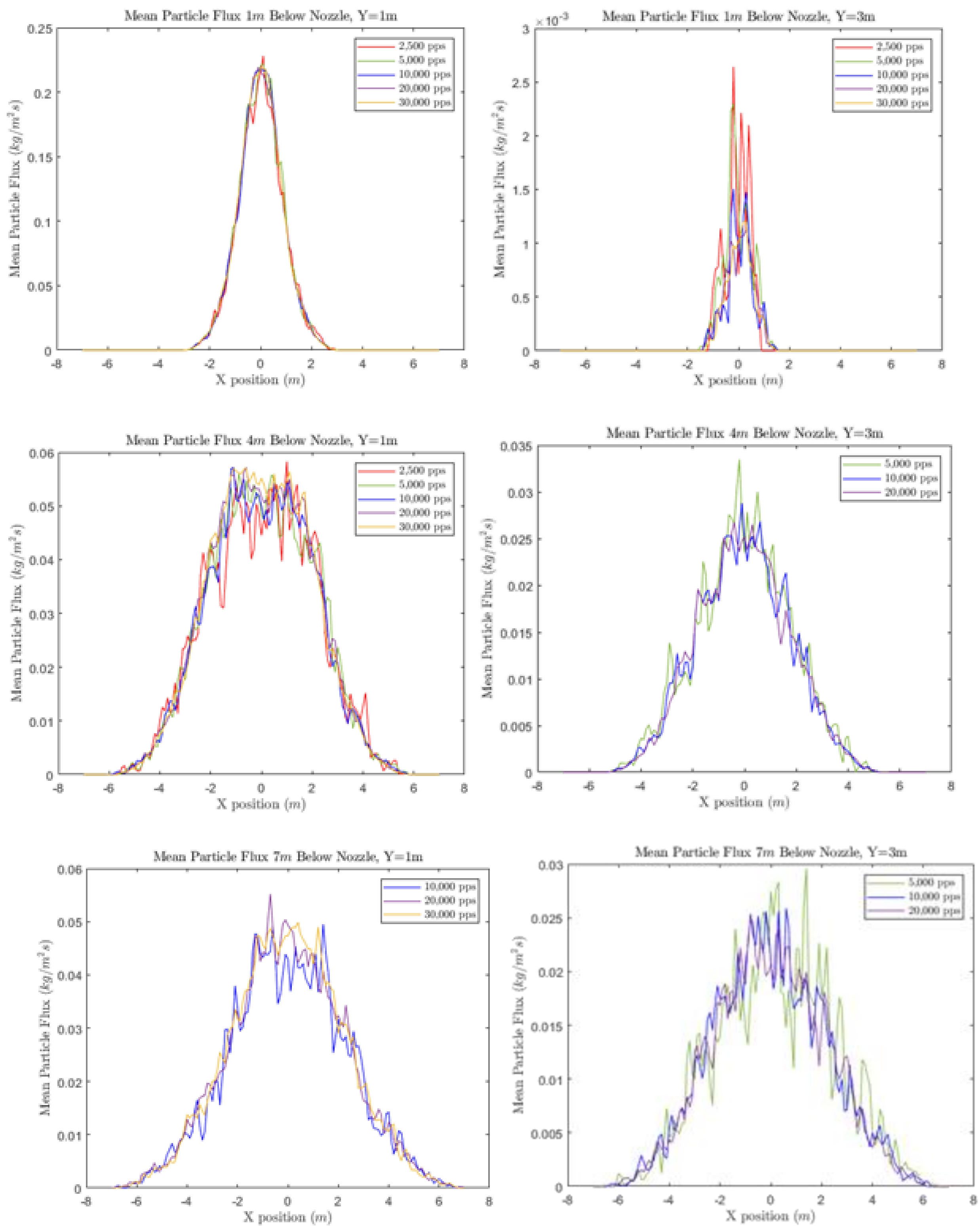

Figure 3-7: Basic Nozzle PPS analysis Y slices

Looking at the flow check in Figure 3-8, the majority of water remains in the domain, with a total error of less than 0.5% from the specified flow rate of 94.8 liters per minute.

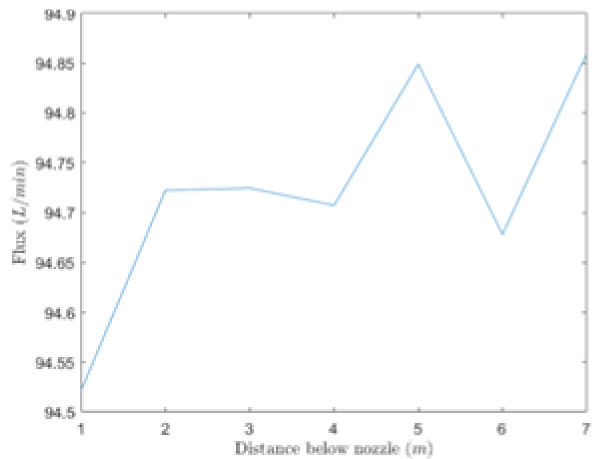

Figure 3-8: Basic Nozzle Flux Check

3.3 4S and Basic Nozzle Comparison

Comparing the basic nozzle mean particle flux distribution maps, as seen in Figure 3-9, several differences can be seen from the 4S nozzle. The most apparent is that at all distances below the nozzle, the basic nozzle does not reach as far as the 4S nozzle. Second, there is no azimuthal variation with the basic nozzle.

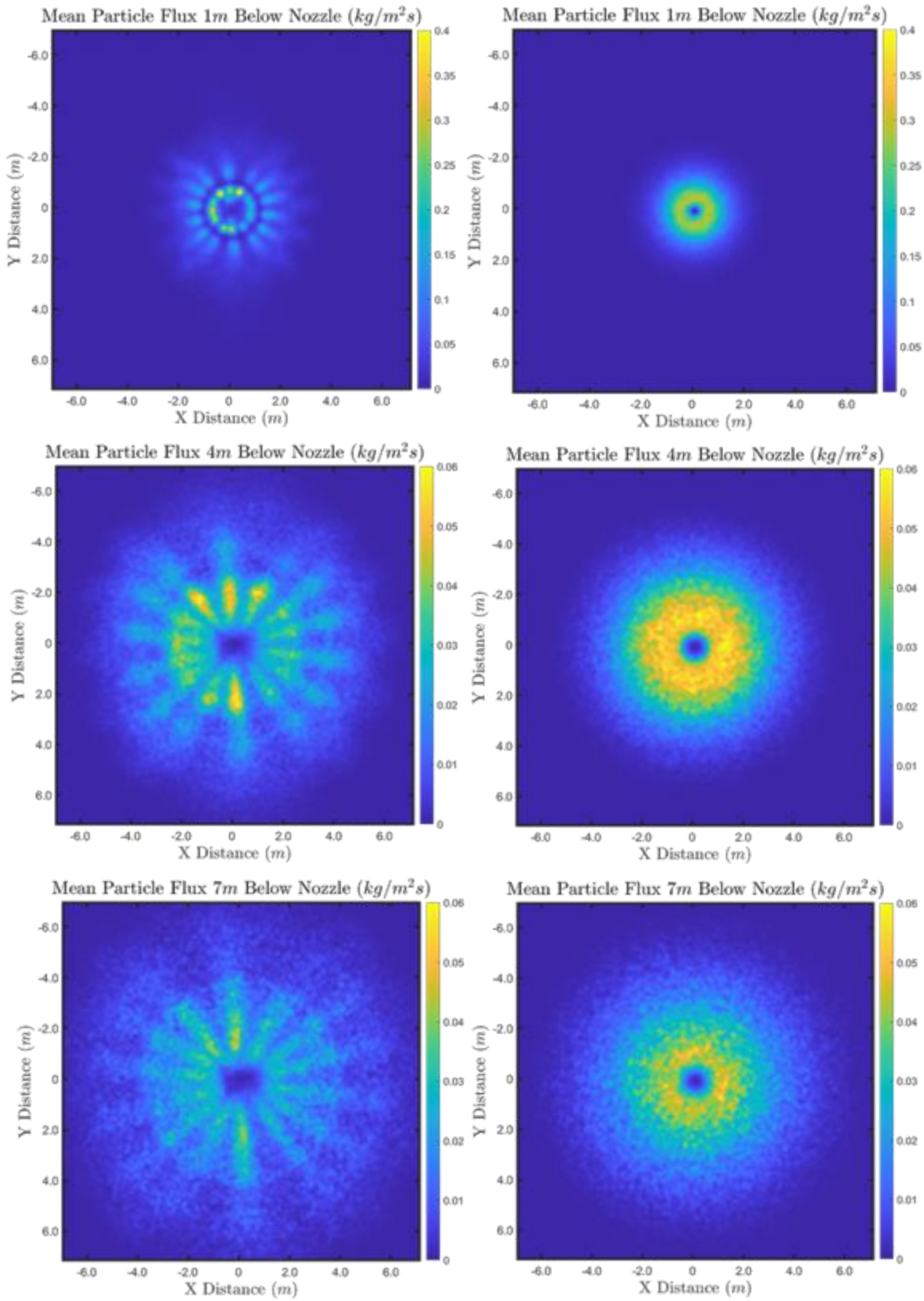

Figure 3-9: 4S (Left column) vs. Basic Nozzle (Right column) Patternation

Analyzing the Y slices in Figure 3-10, the magnitude and overall shape of the water flux distribution vary greatly between the 4S and basic nozzle. One trend that can be drawn across all slices is that the 4S nozzle has a lower particle flux closer to the nozzle than the basic nozzle, and a higher particle flux farther away. There are two exceptions to this conclusion, at Y = 3 m for a distance of 4 and 7 m below the nozzle, the 4S particle flux spikes and exceeds the basic nozzle particle flux at X = 0. Looking again at Figure 3-9, there are strong azimuthal concentrations in the corresponding regions that explains this.

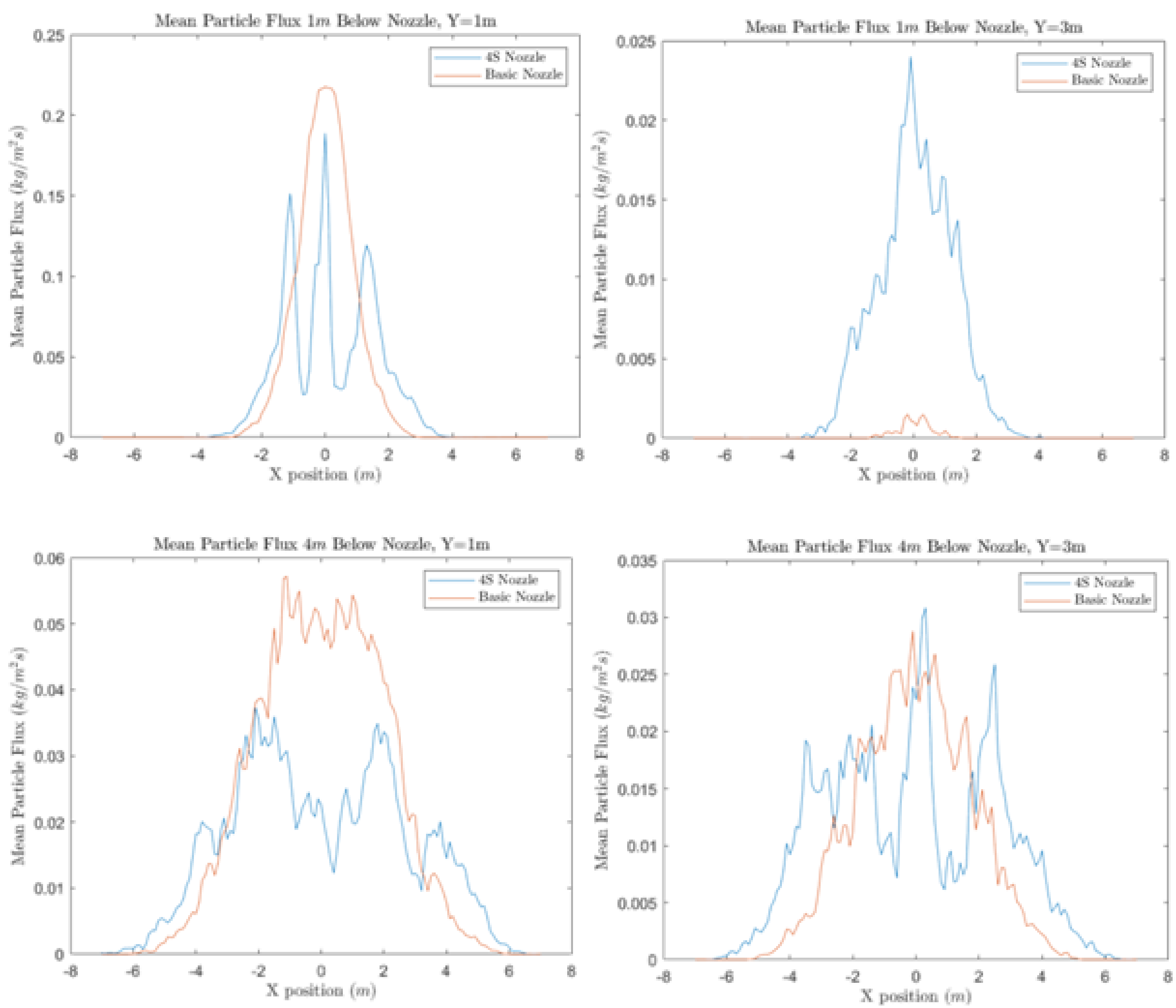

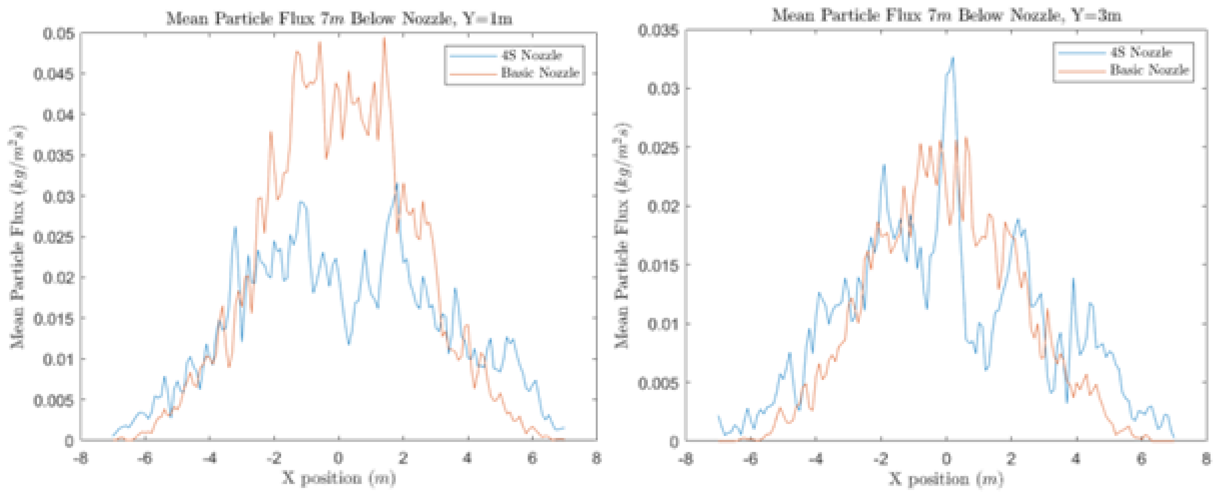

Figure 3-10: 4S (Left Column) vs Basic (Right column) Nozzle Y slices

The previous observation that the 4S nozzle has a lower particle flux closer to the nozzle, and a higher particle flux farther away is confirmed with the average radial particle flux comparison presented in Figure 3-11. Additionally, the basic nozzle only has a single peak at each elevation and overall is smoother than the 4S nozzle.

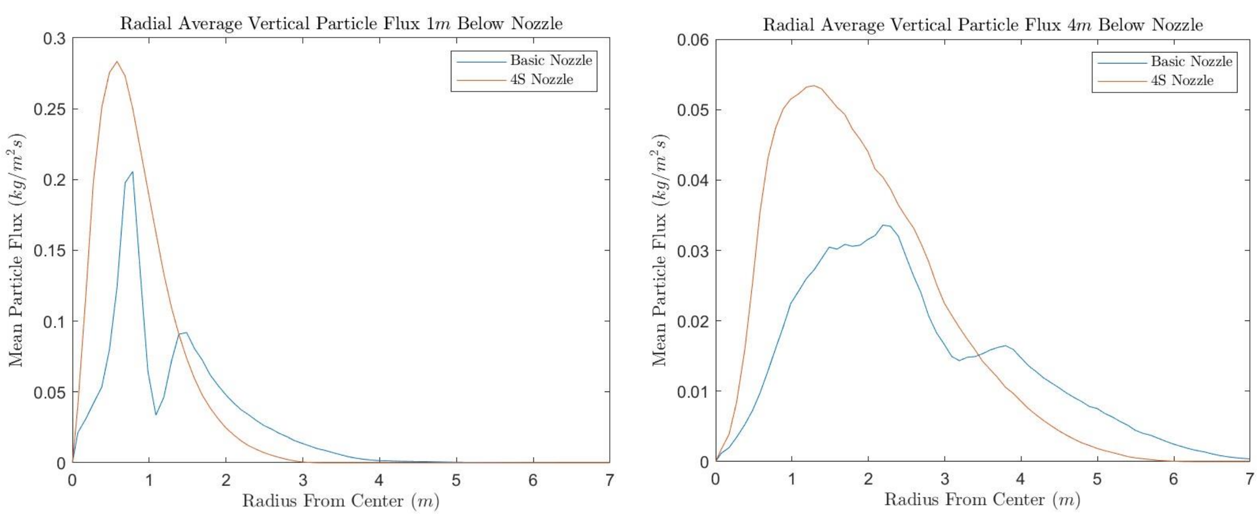

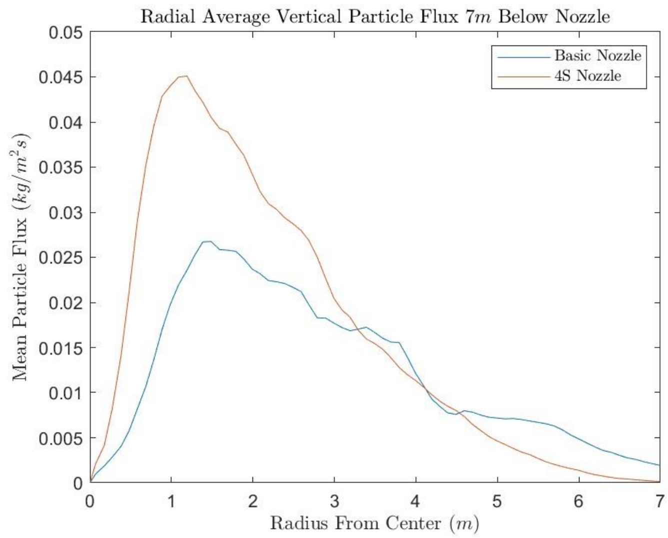

Figure 3-11: Average Radial Water Flux Distribution, 4S vs Basic Nozzle

Chapter 4 : Bucket Test Comparison Crossflow

4.1 Model Set Up

After analyzing the 4S and basic nozzles in quiescent air, a crossflow was introduced to see the effects of air movement on the sprays. Air movement in a fire scenario could be caused by natural ventilation, mechanical ventilation, or by the fire itself. Buoyant, hot combustion gasses rise up and entrain surrounding air to create the fire plume and ceiling jet [20]. The enclosure fire experiment in Chapter 5 involves three burning objects, with the maximum heat release rate (HRR) of a single object of 160 kW. Using Heskestad's correlations for plume velocities, the fire in the experiment creates a maximum vertical plume velocity of 3.3 m/s at 3 m elevation. As such, crossflows from 0 m/s to 3 m/s are considered in these tests.

For this crossflow bucket test, the same 4S and Basic sprinkler characterizations discussed in Chapter 3 were analyzed. First, the 4S nozzle is analyzed in increasing crossflow to determine the effect on the features of the spray, then the 4S nozzle is compared to the basic nozzle to see the effect of the crossflow on the differences between nozzles discussed previously. To allow for the effects of the crossflow, the domain was doubled in the X direction for a total size of 28 m x 14 m x 7.6 m. The pendant sprinkler was once again placed 0.6 m below the ceiling and boundaries, grid size, humidity, and timing remain the same as the quiescent bucket test. The airflow in this simulation originates from the negative X boundary at 0, 1, 2, and 3 m/s.

4.2 4S Results

First, the SmokeView representations of the simulations were analyzed side by side. In Figure 4-1, it can be seen that any magnitude of crossflow displaces the smallest particles significantly. At 0 m/s the smallest particles (deep blue) of approximately 50-100 μm remain within 2 m of the center, but reach the positive X boundary 21 m from center in all crossflows. As the velocity of the crossflow increases from 1 to 3 m/s the number of small particles exiting the domain and the height at which they exit both increases. The slightly larger particles of approximately 500-700 μm (light blue/ teal) land 5 m from center downwind at 1 m/s, 7 m from center at 2 m/s, and 9 m from center at 3 m/s. This corresponds to a difference of approximately 2 m displacement per 1 m/s crossflow at 7 m below the nozzle. The largest particles of greater than 2000 μm (orange / red) are easier to analyze on the upwind side of the spray. The largest particles land approximately 6 m from the center at 1 m/s, 5 m from center at 2 m/s and 4 m from center at 3 m/s. This is a difference of approximately 1 m distance per 1 m/s crossflow at 7 m below the nozzle. In summary, the smallest particles are heavily influenced by even slight crossflow, and small particles are influenced more than larger particles by crossflow.

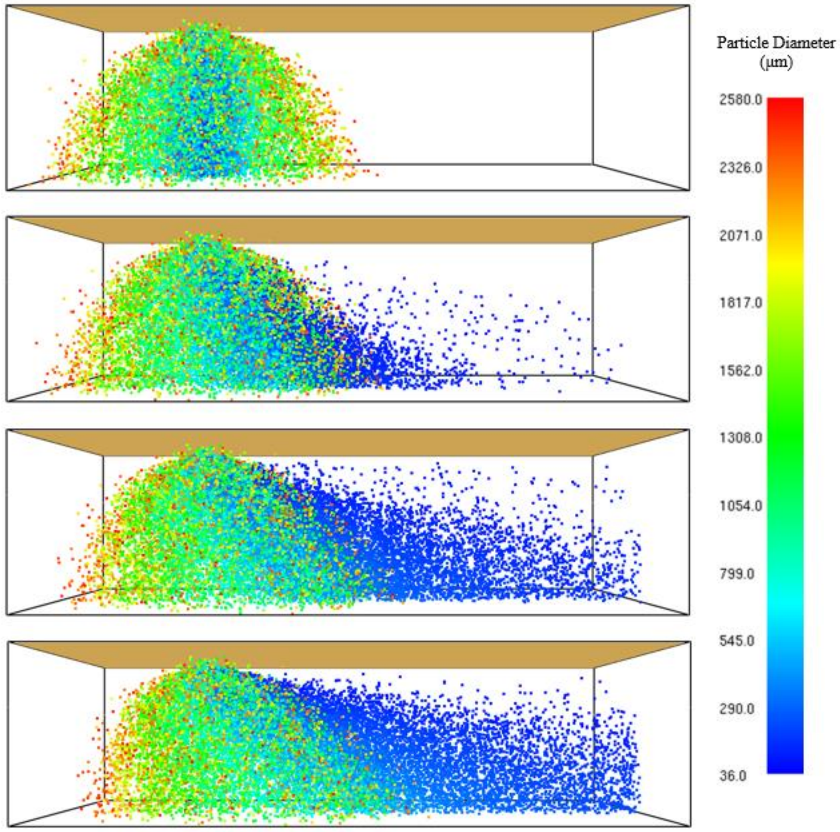

Figure 4-1: 4S Nozzle at 0, 1, 2, 3 m/s Crossflow (Top to Bottom)

Next, the mean particle flux distribution maps at the Y= 0, 2, 4, and 6 axis are analyzed 1, 4, and 7 m below the nozzle. An example of these axis of intrest can be seen in Figure 4-2.

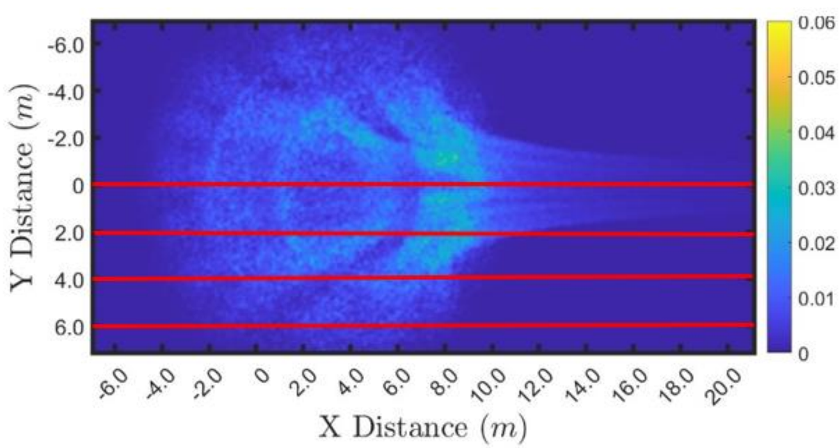

Figure 4-2: Y slices at 7 m Below the Nozzle, 3 m/s Crossflow

At an elevation of 1 m below the nozzle, there is not much difference between the crossflow velocities, see Figure 4-3. The spray is shifted slightly, less than 0.5 m in some locations, however it retains all the features of the spray in magnitude and shape. All visual azimuthal and radial variations are apparent at 3 m/s.

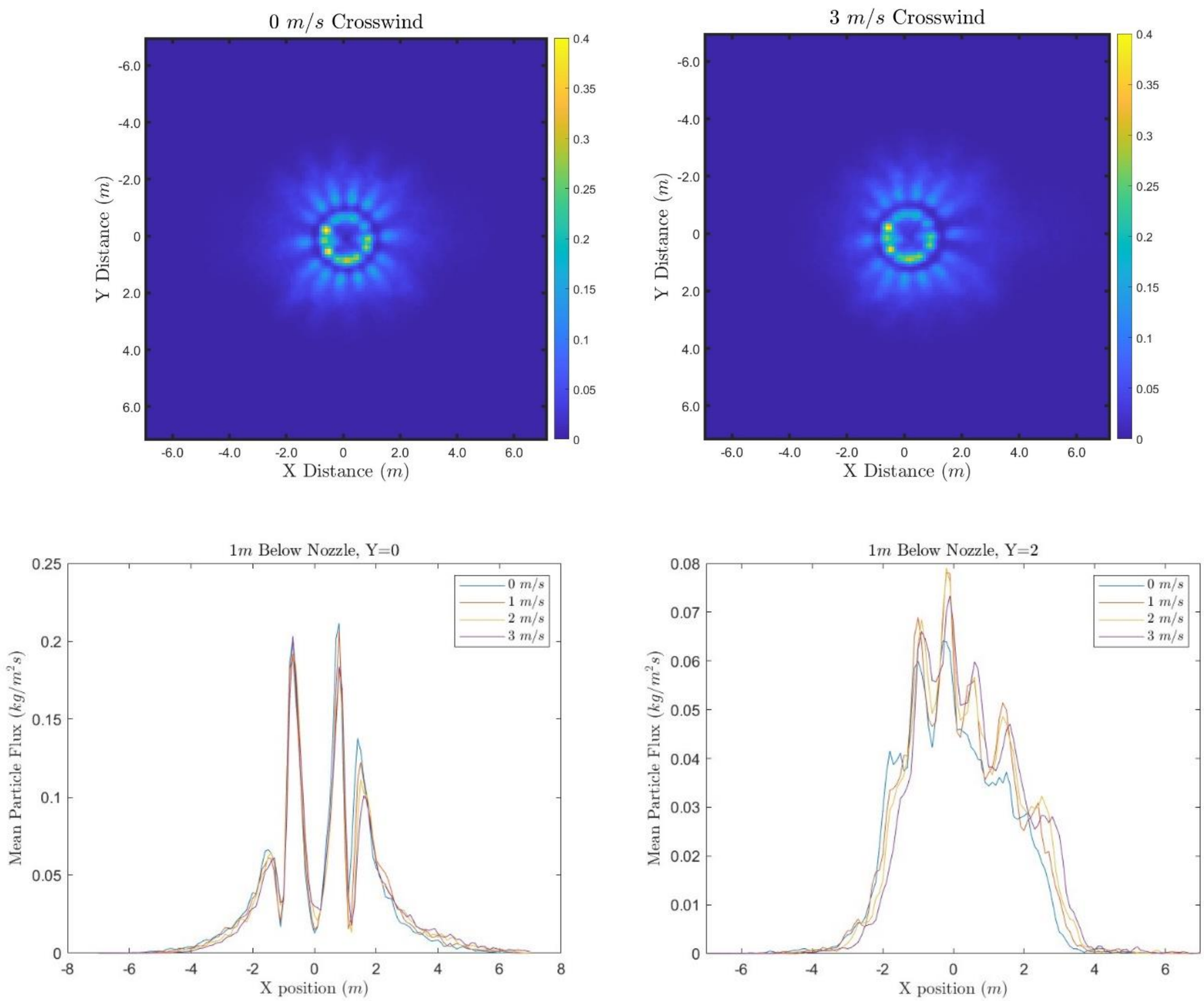

Figure 4-3: 1 m below 4S nozzle, 0 and 3 m/s Crossflow

At 4 m below the nozzle, the crossflow has a larger effect. Where smaller particles are present in the spray, the magnitude of the peaks decreases with increasing wind, and the overall distribution flattens and elongates. This can be seen in Figure 4-4, at the center of the spray in the mean particle flux distribution maps, and in corresponding Y slice plots at Y = 0 and Y = 2 from X = -3 onward. Where the largest particles are present in the spray, the distribution remains largely intact, with a shift proportional to the crossflow. This can be seen in the mean particle distribution maps at the outer edge of the spray and the corresponding Y slice plots at Y = 4 and Y = 6. This difference in behavior is due to the difference in momentum and drag coefficients between the smaller and larger particles.

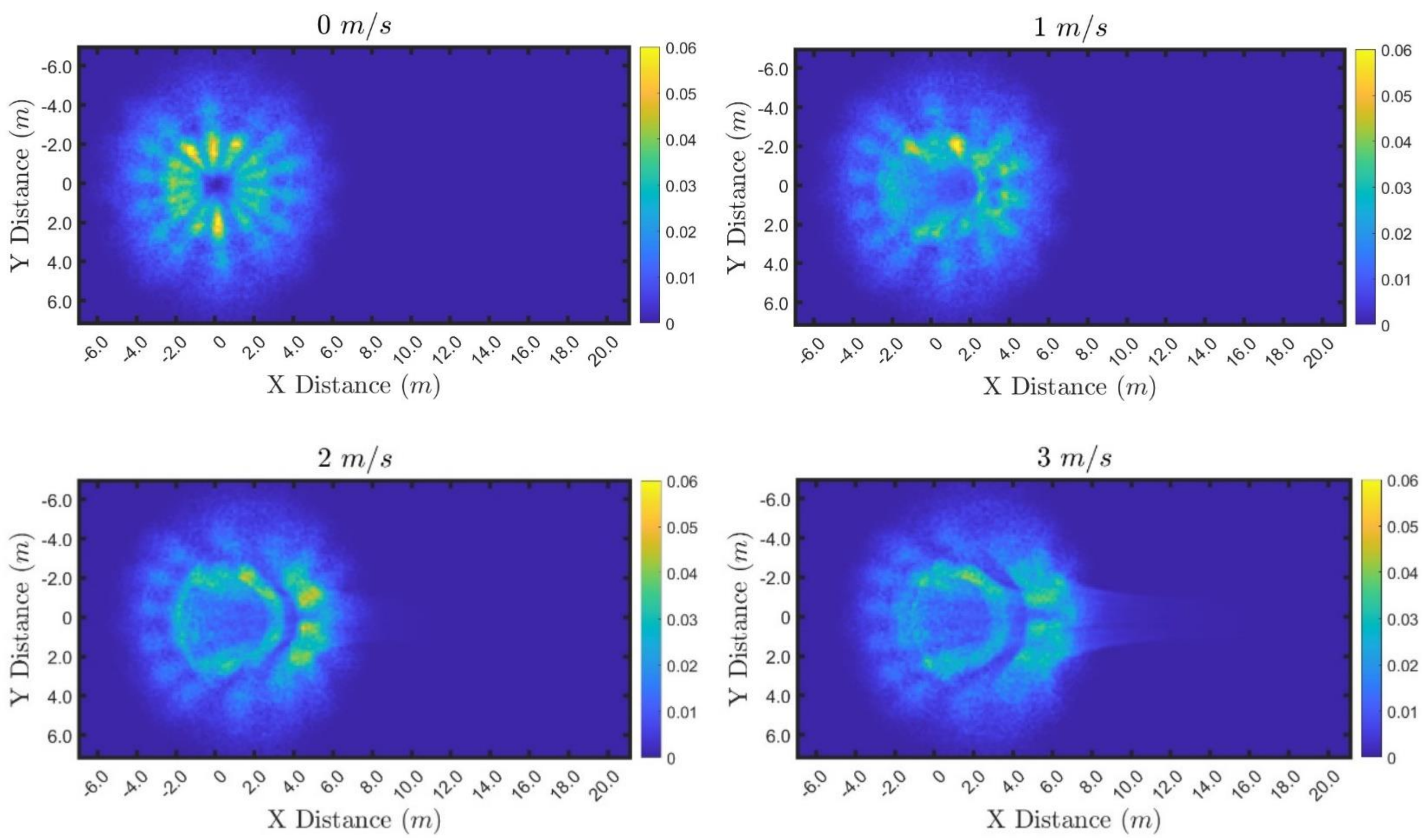

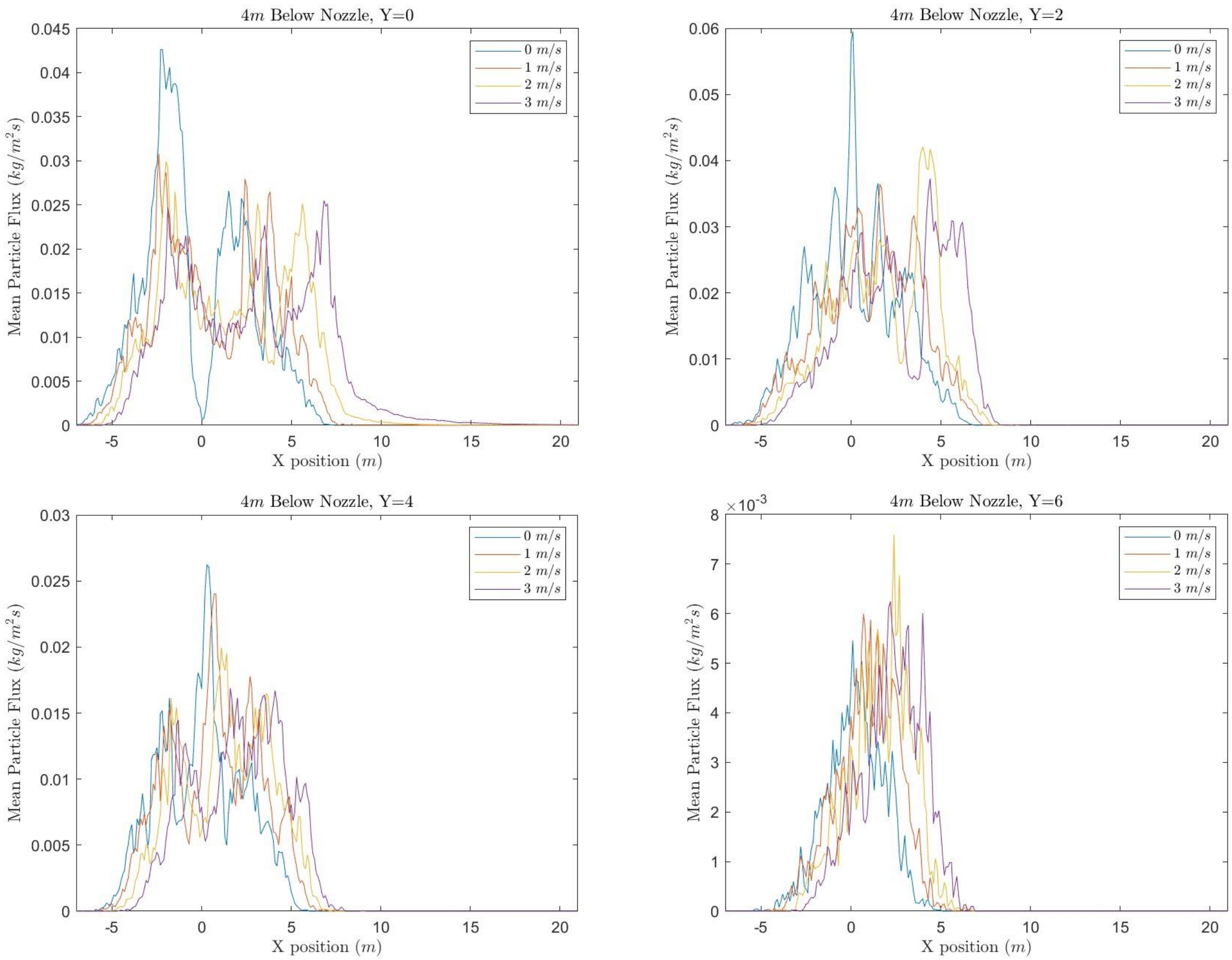

Figure 4-4: Crossflow Analysis 4 m Below Nozzle

At 7 m below the nozzle, in Figure 4-5, the trends from 4 m below the nozzle continue with a greater magnitude. Where smaller particles are present in the spray, the magnitude of the peaks still decreases with increasing wind, however the displacement is increased. At 4 m there was noticeable particle flux along Y = 0 up to 15 m from the center, whereas at 7 m below the nozzle there is noticable particle flux to the edge of the domain at 21 m from center. Where large particles are present, the overall shape of the particle flux distrubution at Y=4 is no longer symmetrical and skews left at higher crossflows in addition to a larger displacement. At Y = 6 the shape of the distribution remains relatively uniform and symmetric but has a larger displacement. Additionally the strong azimutal features of the spray are no longer visible at 2 and 3 m/s.

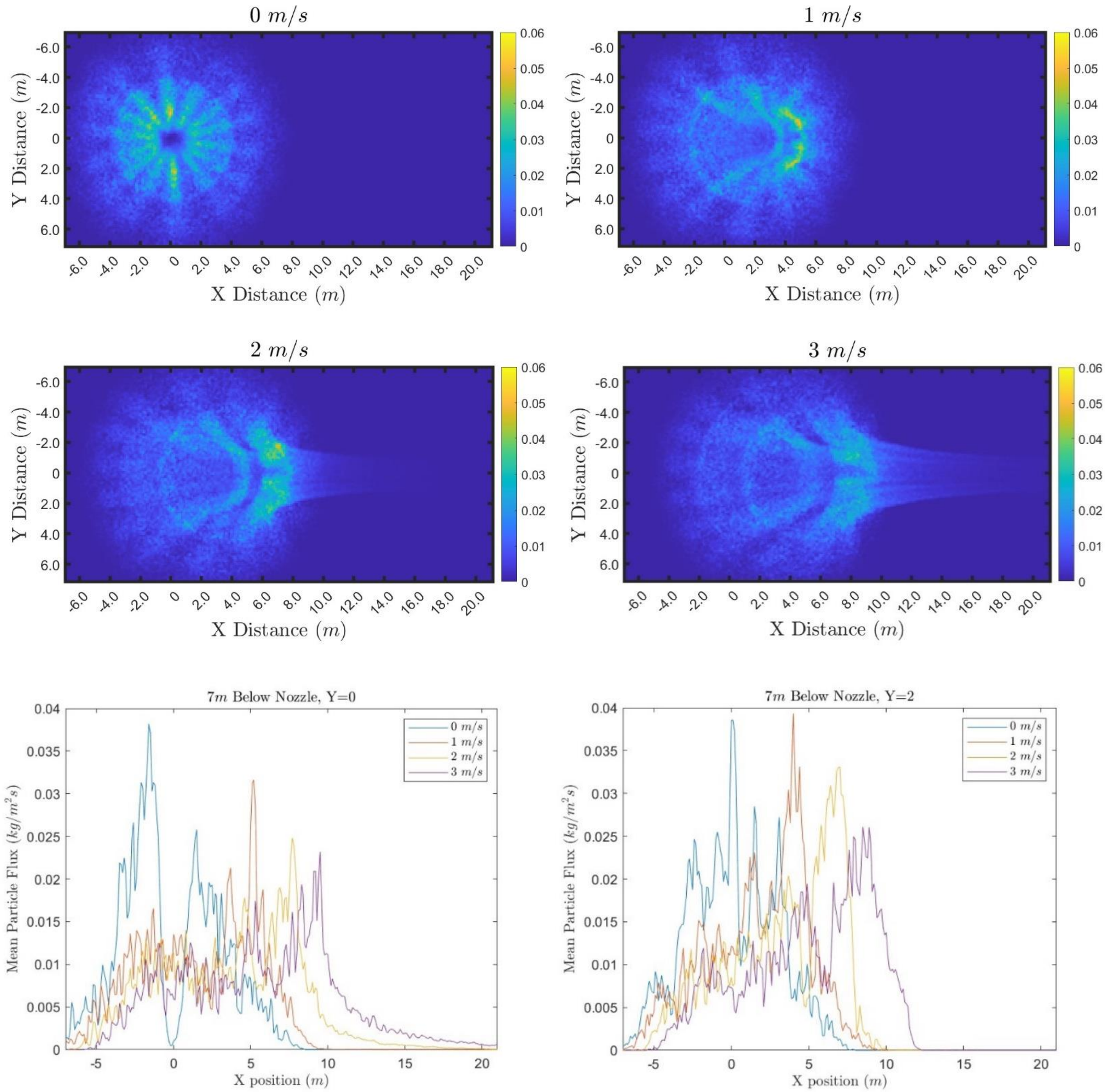

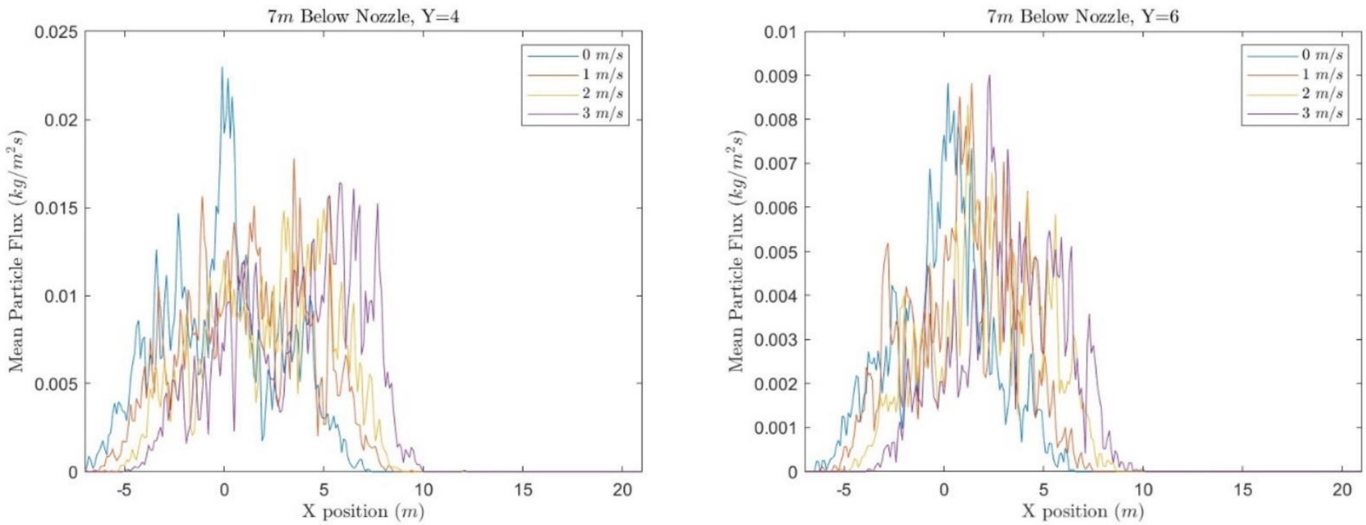

Figure 4-5: Crossflow Analysis 7 m Below Nozzle

In summary, at 1 m below the nozzle, all crossflows have little effect on the magnitude and shape of the distribution of the particle flux. At 4 m below the nozzle, strong azimuthal features developed by larger particles remain, however substantial changes in magnitude and shape of the distribution can be seen due to smaller particles. At 7 m below the nozzle, strong azimuthal features are no longer significant, and the overall shape and magnitude of the distribution is largely affected.

4.3 4S and Basic Nozzle Comparison

Next the basic nozzle was simulated in the domain at the same magnitudes of crossflow for comparison with the 4S nozzle. The effect of the crossflow is the greatest at 3 m/s velocity, 7 m below the nozzle as seen in Figure 4-6. Just like in quiescent air, the basic nozzle delivers more water closer to the center of the sprinkler and the 4S nozzle delivers more water farther from the center. The overall shape of the distribution is still smoother in the basic nozzle than the 4S. All Y slices can be seen in Appendix F.

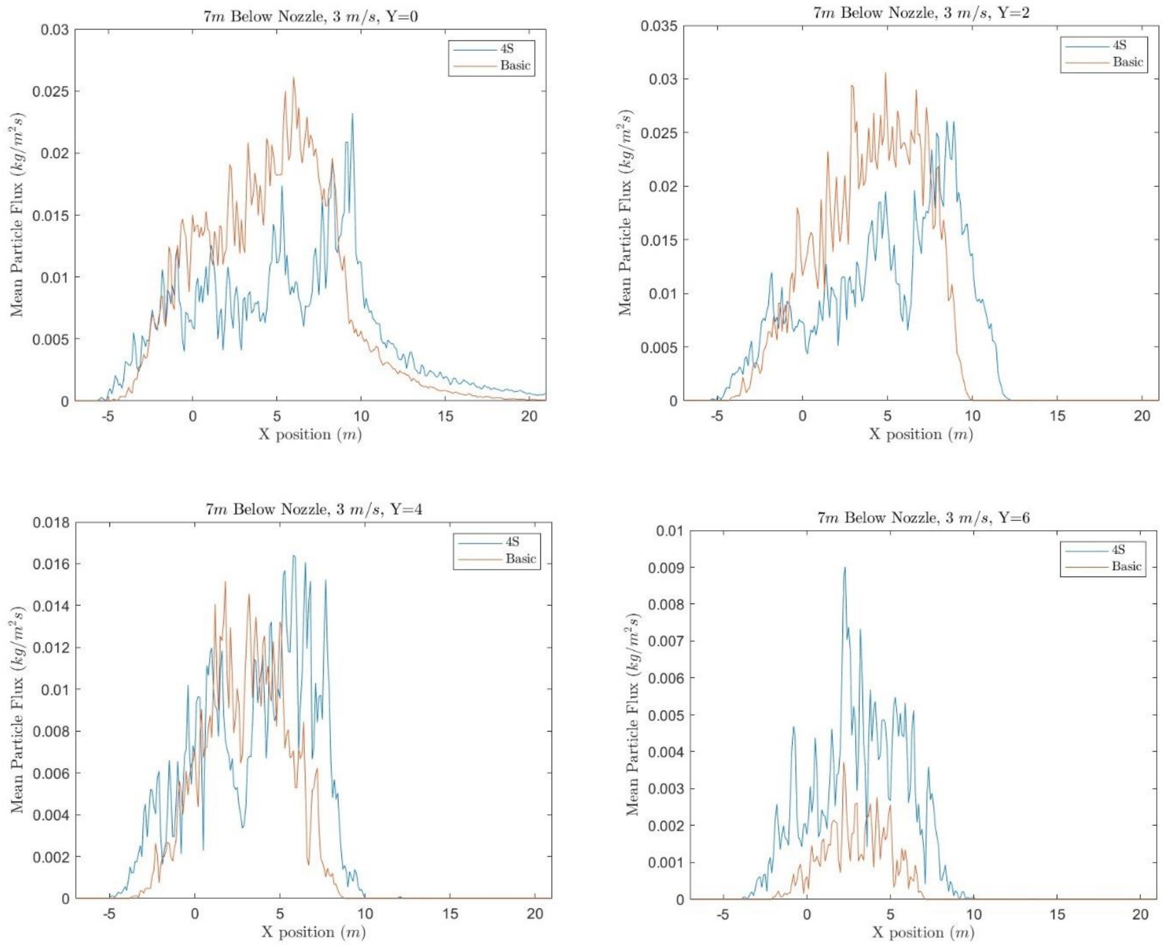

Figure 4-6: 4S vs Basic Nozzle Crossflow Comparison

Chapter 5 : Enclosure Fire Model

5.1 Model Set Up

A small enclosure fire experiment with sprinkler activation was modeled after an experiment performed by Khoat, et al [21]. Following the experiment, Khoat used data gathered to create and validate a CFD model of the enclosure fire for use in an analysis of spray and plume interactions. The same steps to build and validate the fire model are followed in this study, after which the model will be used to gather quantitative data on the 4S and basic nozzles.

The room construction is a simple rectangular box 7 m x 3 m x 3 m with two doorways. The fire source consists of a wood crib and two vertical polyurethane boards attached to support structures. In the ceiling there was a K 4.8 sprinkler and two K-type thermocouples to measure the temperatures used to calibrate the FDS model. Details of specific set up, equipment, and materials can be read in the report. All dimensions can be seen in Figure 5-1 below, as well as an outside view of the test [21].

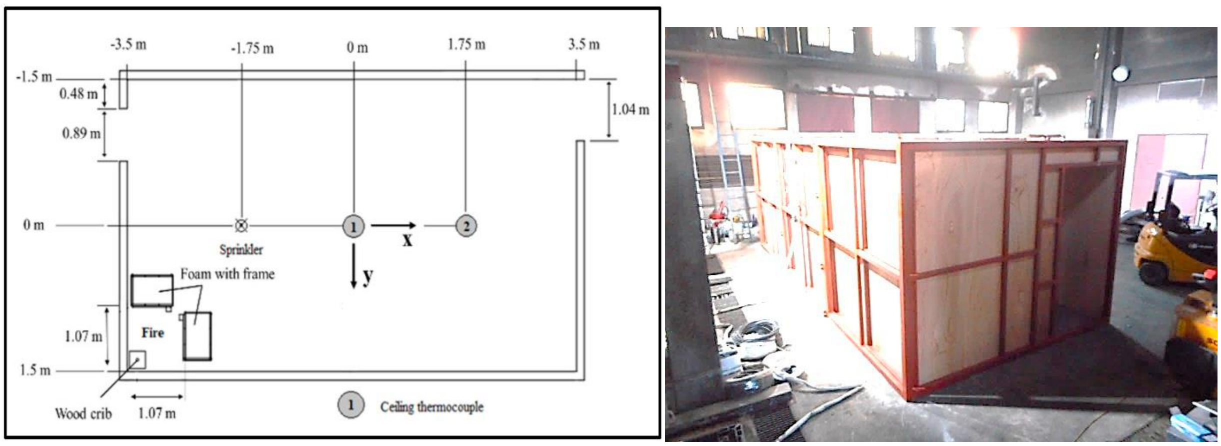

Figure 5-1: Enclosure Fire Set Up [21]

The wood crib measured 305 mm x 305 mm x 152 mm and each foam board measured 810 mm x 760 mm x 76 mm. The foam boards were supported vertically by a metal support structure with plywood backing. The HRR of each object was measured separately using a large-scale calorimeter under ISO 13784 through oxygen consumption calorimetry. The calorimetry experiment set up and resulting HRR curves can be seen in Figure 5-2 [21].

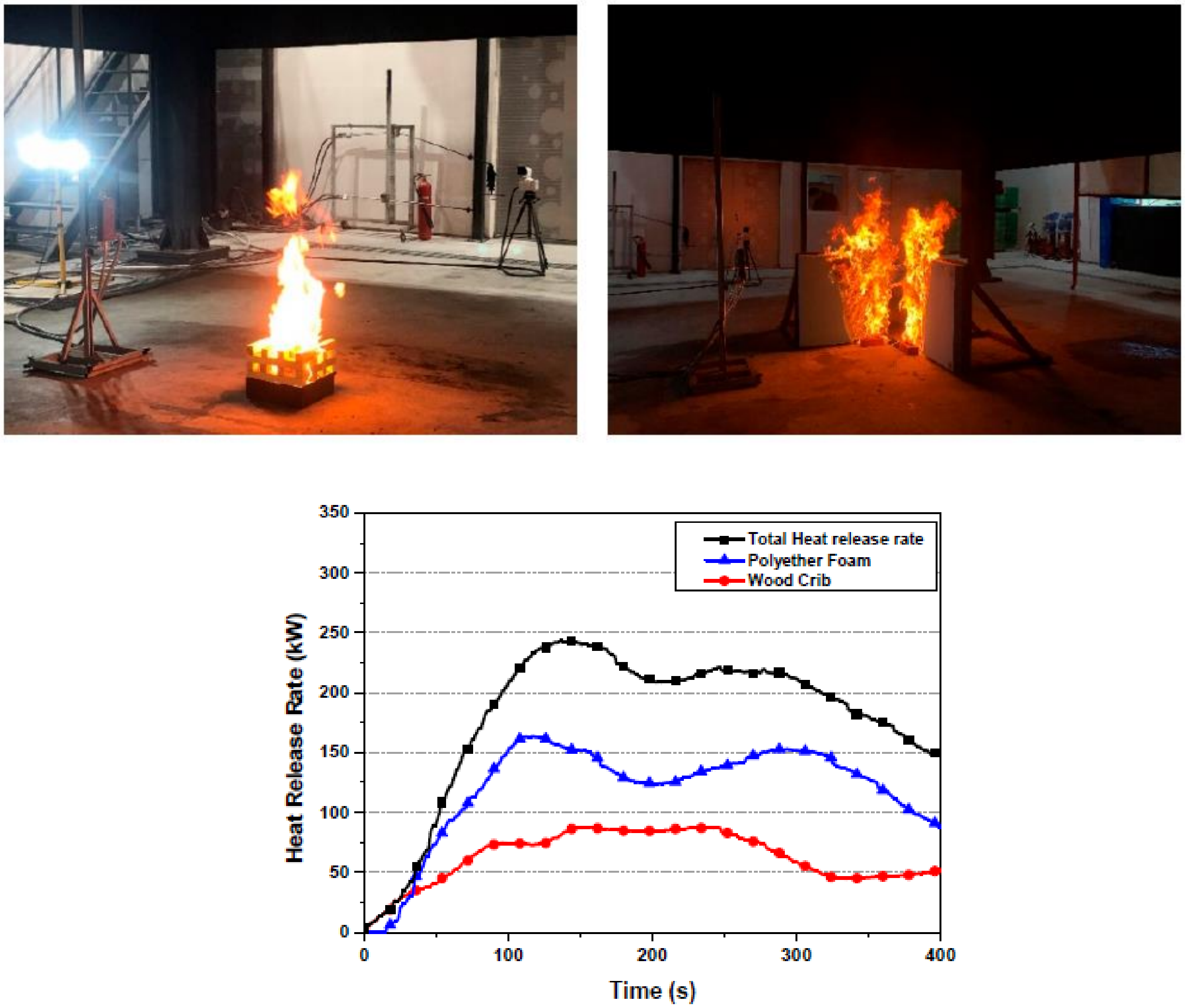

Figure 5-2: Cone Calorimetry and HRR Curves [21]

In building the FDS model, a simple pyrolysis model utilizing a gas burner with a specified HRR was used. This pyrolysis model is appropriate when modeling a fire of a known HRR [12]. The maximum HRR was specified per unit area for each individual object by the input HRRPUA in units of kW/m^2, and was varied in time through the RAMP_Q function to match the unsteady values from cone calorimetry data. The burner for the wood crib was prescribed as the top surface, and for the foam boards was the vertical surfaces facing negative Y and negative X.

Other details of the experimental domain expressed in the study are as follows. Ambient temperature was 29 degrees C. The floor, walls, and ceilings of the compartment were concrete, plywood, and gypsum board respectively. For the FDS simulation, the floor and walls were ADIABATIC. Grid analysis was conducted by Khoat without sprinkler activation as seen in Figure 5-3 and a grid size of 10 cm was selected [21].

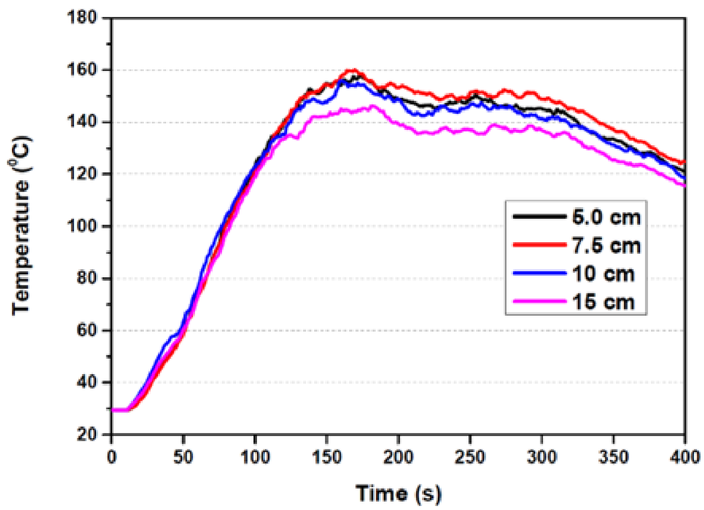

Figure 5-3: Enclosure Fire Grid Convergence [21]

Some details not discussed in the report that had to be estimated were as follows. There was no mention of the ceiling, so it was set to half inch thick gypsum. There was no mention of humidity so 40% was used in this FDS study. In order to match the thermocouple data, thermocouples were modeled in FDS with the built in thermocouple device with a 1 mm bead and emissivity of 0.9.

In the simple pyrolysis model used, water accumulating on the burner results in a reduction of burning rate based on the mass of water per unit area on the burner. To calibrate this extinguishing method, a parameter called the extinguishing coefficient (Alpha) must be specified that reduces the mass lot rate of fuel through an exponential function seen in equation 11. This coefficient must be experimentally obtained. $m"_w(t)$ is the mass of water per unit area on the burner, and $\dot{m}"_{f,0}(t)$ is the specified burning rate, in this case given by the heat release rate curves.

$$\dot{m}"_f(t) = \dot{m}"_{f,0}(t)e^{-\int E\_COEFFICIENT\ m"_w(t)\ dt} \qquad \text{(Eq. 11)}$$

For water impinging on the wood crib, the water can spray directly on the top surface of the wood and this mass is used to reduce the burning rate as above. For the foam boards however, the burning surfaces are vertical and oriented away from the sprinkler so that normal trajectory will not allow the droplets to land directly on the burner. One way particles could land on the vertical surface is through turbulence of the fire, although particles affected most by turbulence are small particles. The other way is through FDS's model of droplet movement on solid surfaces. In this model when a droplet hits a solid surface it sticks to it and is reassigned a new velocity and direction. In the case of the horizontal top of the foam board, this direction is random with a horizontal velocity of 0.2 m/s. Once the droplet reaches the edge of the horizontal surface it will transition to the vertical face with a downward velocity of 0.5 m/s. This water on the vertical surface of the burner would then affect heat release rate reduction in the extinguishment model.

The sprinkler in the experimental set up was 76 mm below the ceiling. It was a K 4.8 with a 68 degree C activation temperature. Operational pressure was 1 bar. FDS sprinkler parameters were estimated in the study and can be seen in Table 5. These sprinkler parameters were used for the validation of this model.

Table 5: Enclosure Fire Sprinkler Spray Parameters [21]

Sprinkler Parameter	Value
Flow rate	50 L/min
Velocity	6.01 m/s
Droplet size	954 μm
Atomization distance	0.2 m
Angles	10–80°
Activation temperature	68 °C

RTI of the sprinkler was not mentioned in the report, so it was varied until activation time of 70 seconds was achieved with an RTI of 75. The front wall of the room was set to transparent for visualization purposes. Full input code can be seen in Appendix D.

5.2 Validation

Validation was based on the experimental ceiling temperature measurements seen in Figure 5-4. To calibrate the extinguishing model, the extinguishing coefficient (Alpha) was varied from 1 to 3 in separate simulations with the resulting ceiling temperatures plotted against experimental data in Figure 5-5. All values of the extinguishing coefficient matched prior to activation. After activation, Alpha = 1 matched from 70 s to 150 seconds but diverged after that. Alpha = 2 was close from 200 to 350 seconds. Alpha = 3 was consistently lower. Alpha = 1.5 provided a good balance throughout the entire simulation and was selected.

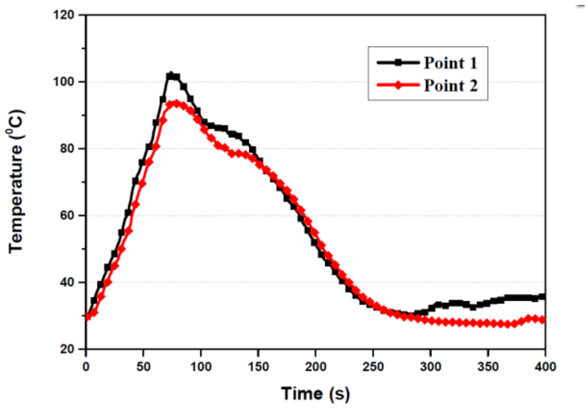

Figure 5-4: Experimental Ceiling Temperatures at Point 1 and Point 2 [21]

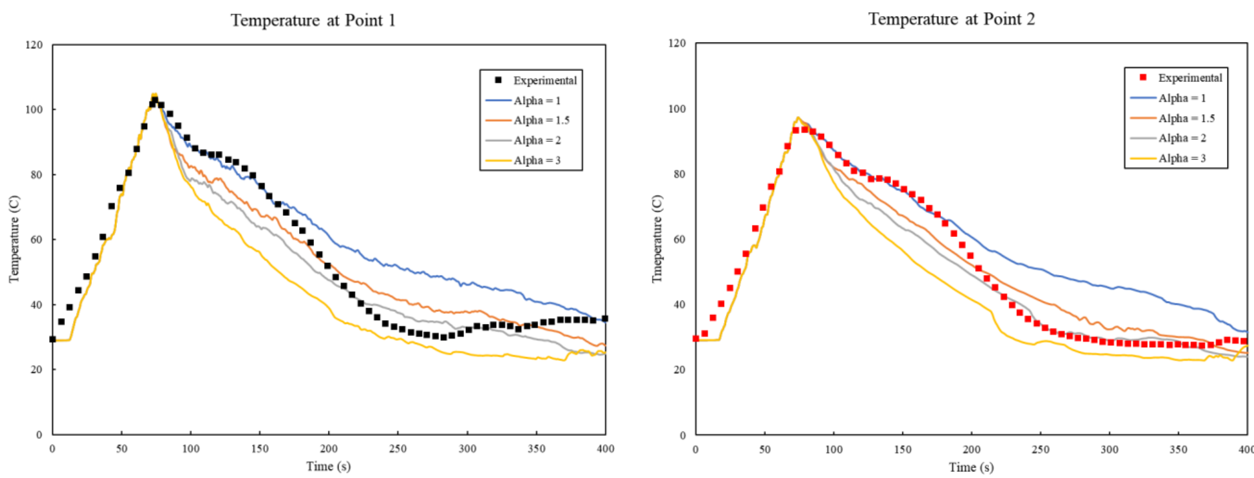

Figure 5-5: Validation Ceiling Temperatures vs. Extinguishing Coefficient

5.3 Experimental Results

With the validation of the FDS simulation and the selection of the extinguishing coefficient complete, the 4S and basic nozzle were tested to quantify the trends observed in previous chapters. All simulation parameters remained the same as the validation case with the exception of the nozzle characterizations. Additionally, a device was added to measure the total accumulated water over time on the surface of each the burner. Smokeview display of the simulation with the 4S nozzle characterization can be seen in Figure 5-6.

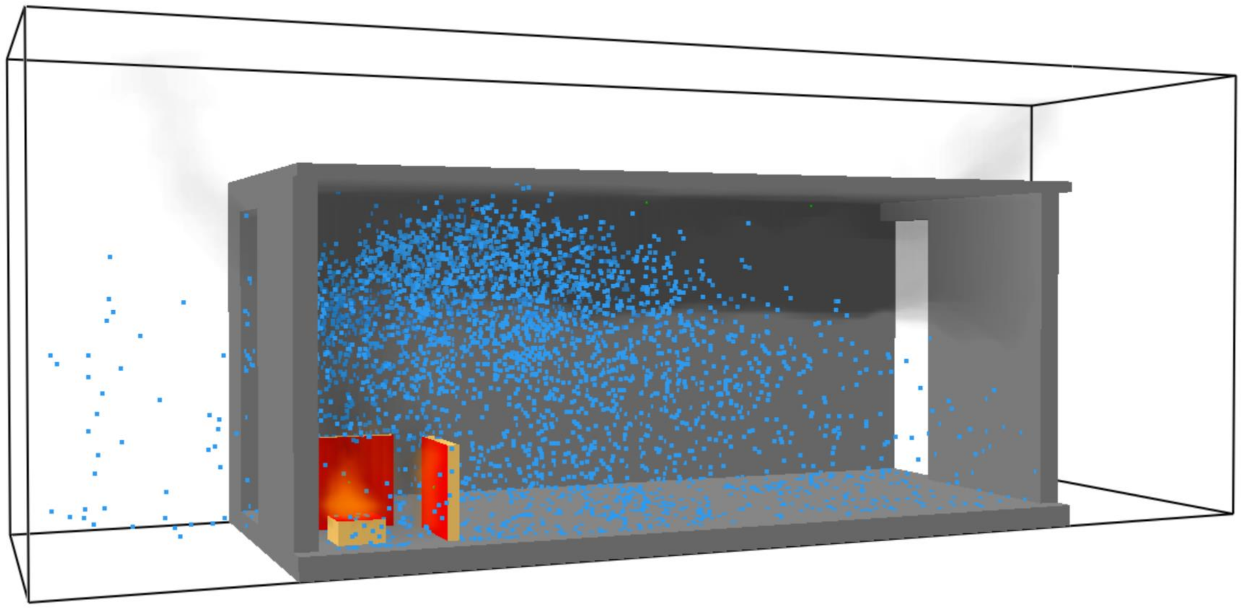

Figure 5-6: FDS Simulation with 4S Nozzle Characteristics of K5.6 at 14 psi

The 4S and basic nozzles were run separately, and the accumulated water on the burner surfaces were plotted against each other in Figure 5-7 along with the resulting total HRR and ceiling temperature. From sprinkler activation to 400 seconds, a total of around 310 seconds, the wood crib accumulated 1.8 kg of water for the 4S nozzle and 2 kg of water for the basic nozzle. The back foam accumulated 0.95 kg of water for the 4S nozzle and 0.9 kg of water for the basic nozzle. The right foam board accumulated 0.75 kg of water for the 4S nozzle and 0.95 kg of water for the basic nozzle. These differences correspond to a 10%, -3%, and 23% difference respectively between the 4S nozzle and the basic nozzle. The effect of this difference in water on the total HRR throughout the simulation was less than 10 kW and the difference in ceiling temperature is almost negligible.

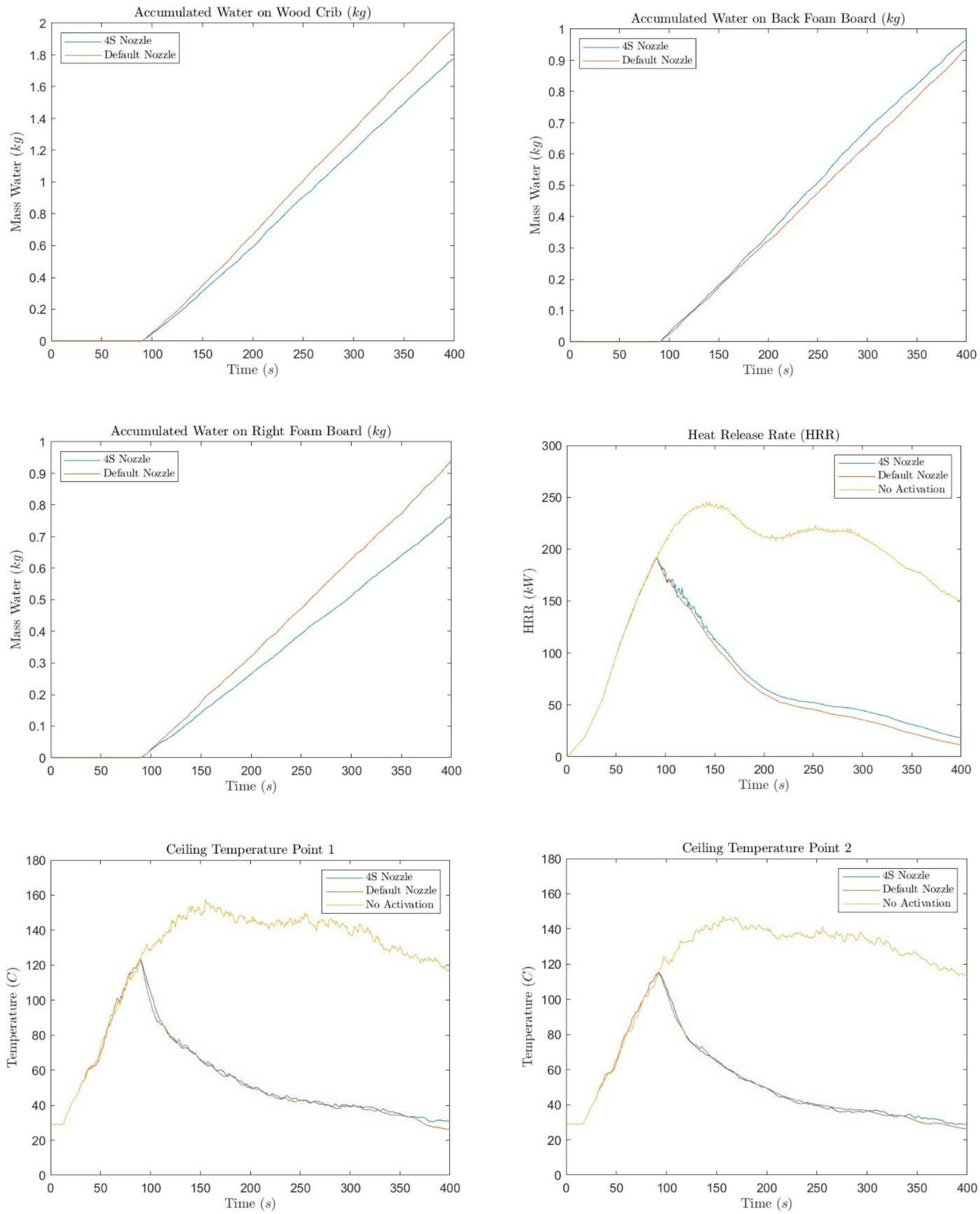

Figure 5-7: Enclosure Fire 4S vs Basic Nozzle

To understand these results, the relation from the burners to the center of the sprinkler was analyzed and compared to data from the quiescent bucket test in Chapter 3. Although the quiescent bucket test results do not include the effects of room geometry or turbulence, they provide a good reference to compare results. The center of the wood crib was 1.75 m from the center of the sprinkler, with the burner surface 2.6 m below the sprinkler. The radial flux distribution at a distance of 3 m below the nozzle from a quiescent bucket test was plotted in Figure 5-8. The average radial particle flux predicts more water flux delivered by the basic nozzle than the 4S at radial distances less than 3 m from the center of the spray. This is consistent with the results of the enclosure fire with exception of the back foam board that the 4S had 3% more flux than the basic nozzle. The 3% difference could possibly be caused by plume spray interactions, room geometry, or azimuthal features of the 4S spray and will be investigated further in Chapter 6.

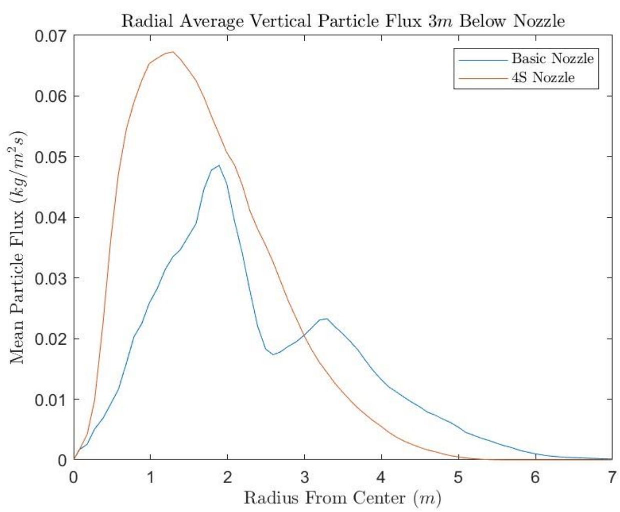

Figure 5-8: 4S and Basic Average Radial Particle Flux 3 m Below Nozzle

This result however only presents the differences between the 4S and basic nozzle at one radial distance. As the differences between the 4S and basic nozzle are larger at different radial distances, the sprinkler was moved to five other positions with different radial distances ranging from 1.1 m to 5.2 m from the center of the wood crib. Position B is the original placement discussed above and all positions can be seen in Figure 5-9.

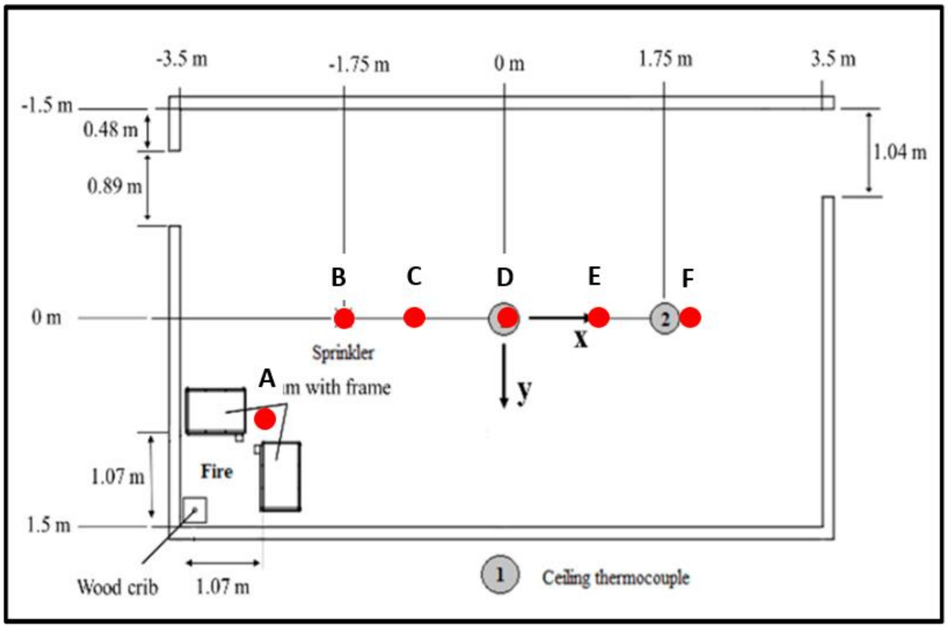

Figure 5-9. Enclosure Fire Positions of Sprinklers

At each of these positions, the same fire scenario was run with both the 4S and basic nozzles as before. Individual graphs of accumulated water per burner, HRR, and ceiling temperatures can be seen for each position in Appendix G. Differences between the nozzles at each position were calculated as percent increase or decrease from the 4S nozzle to the basic nozzle and presented in Table 6 along with the mass of accumulated water. A positive number means that the basic nozzle delivered more water mass and a negative number indicates the 4S nozzle delivered more water mass.

Table 6: Accumulated Water 4S vs Basic Nozzle Comparison

Position	Radial Distance (m)	Wood Crib			Back Foam Board			Righ Foam Board		
		4S (kg)	Basic (kg)	% Change	4S (kg)	Basic (kg)	% Change	4S (kg)	Basic (kg)	% Change
A	1.1	0.86	1.95	127	0.32	1.10	240	0.73	1.10	50
B	1.75	1.78	1.97	10	0.97	0.93	-3	0.76	0.94	23
C	2.4	1.35	1.57	16	0.58	0.70	19	0.78	0.79	1
D	3.3	0.98	0.89	-9	0.73	0.35	-52	0.69	0.47	-31
E	4.2	0.41	0.35	-16	0.15	0.13	-16	0.29	0.20	-31
F	5.2	0.08	0.11	44	0.02	0.04	79	0.06	0.08	23

Position A had the largest differences between the nozzles, and with the resulting HRR and Ceiling Temperature curves showing significant differences as seen in Figure 5-10.

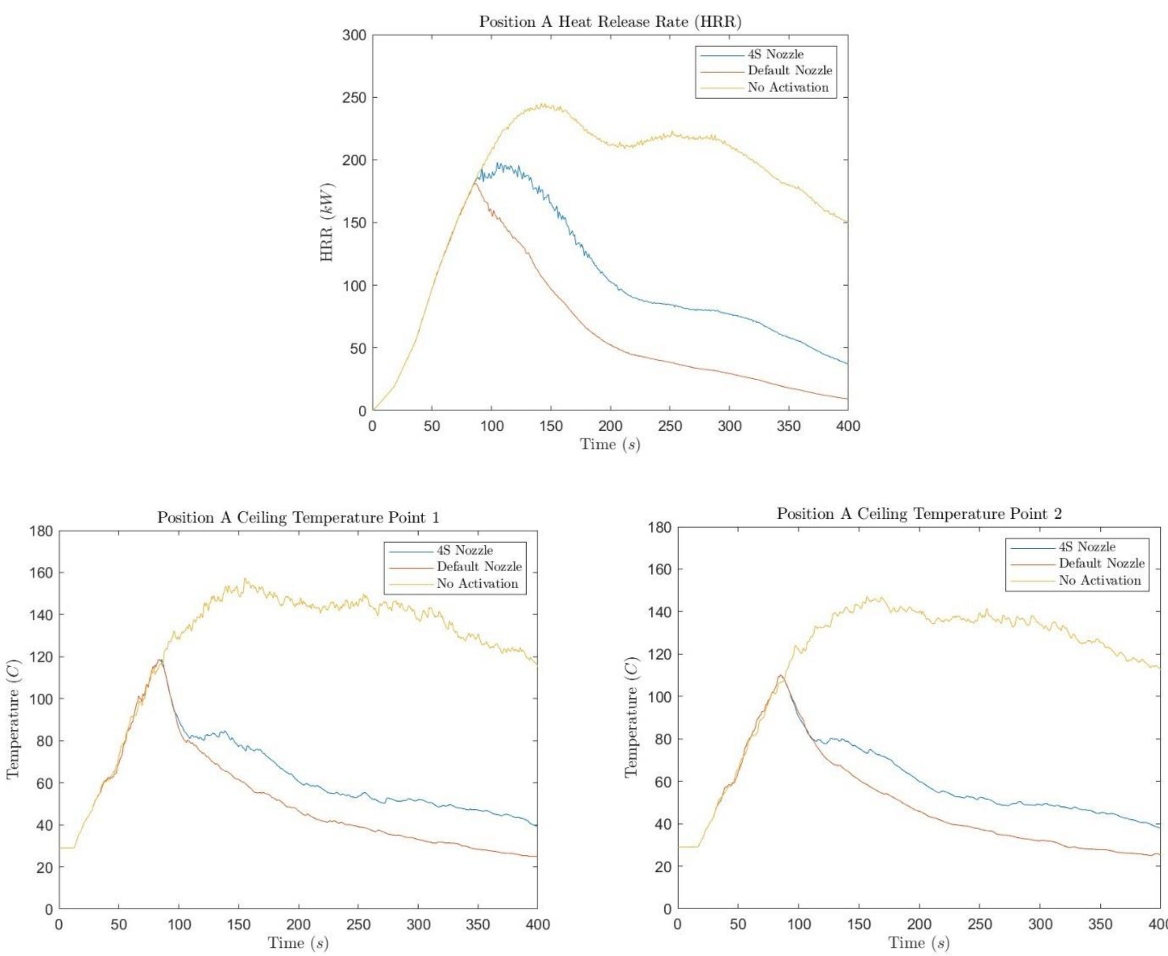

Figure 5-10: Position A HRR and Ceiling Temperature

As the average radial particle flux distribution predicts, at distances less than 3 m from the center of the nozzle the basic nozzle provides more water except for the Back Foam board at position B discussed previously. At distances greater than 3 m the 4S provides more water flux as predicted except for position F.

To understand the differences at position F, the mean particle flux distribution at 3 m below the nozzle from the quiescent bucket test was plotted and scale adjusted to show variation of lower particle fluxes around the edges of the spray in Figure 5-11. The outer edges of spray are elongated about the Y axis, creating an elliptical shape. Unlike strong local azimuthal concentrations seen previously, this indicates a more global azimuthal trend. As the sprinkler in Position F is at the edge of this ellipse along the negative X axis, this explains the difference.

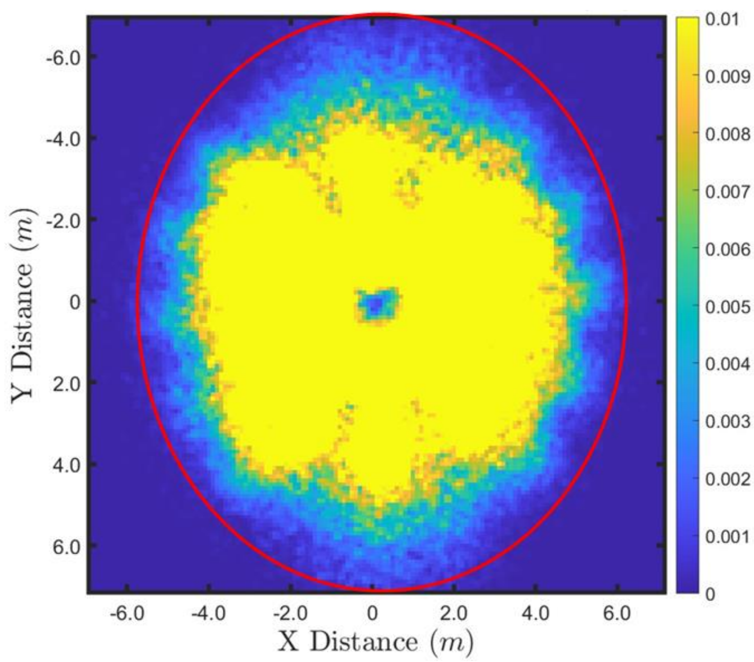

Figure 5-11: 4S Mean Particle Flux Distribution 3 m Below Nozzle, Scaled

Additionally, as discussed previously the particle flux at position F was an order of lower than the other positions and small changes could have larger effects.

In general, the radial water flux distribution was the best predictor of the differences between the nozzles. Local azimuthal differences did not play a large role in the quantitative results however a global azimuthal trend effected the farthest position.

After the 4S and basic nozzle were compared, the 4S nozzle was run at all positions without fire to analyze the effect of the turbulence created by the fire on the accumulated water. This data was compared to the accumulated water on burner surfaces with the prescribed fire. The percentage increase or decrease from the no fire to the fire scenario was calculated for each position and results presented in Table 7 along with the mass of accumulated water on each burner. Plots showing accumulated water over time on burner surfaces can be seen in Appendix H.

Table 7: Accumulated Water of Enclosure Fire 4S Nozzle, Fire vs. No Fire

Position	Radial Distance (m)	Wood Crib			Back Foam Board			Righ Foam Board		
		No Fire (kg)	Fire (kg)	% Change	No Fire (kg)	Fire (kg)	% Change	No Fire (kg)	Fire (kg)	% Change
A	1.1	1.01	0.86	-15	0.43	0.32	-24	0.78	0.73	-6
B	1.75	1.60	1.78	11	1.05	0.97	-8	0.94	0.76	-19
C	2.4	1.10	1.35	23	0.62	0.58	-6	0.73	0.78	7
D	3.3	0.93	0.98	5	0.74	0.73	-1	0.70	0.69	-2
E	4.2	0.42	0.41	-3	0.15	0.15	0	0.30	0.29	-1
F	5.2	0.07	0.08	7	0.02	0.02	32	0.07	0.06	-8

In general, larger differences occur at lesser radius where small particles are present in the spray. Positions A, B, and C all range from 6 to 24 percent difference. Positions D and E where larger particles are present range only range from 3 to 7 percent different. This reinforces what was seen in the crosswind analysis that the areas of the spray where larger particles are present resist crosswind, or turbulence more than the areas with smaller particles. Position F, however, has a 32 percent difference, possibly from turbulence associated with the fire plume or room geometry. Additionally, the lower particle flux at this location could be amplifying a small effect.

Chapter 6 : Parameter Comparison

Now that the differences between the 4S and basic nozzle have been quantified and shown to be significant, it is important to identify which of the particular aspects of the 4S nozzle characterization was the most impactful on the results in this case. In order to do that, the characteristics of the basic nozzle were manipulated one at a time to match those of the 4S nozzle, keeping all other parameters that of the basic nozzle. The quiescent bucket test simulation was used as the framework for these tests and all specifics remain the same as Section 3.1 with the exception of the parameters discussed below. Since the average radial particle flux distribution was shown to be a good indicator of performance of the different nozzles, the radial profiles will be analyzed to determine effect of the manipulation.

In the first test, the droplet diameter distribution was changed to include DIAMETER and GAMMA_D, with all other characteristics and parameters remaining constant to the basic nozzle. The diameter was changed from the estimated 954 μm to the 4S measured 967 μm and distribution parameter changed from FDS default 2.4 to the 4S measured 2.07. In the second test, an average particle velocity from the 4S nozzle spray table was calculated to be 12.60 m/s and utilized in the basic nozzle compared to the calculated 12.47 m/s. The third and fourth tests manipulate the polar angle distribution of water flux. By averaging the 360 azimuthal water flux segments from the 4S nozzle spray table at each polar angle, one average flux was calculated for each polar angle, seen in Figure 6-1. The third test takes these averaged values and uses them in an 11 line spray table to prescribe a spray pattern that is uniform in azimuthal angle but varies with polar angle. The fourth test simplifies this polar angle distribution one step further and prescribes a uniform distribution of particle flux within the spray angles of 35 to 85 degrees where the maximum flux occurs.

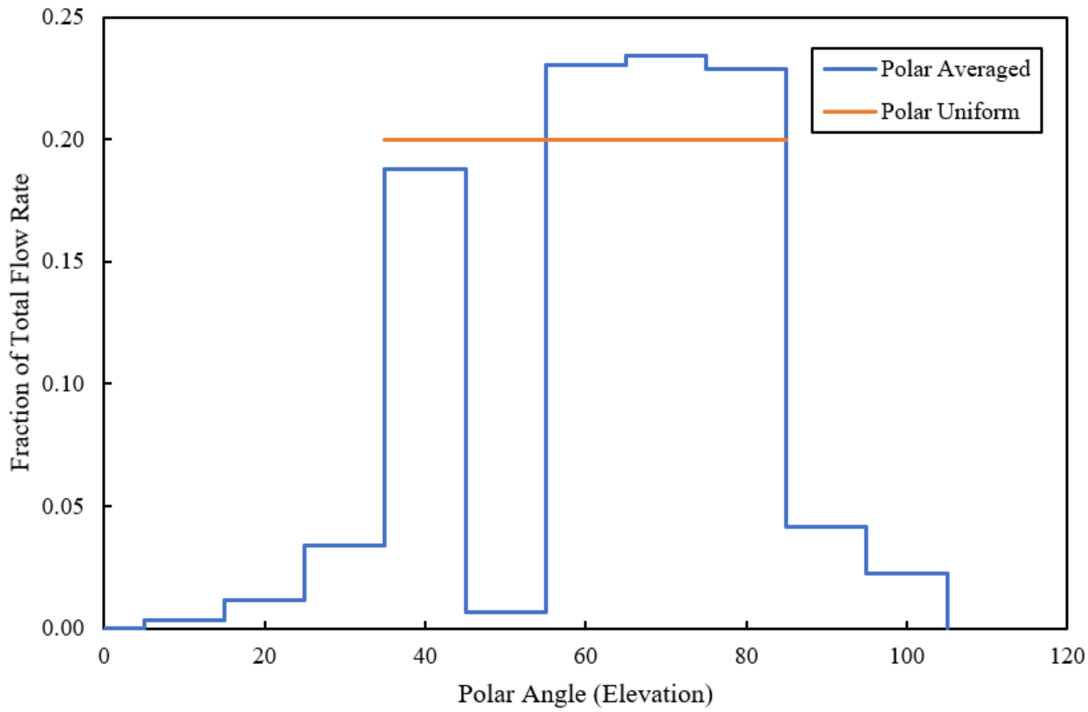

Figure 6-1: 4S Nozzle Polar Water Flux Distribution

The average radial particle flux distributions from these four tests along with the 4S and basic nozzles were plotted for comparison in Figure 6-2. Neither changing the droplet diameter and distribution parameter nor the particle velocity had substantial changes. This is likely because estimations were close to measured values. Changing both the polar averaged and uniform distribution greatly increased the similarity to the 4S nozzle.

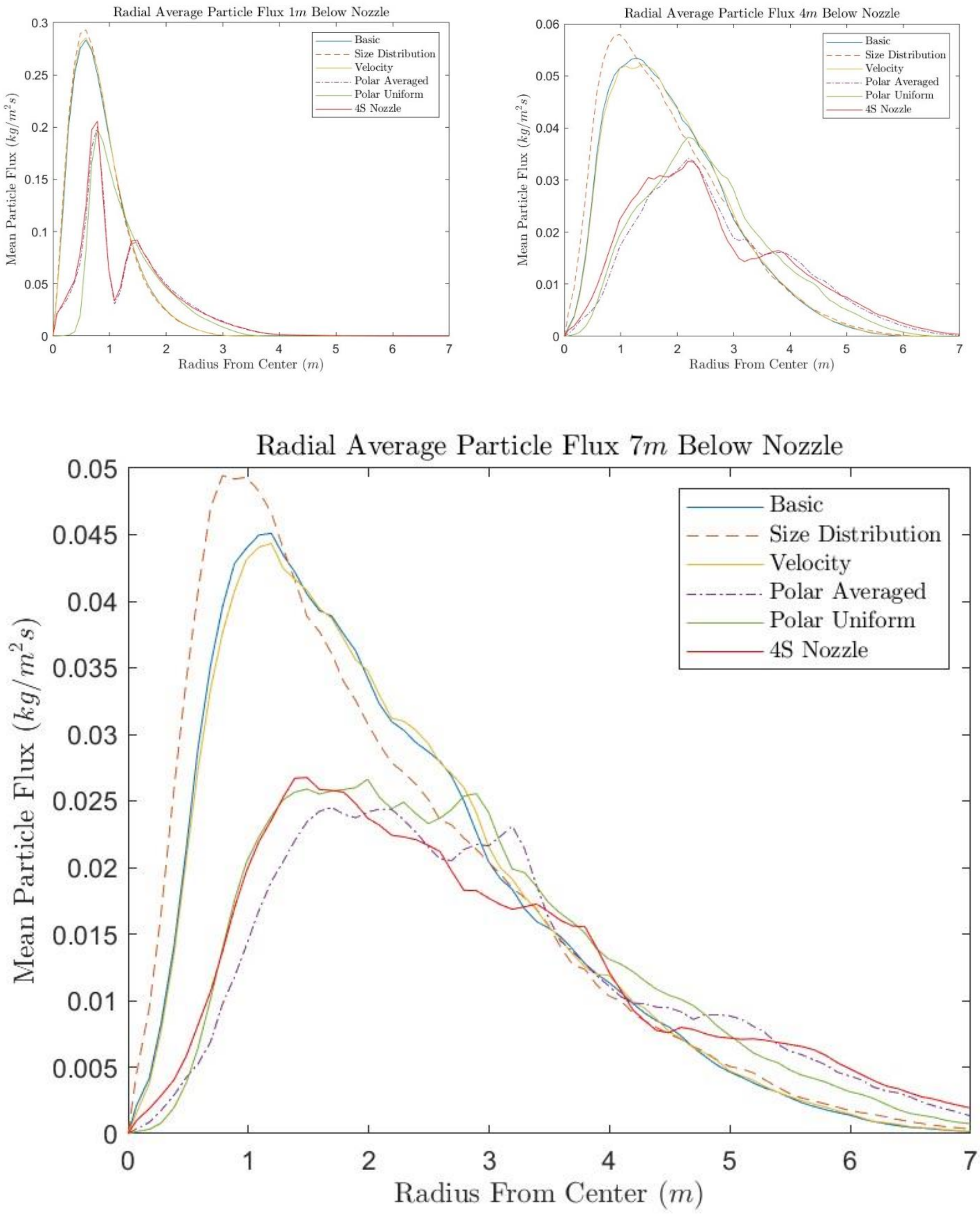

Figure 6-2: Parameter Comparison, Radial Water Flux Distributions

At 1 m below the nozzle, the Polar Averaged test matched the 4S nozzle almost exactly, where the Polar Uniform distribution test deviated less than 0.5 m from center and between 1 m and 1.5 m from center. At 4 m and 7 m below the nozzle, both the Polar Averaged and Polar Uniform curves match the 4S curve reasonably with minimal differences. Since changing the polar water distribution had the largest effect on the basic nozzle, this polar water distribution was the most important input parameter provided by the 4S when compared to estimations from literature.

To investigate the effect of local azimuthal variations on the spray, the enclosure fire model was utilized with the prescribed burner HRR and the 4S sprinkler was rotated a number of degrees between tests. Looking at the mean particle flux distribution map 3 m below the nozzle in Figure 6-3, the largest local azimuthal variation appears between 0.5 m and 2 m from the nozzle, so Position B was selected with the wood crib 1.75 m from the center of the nozzle. The foam boards are both approximately 1.2 m away from the center of the nozzle.

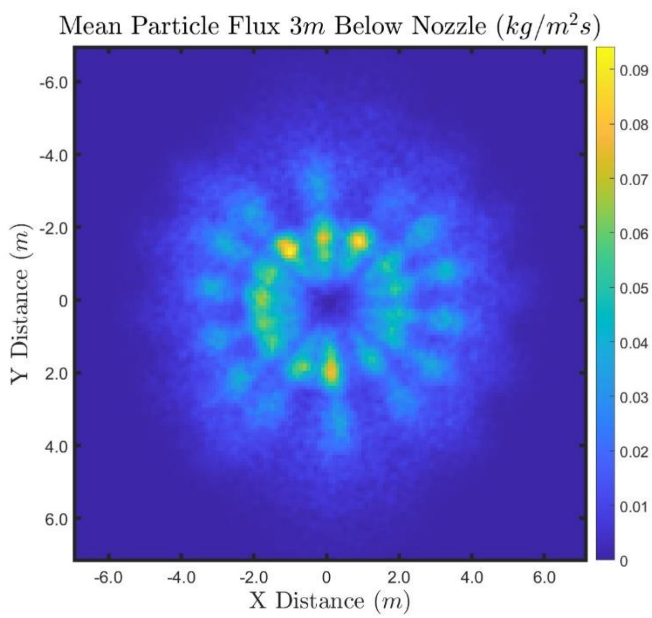

Figure 6-3: 4S Nozzle Mean Particle Flux Distribution 3 m Below Nozzle

A MATLAB script was utilized to rotate the spray within the spray table by 5, 12.5, 30, 50 and 90 degrees from the standard, or 0 degree position. Each simulation was run with the fire and the total accumulated water along with the percent difference from 0 degrees rotation was calculated and presented in Table 8.

Table 8: Azimuthal Enclosure Fire Test Accumulated Water

Rotation	Wood		Back Foam		Right Foam	
	kg	% Difference	kg	% Difference	kg	% Difference
0	1.78	0	0.97	0	0.76	0
5	1.83	3	1.08	11	1.00	31
12.5	2.55	43	1.27	31	1.18	54
30	2.82	58	1.08	12	0.54	-30
50	2.97	67	0.99	2	0.82	7
90	1.33	-25	0.90	-7	0.86	13

Azimuthal features created substantial differences in accumulated water, with percentage differences ranged up to 67%, however they did not have a large effect on overall HRR and Ceiling Temperatures seen in Appendix I. Figure 6-4 shows the 12.5-degree rotation which had the largest impact on HRR of and ceiling temperatures, however the differences are not significant. The Azimuthal differences are strong enough to explain the previous variation where the Basic vs 4S enclosure fire data did not align with what the average radial particle flux distribution predicted.

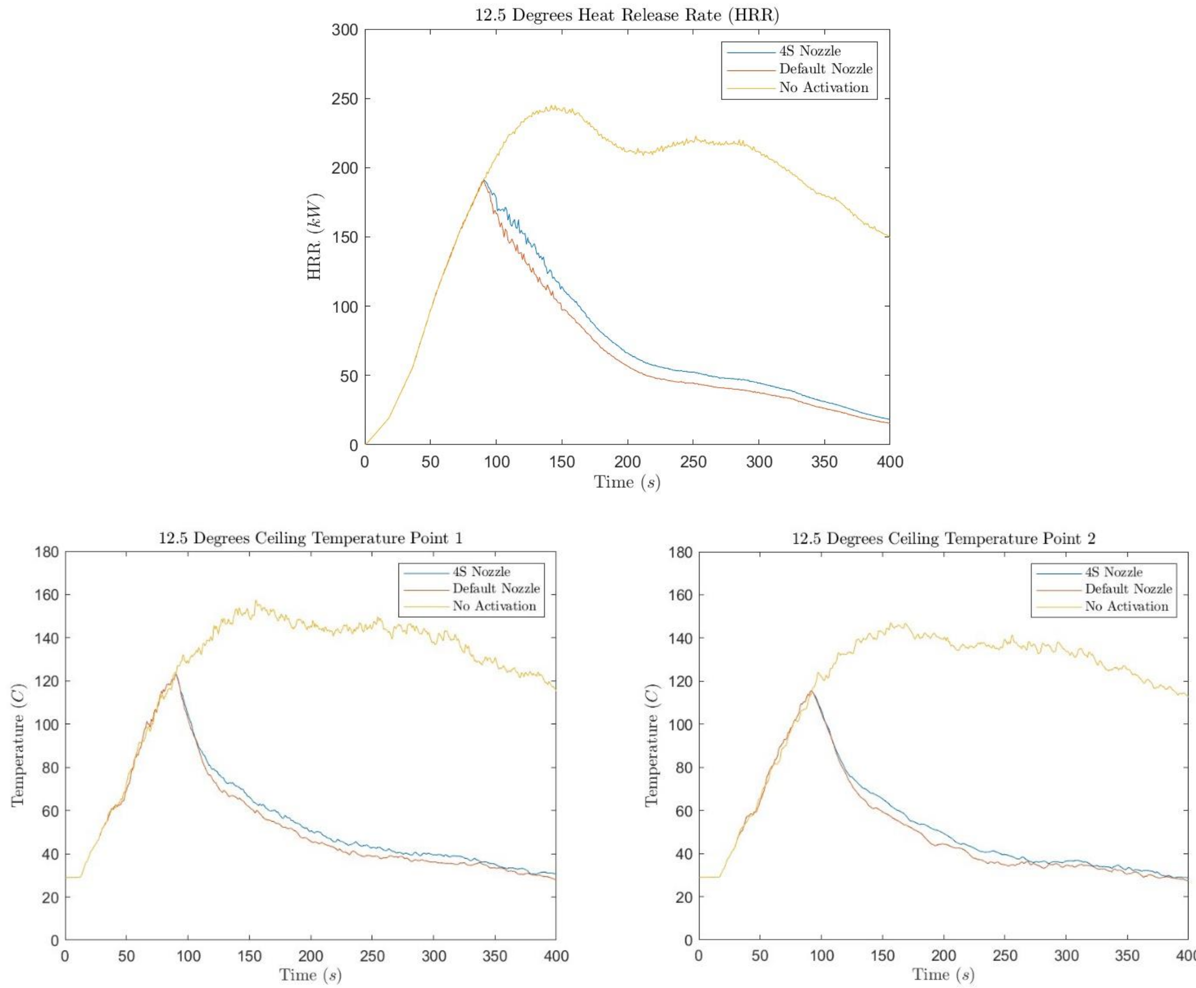

Figure 6-4: 12.5 Degree Rotation HRR and Ceiling Temperature

Chapter 7 : Conclusions and Future Work

While the 4S and basic nozzles both deliver the same flow rate of water to a similar footprint, there are substantial differences in the mass of water delivered to specific locations. Within the enclosure fire scenario, the accumulated water on the surface of the burner varied up to 240% between the 4S and basic nozzles, with noticeable effect on the overall HRR and ceiling temperatures. These differences in performance can be predicted with reasonable accuracy by the average radial water flux distribution of each nozzle. Of the data provided by the 4S, the polar water distribution was the most impactful parameter in the difference between the 4S and basic nozzle noted in the enclosure fire scenario. Local azimuthal variations within the 4S spray, while accounting for up to a 67% difference in accumulated water, did not lead to significant differences in the HRR rates and ceiling temperatures of the enclosure fire. Global azimuthal distributions led to a 79 percent change in water accumulated, but the with a water flux that impacted the overall HRR and ceiling temperatures less than local azimuthal variations.

Varying sizes of particles within the spray affected the spray with increasing crosswind and turbulence in the enclosure fire. Where larger particles were present in the 4S spray, the overall shape and magnitude of the water flux distribution resisted the airflow. The areas of the 4S spray where smaller particles were present showed changing shape and magnitude of particle flux distribution. Local azimuthal variations were lost in the crosswind bucket test by 7 m below the nozzle. Within the enclosure fire, the fire plume and turbulence caused by room geometry confirmed these findings.

There are two large limitations of this study, the first being that only one combination of 4S nozzle and estimated parameters was studied. In this combination the particle diameter, diameter distribution parameter, and particle velocity estimations were very close to 4S measurements. That might not always be the case and the effect of these parameters on the overall spray performance was not addressed in this study. Future work should include testing multiple sprinklers and the same sprinkler at multiple pressures to ensure universality of conclusions in this study. Additionally, fire scenarios where multiple sprinklers are activated should be tested.

The second large limitation of this study was that only one fire simulation was analyzed. While the situation was realistic, it presented one room geometry, one distance below the nozzle of burner surface, one FDS model of extinguishment, one burner size, one prescribed HRR. All of these factors affect the interaction between a sprinkler spray and a fire and could impact results. For example, an ESFR sprinkler in a storage facility could see much higher HRR where large plume velocities are developed and the most important factor in extinguishment could be water drop size and velocity as the droplets must have momentum to penetrate the plume and reach burning surfaces. Additionally, a larger fire or burner surface relative to the spray area of the sprinkler might be less susceptible to local azimuthal changes or radial changes. The pyrolysis model utilizing the extinguishing coefficient saw large differences in accumulated water flux that had little effect on the HRR, and in other models, a 70% increase in water flux might have a larger effect. Future work should include testing multiple configurations, fire sizes, and pyrolysis models.

Appendix A: 4S Nozzle Characterization

```
&PART ID='water drops',
        WATER=.TRUE.,
        QUANTITIES(1:3)=   'PARTICLE_DIAMETER',
                 'PARTICLE_TEMPERATURE',
                 'PARTICLE_AGE',
         DIAMETER=967.148,
         GAMMA_D=2.07178,
         SAMPLING_FACTOR=1/

&PROP ID='K5.6',
        QUANTITY='SPRINKLER LINK TEMPERATURE',
        OFFSET=0.3,
        PARTICLES_PER_SECOND=5000,
        PART_ID='water drops',
        FLOW_RATE=94.8017,
        SPRAY_PATTERN_TABLE='table_k5.6',
        PARTICLE_VELOCITY=13.2858,
        SMOKEVIEW_ID='sprinkler_pendent'/

&SPEC ID='WATER VAPOR'/

&TABL ID='table_k5.6',TABLE_DATA=95,105,-0.5,0.5,12.3919,0.0000079280456038867 39/
&TABL ID='table_k5.6',TABLE_DATA=95,105,0.5,1.5,12.3919,0.000010807252882256 67/
&TABL ID='table_k5.6',TABLE_DATA=95,105,1.5,2.5,12.3919,0.000012421502253624 08/
&TABL ID='table_k5.6',TABLE_DATA=95,105,2.5,3.5,12.3919,0.000011548725320856 69/
…
```

(‘table_k5.6’ has 3600 lines of code total)

Appendix B: Basic Nozzle Characterization

```
&PART ID='water drops',
        SPEC_ID='WATER VAPOR',
        QUANTITIES(1:3)='PARTICLE DIAMETER','PARTICLE
TEMPERATURE','PARTICLE VELOCITY',
        DIAMETER=954,
        SAMPLING_FACTOR=1/

&PROP ID='K5.6_01',
        QUANTITY='SPRINKLER LINK TEMPERATURE',
        OFFSET=0.05,
        PARTICLES_PER_SECOND=10000,
        PART_ID='water drops',
        FLOW_RATE=94.79,
        SPRAY_ANGLE=10.,80.,
        ORIFICE_DIAMETER=0.0127,
        SMOKEVIEW_ID='sprinkler_pendent'/

&DEVC XYZ=0.0,0.0,7,
        PROP_ID='K5.6_01',
        ID='Spr_1',
```

Appendix C: Bucket Test Model w/ Basic Nozzle

```
&HEAD CHID='bt_k5o6_20psi' /

&MESH IJK=140,140,23, XB=-7,7,-7,7,0.0,2.3 / 10 cm grid.
&MESH IJK=140,140,23, XB=-7,7,-7,7,2.3,4.6 / 10 cm grid.
&MESH IJK=140,140,25, XB=-7,7,-7,7,4.6,7.1 / 10 cm grid.

//

&MISC SIMULATION_MODE='LES',
        HUMIDITY=100.,
        PARTICLE_CFL=T, /
&RADI RADIATION=F, /
&TIME T_END=70., /

// Vents

&VENT MB='XMIN', SURF_ID='OPEN' /
&VENT MB='XMAX', SURF_ID='OPEN' /
&VENT MB='YMIN', SURF_ID='OPEN' /
&VENT MB='YMAX', SURF_ID='OPEN' /
&VENT Mb='ZMIN', SURF_ID='OPEN' /

// Spray

&SPEC ID='WATER VAPOR'/

&PART ID='water drops',
        SPEC_ID='WATER VAPOR',
        QUANTITIES(1:3)='PARTICLE DIAMETER','PARTICLE TEMPERATURE','PARTICLE VELOCITY',
        DIAMETER=954,
        SAMPLING_FACTOR=1/

&PROP ID='K5.6_01',
        QUANTITY='SPRINKLER LINK TEMPERATURE',
        OFFSET=0.05,
        PARTICLES_PER_SECOND=10000,
        PART_ID='water drops',
        FLOW_RATE=94.79,
        SPRAY_ANGLE=10.,80.,
        ORIFICE_DIAMETER=0.0127,
        SMOKEVIEW_ID='sprinkler_pendent'/

&DEVC XYZ=0.0,0.0,7,
        PROP_ID='K5.6_01',
        ID='Spr_1',
        QUANTITY="TIME",
        SETPOINT=0. / Activates at t=0

// Slice Files

&SLCF PBZ=0.0,QUANTITY='PARTICLE FLUX Z', PART_ID='water drops' /
```

```
&SLCF PBZ=1.0,QUANTITY='PARTICLE  FLUX  Z', PART_ID='water drops' /
&SLCF PBZ=2.0,QUANTITY='PARTICLE  FLUX  Z', PART_ID='water drops' /
&SLCF PBZ=3.0,QUANTITY='PARTICLE  FLUX  Z', PART_ID='water drops' /
&SLCF PBZ=4.0,QUANTITY='PARTICLE  FLUX  Z', PART_ID='water drops' /
&SLCF PBZ=5.0,QUANTITY='PARTICLE  FLUX  Z', PART_ID='water drops' /
&SLCF PBZ=6.0,QUANTITY='PARTICLE  FLUX  Z', PART_ID='water drops' /

&DEVC XB=-7,7,-7,7,6,6, ID='flux 1m', QUANTITY='PARTICLE  FLUX Z', STATISTICS='AREA INTEGRAL'  /
&DEVC XB=-7,7,-7,7,0,0, ID='flux 7m', QUANTITY='PARTICLE  FLUX Z', STATISTICS='AREA INTEGRAL'  /
&DEVC XB=-7,7,-7,7,0,0, ID='total', QUANTITY='AMPUA',  PART_ID='water drops', STATISTICS='SURFACE
INTEGRAL'  /

&TAIL /
```

Appendix D: Enclosure Fire FDS Model w/ 4S Nozzle

```
&HEAD CHID='et_4S_Nozzle,  /

&MESH IJK=20,34,44, XB=-5.7,-3.7,-1.7,1.7,-0.2,4.2  / 10 cm grid.
&MESH IJK=74,34,44, XB=-3.7,3.7,-1.7,1.7,-0.2,4.2  / 10 cm grid.
&MESH IJK=20,34,44, XB=3.7,5.7,-1.7,1.7,-0.2,4.2  / 10 cm grid.

//

&MISC SIMULATION_MODE='LES',
 HUMIDITY=40.,
 PARTICLE_CFL=T,
 TMPA=29.,
 BNDF_DEFAULT=.FALSE.  /
&RADI RADIATION=T,  /
&TIME T_END=400., /

&DUMP DT_HRR=1. /

// Vents

&VENT MB='XMIN',  SURF_ID='OPEN'  /
&VENT MB='XMAX',  SURF_ID='OPEN'  /
&VENT MB='YMIN',  SURF_ID='OPEN'  /
&VENT MB='YMAX',  SURF_ID='OPEN'  /
&VENT MB='ZMIN', SURF_ID='OPEN'  /
&VENT MB='ZMAX',  SURF_ID='OPEN'  /

// Materials

&REAC FUEL='PROPANE',  SOOT_YIELD=0.01  /


&SURF ID          ='WOOD  BURNER',
         HRRPUA = 546.0,
 RAMP_Q="WOOD",
 COLOR = 'RED',
 E_COEFFICIENT=1.5/

&SURF ID          ='FOAM  BURNER',
         HRRPUA = 127.5,
 RAMP_Q="FOAM",
 COLOR = 'RED',
 E_COEFFICIENT=1.5/

&SURF ID                         ='ROOM',
 ADIABATIC=T,
 COLOR = 'GRAY'  /

&SURF ID                         ='SEETHROUGH',
 ADIABATIC=T,
```

```
  COLOR = 'GRAY',
  TRANSPARENCY=0.0  /

// Walls

&OBST XB= -3.7, 3.7, -1.7, 1.7, -0.2, 0.0, SURF_ID="ROOM",  BNDF_FACE(3)=.TRUE.  / Floor
&OBST XB= -3.7, 3.7, -1.7, 1.7,  3.0, 3.1, SURF_ID="ROOM"  / Ceiling
&OBST XB= -3.7, 3.7, -1.7,-1.5,  0.0, 3.0, SURF_ID="SEETHROUGH"  / Front Wall
&OBST XB= -3.7, 3.7,  1.5, 1.7,  0.0, 3.0, SURF_ID="ROOM"  / Back Wall
&OBST XB= -3.7,-3.5, -1.5, 0.1,  0.0, 3.0, SURF_ID="ROOM"  / Left Wall
&OBST XB= -3.7,-3.5,  0.1, 1.0,  2.8, 3.0, SURF_ID="ROOM"  / Left Wall
&OBST XB= -3.7,-3.5,  1.0, 1.5,  0.0, 3.0, SURF_ID="ROOM"  / Left Wall
&OBST XB=  3.5, 3.7, -1.5, 0.5,  0.0, 3.0, SURF_ID="ROOM"  / Right Wall
&OBST XB=  3.5, 3.7,  0.5, 1.5,  2.8, 3.0, SURF_ID="ROOM"  / Right Wall

// Wood Crib

&OBST XB= -3.3, -2.9, -1.3,-0.9,  0.0, 0.2,
  SURF_ID6= 'INERT','INERT','INERT','INERT','INERT','WOOD  BURNER',
  BNDF_FACE(3)=.TRUE.  / Wood Crib

&RAMP ID='WOOD',  T=0, F=0/
&RAMP ID='WOOD',  T=17.7, F=0.22/
&RAMP ID='WOOD',  T=35.6, F=0.41/
&RAMP ID='WOOD',  T=53.5, F=0.52/
&RAMP ID='WOOD',  T=71.4, F=0.69/
&RAMP ID='WOOD',  T=89.5, F=0.84/
&RAMP ID='WOOD',  T=107.6, F=0.85/
&RAMP ID='WOOD',  T=125.6, F=0.86/
&RAMP ID='WOOD',  T=143.5, F=0.99/
&RAMP ID='WOOD',  T=161.7, F=1/
&RAMP ID='WOOD',  T=179.6, F=0.98/
&RAMP ID='WOOD',  T=197.7, F=0.97/
&RAMP ID='WOOD',  T=215.5, F=0.99/
&RAMP ID='WOOD',  T=233.7, F=1/
&RAMP ID='WOOD',  T=251.5, F=0.95/
&RAMP ID='WOOD',  T=269.7, F=0.87/
&RAMP ID='WOOD',  T=287.8, F=0.77/
&RAMP ID='WOOD',  T=305.9, F=0.64/
&RAMP ID='WOOD',  T=323.9, F=0.53/
&RAMP ID='WOOD',  T=342.1, F=0.52/
&RAMP ID='WOOD',  T=360.1, F=0.54/
&RAMP ID='WOOD',  T=378.3, F=0.55/
&RAMP ID='WOOD',  T=400, F=0.59/

// Foam

&OBST XB= -3.4,-2.6,  -0.4,-0.3,  0.0, 0.8,
  SURF_ID6= 'INERT','INERT','FOAM  BURNER','INERT','INERT','INERT',
  BNDF_FACE(-2)=.TRUE.  / Back Foam

&OBST XB= -2.4,-2.3, -1.4,-0.6,  0.0, 0.8,
  SURF_ID6= 'FOAM BURNER','INERT','INERT','INERT','INERT','INERT',
  BNDF_FACE(-1)=.TRUE.  / Right Foam
```

```
&RAMP ID='FOAM',  T=0, F=0/
&RAMP ID='FOAM',  T=14.5, F=0/
&RAMP ID='FOAM',  T=17.7, F=0/
&RAMP ID='FOAM',  T=35.6, F=0.12/
&RAMP ID='FOAM',  T=53.5, F=0.39/
&RAMP ID='FOAM',  T=71.4, F=0.57/
&RAMP ID='FOAM',  T=89.5, F=0.72/
&RAMP ID='FOAM',  T=107.6, F=0.9/
&RAMP ID='FOAM',  T=125.6, F=1/
&RAMP ID='FOAM',  T=143.5, F=0.96/
&RAMP ID='FOAM',  T=161.7, F=0.93/
&RAMP ID='FOAM',  T=179.6, F=0.84/
&RAMP ID='FOAM',  T=197.7, F=0.78/
&RAMP ID='FOAM',  T=215.5, F=0.76/
&RAMP ID='FOAM',  T=233.7, F=0.79/
&RAMP ID='FOAM',  T=251.5, F=0.84/
&RAMP ID='FOAM',  T=267.7, F=0.86/
&RAMP ID='FOAM',  T=287.8, F=0.92/
&RAMP ID='FOAM',  T=305.9, F=0.93/
&RAMP ID='FOAM',  T=323.9, F=0.92/
&RAMP ID='FOAM',  T=342.1, F=0.84/
&RAMP ID='FOAM',  T=360.1, F=0.79/
&RAMP ID='FOAM',  T=378.3, F=0.69/
&RAMP ID='FOAM',  T=400, F=0.6/

// Sprinkler

&SPEC ID='WATER VAPOR'/

&PART ID='water drops',
 SPEC_ID='WATER VAPOR',
 QUANTITIES(1:3)='PARTICLE DIAMETER','PARTICLE VELOCITY','PARTICLE AGE',
 DIAMETER=967.148,
 GAMMA_D=2.07178,
 SAMPLING_FACTOR=5.,
 AGE=5./

&PROP ID='4SK5.6',
 QUANTITY='SPRINKLER LINK TEMPERATURE',
 RTI=75.,
		ACTIVATION_TEMPERATURE=68.,
 OFFSET=0.3,
 PARTICLES_PER_SECOND=15000,
 PART_ID='water drops',
 FLOW_RATE=94.8017,
 SPRAY_PATTERN_TABLE='table_RA1414_01',
 PARTICLE_VELOCITY=13.2858,
 SMOKEVIEW_ID='sprinkler_pendent'/

&DEVC XYZ=-1.75,0.0,2.8,
 PROP_ID='4SK5.6',
 ID='Spr_1', /
```

```
// Temperature Probes

&PROP ID='Small TC', EMISSIVITY=0.9, DIAMETER=0.001, /

&DEVC ID='Point 1', XYZ=0,0,2.9, QUANTITY='TEMPERATURE' /
&DEVC ID='TC_1S', XYZ=0,0,2.9, QUANTITY='THERMOCOUPLE', PROP_ID='Small TC' /

&DEVC ID='Point 2', XYZ=1.8,0,2.9, QUANTITY='TEMPERATURE' /
&DEVC ID='TC_2S', XYZ=1.8,0,2.9, QUANTITY='THERMOCOUPLE', PROP_ID='Small TC' /

// Slice Files

&SLCF PBZ=0.01, QUANTITY='PARTICLE FLUX Z', PART_ID='water drops' /
&SLCF PBZ=0.5, QUANTITY='PARTICLE FLUX Z', PART_ID='water drops' /
&SLCF PBZ=1.0, QUANTITY='PARTICLE FLUX Z', PART_ID='water drops' /
&SLCF PBZ=1.5, QUANTITY='PARTICLE FLUX Z', PART_ID='water drops' /
&SLCF PBZ=2.0, QUANTITY='PARTICLE FLUX Z', PART_ID='water drops' /

&SLCF PBY=0.0, QUANTITY='TEMPERATURE', /
&SLCF PBY=0.0, QUANTITY='VELOCITY', VECTOR=T /

//

&BNDF QUANTITY='AMPUA', CELL_CENTERED=T, PART_ID='water drops' /

// HRR

&DEVC XB=-3.3,-2.9,-1.3,-0.9,0.2,0.2, QUANTITY='HRRPUA', ID='HRR_WOOD', SPATIAL_STATISTIC='SURFACE
INTEGRAL' /
&DEVC XB=-3.4,-2.6,-0.4,-0.4,0.0,0.8, QUANTITY='HRRPUA', ID='HRR_BACKFOAM', SPATIAL_STATISTIC='SURFACE
INTEGRAL' /
&DEVC XB=-2.4,-2.4,-1.4,-0.6,0.0,0.8, QUANTITY='HRRPUA', ID='HRR_RIGHTFOAM', SPATIAL_STATISTIC='SURFACE
INTEGRAL' /

// Water

&DEVC XB=-3.3,-2.9,-1.3,-0.9,0.2,0.2, ID='WATER_WOOD', QUANTITY='MPUA', PART_ID='water drops',
STATISTICS='SURFACE INTEGRAL' /
&DEVC XB=-3.4,-2.6,-0.4,-0.4,0.0,0.8, ID='WATER_BACKFOAM', QUANTITY='MPUA', PART_ID='water drops',
STATISTICS='SURFACE INTEGRAL' /
&DEVC XB=-2.4,-2.4,-1.4,-0.6,0.0,0.8, ID='WATER_RIGHTFOAM', QUANTITY='MPUA', PART_ID='water drops',
STATISTICS='SURFACE INTEGRAL' /

// Spray Table

&TABL ID='table_RA1414_01',TABLE_DATA=95,105,-0.5,0.5,12.3919,0.000007928045603886739/
&TABL ID='table_RA1414_01',TABLE_DATA=95,105,0.5,1.5,12.3919,0.00001080725288225667/
&TABL ID='table_RA1414_01',TABLE_DATA=95,105,1.5,2.5,12.3919,0.0000124215022 5362408/
&TABL ID='table_RA1414_01',TABLE_DATA=95,105,2.5,3.5,12.3919,0.00001154872532085669/
… (continued)


&TAIL /
```

Appendix E: MATLAB Bucket Test Post Processing Script

```
clc
clear
close all
set(0,'DefaultFigureVisible','on');
[filepath,name,ext] = fileparts(mfilename('fullpath'));
read=name;

[Flux7m,Time]=slread([num2str(read) '_1_1.sf'],10,70);
[Flux6m,Time]=slread([num2str(read) '_1_2.sf'],10,70);
[Flux5m,Time]=slread([num2str(read) '_1_3.sf'],10,70);
[Flux4m,Time]=slread([num2str(read) '_2_1.sf'],10,70);
[Flux2m,Time]=slread([num2str(read) '_3_1.sf'],10,70);
[Flux1m,Time]=slread([num2str(read) '_3_2.sf'],10,70);

Mflux1m = -1*mean(Flux1m,3);
Mflux2m = -1*mean(Flux2m,3);
Mflux3m = -1*mean(Flux3m,3);
Mflux4m = -1*mean(Flux4m,3);
Mflux5m = -1*mean(Flux5m,3);
Mflux6m = -1*mean(Flux6m,3);
Mflux7m = -1*mean(Flux7m,3);

fluxcheck1m = 60*sum(0.1*0.1*Mflux1m,"all");
fluxcheck2m = 60*sum(0.1*0.1*Mflux2m,"all");
fluxcheck3m = 60*sum(0.1*0.1*Mflux3m,"all");
fluxcheck4m = 60*sum(0.1*0.1*Mflux4m,"all");
fluxcheck5m = 60*sum(0.1*0.1*Mflux5m,"all");
fluxcheck6m = 60*sum(0.1*0.1*Mflux6m,"all");
fluxcheck7m = 60*sum(0.1*0.1*Mflux7m,"all");


%Radial_ave

xM = 0:.1:7;

[Tics1,RadialMflux1m]=radial_profile(Mflux1m,1);
[Tics2,RadialMflux2m]=radial_profile(Mflux2m,1);
[Tics3,RadialMflux3m]=radial_profile(Mflux3m,1);
[Tics4,RadialMflux4m]=radial_profile(Mflux4m,1);
[Tics5,RadialMflux5m]=radial_profile(Mflux5m,1);
[Tics6,RadialMflux6m]=radial_profile(Mflux6m,1);
[Tics7,RadialMflux7m]=radial_profile(Mflux7m,1);

%

Mflux_1m_y0   = mean((Mflux1m (70,:)),1);
mfluxpos1m    = RadialMflux1m (1:71);
PosMflux_1m_y0   = Mflux_1m_y0(71:141);

%Export Slices
```

```
writematrix(Mflux1m,      ['Mflux_' num2str(name) '.xls'],'Sheet',1);
writematrix(Mflux2m,      ['Mflux_' num2str(name) '.xls'],'Sheet',2);
writematrix(Mflux3m,      ['Mflux_' num2str(name) '.xls'],'Sheet',3);
writematrix(Mflux4m,      ['Mflux_' num2str(name) '.xls'],'Sheet',4);
writematrix(Mflux5m,      ['Mflux_' num2str(name) '.xls'],'Sheet',5);
writematrix(Mflux6m,      ['Mflux_' num2str(name) '.xls'],'Sheet',6);
writematrix(Mflux7m,      ['Mflux_' num2str(name) '.xls'],'Sheet',7);

writematrix(RadialMflux1m,       ['RadMflux_' num2str(name) '.xls'],'Sheet',1);
writematrix(RadialMflux2m,       ['RadMflux_' num2str(name) '.xls'],'Sheet',2);
writematrix(RadialMflux3m,       ['RadMflux_' num2str(name) '.xls'],'Sheet',3);
writematrix(RadialMflux4m,       ['RadMflux_' num2str(name) '.xls'],'Sheet',4);
writematrix(RadialMflux5m,       ['RadMflux_' num2str(name) '.xls'],'Sheet',5);
writematrix(RadialMflux6m,       ['RadMflux_' num2str(name) '.xls'],'Sheet',6);
writematrix(RadialMflux7m,       ['RadMflux_' num2str(name) '.xls'],'Sheet',7);
writematrix(Tics1,                ['RadMflux_' num2str(name) '.xls'],'Sheet',8);

T = 10:20:130;
L = {'-6.0','-4.0','-2.0','0','2.0','4.0','6.0'};

%particle flux

figure (1)

imagesc(Mflux1m);
axis equal tight;
fig=gcf;
fig.Position=[1100,100,800,800];
colorbar;
set(gca,'FontSize',14,'LineWidth',3);
title ('Mean Particle Flux 1$m$ Below Nozzle
($kg/m^2s$)','Interpreter','LaTex','FontSize',22);
set(gca,'XTick',T,'XTickLabel',L)
xlabel('X Distance ($m$)','Interpreter','LaTex','FontSize',20);
set(gca,'YTick',T,'YTickLabel',L)
ylabel('Y Distance ($m$)','Interpreter','LaTex','FontSize',20);
savefig([num2str(name) '_Mflux1m']);

figure (4)
imagesc(Mflux4m);
axis equal tight;
fig=gcf;
fig.Position=[1100,100,800,800];
colorbar;
set(gca,'FontSize',14,'LineWidth',3);
title ('Mean Particle Flux 4$m$ Below Nozzle
($kg/m^2s$)','Interpreter','LaTex','FontSize',22);
set(gca,'XTick',T,'XTickLabel',L)
xlabel('X Distance ($m$)','Interpreter','LaTex','FontSize',20);
set(gca,'YTick',T,'YTickLabel',L)
ylabel('Y Distance ($m$)','Interpreter','LaTex','FontSize',20);
savefig([num2str(name) '_Mflux4m']);
```

```
figure (7)
imagesc(Mflux7m);
axis equal tight;
fig=gcf;
fig.Position=[1100,100,800,800];
colorbar;
set(gca,'FontSize',14,'LineWidth',3);
title ('Mean Particle Flux 7$m$ Below Nozzle
($kg/m^2s$)','Interpreter','LaTex','FontSize',22);
set(gca,'XTick',T,'XTickLabel',L)
xlabel('X Distance ($m$)','Interpreter','LaTex','FontSize',20);
set(gca,'YTick',T,'YTickLabel',L)
ylabel('Y Distance ($m$)','Interpreter','LaTex','FontSize',20);
clim([0 0.05])
savefig([num2str(name) '_Mflux7m']);

%Y Slices

xN = -7:.1:7;

Mflux_1m     =Mflux1m;
Mflux_4m     =Mflux4m;
Mflux_7m     =Mflux7m;

Mflux_1m_yn4   = mean((Mflux_1m (30,:)),1);
Mflux_4m_yn4   = mean((Mflux_4m (30,:)),1);
Mflux_7m_yn4   = mean((Mflux_7m (30,:)),1);
Mflux_1m_yn3   = mean((Mflux_1m (40,:)),1);
Mflux_4m_yn3   = mean((Mflux_4m (40,:)),1);
Mflux_7m_yn3   = mean((Mflux_7m (40,:)),1);
Mflux_1m_yn2   = mean((Mflux_1m (50,:)),1);
Mflux_4m_yn2   = mean((Mflux_4m (50,:)),1);
Mflux_7m_yn2   = mean((Mflux_7m (50,:)),1);
Mflux_1m_yn1   = mean((Mflux_1m (60,:)),1);
Mflux_4m_yn1   = mean((Mflux_4m (60,:)),1);
Mflux_7m_yn1   = mean((Mflux_7m (60,:)),1);
Mflux_1m_y0   = mean((Mflux_1m (70,:)),1);
Mflux_4m_y0   = mean((Mflux_4m (70,:)),1);
Mflux_7m_y0   = mean((Mflux_7m (70,:)),1);
Mflux_1m_y1   = mean((Mflux_1m (80,:)),1);
Mflux_4m_y1   = mean((Mflux_4m (80,:)),1);
Mflux_7m_y1   = mean((Mflux_7m (80,:)),1);
Mflux_1m_y2   = mean((Mflux_1m (90,:)),1);
Mflux_4m_y2   = mean((Mflux_4m (90,:)),1);
Mflux_7m_y2   = mean((Mflux_7m (90,:)),1);
Mflux_1m_y3   = mean((Mflux_1m (100,:)),1);
Mflux_4m_y3   = mean((Mflux_4m (100,:)),1);
Mflux_7m_y3   = mean((Mflux_7m (100,:)),1);
Mflux_1m_y4   = mean((Mflux_1m (110,:)),1);
Mflux_4m_y4   = mean((Mflux_4m (110,:)),1);
Mflux_7m_y4   = mean((Mflux_7m (110,:)),1);
```

```
figure(41)
hold on
plot(xN, Mflux_1m_y0)
plot(xN, Mflux_1m_y1)
plot(xN, Mflux_1m_y2)
plot(xN, Mflux_1m_y3)
plot(xN, Mflux_1m_y4)
title('Mean Particle Flux 1$m$ Below Nozzle','Interpreter','latex')
xlabel('X position ($m$)','Interpreter','latex')
ylabel('Mean Particle Flux ($kg/m^2s$)','Interpreter','latex')
legend('Y = 0$m$','Y = $-$1$m$','Y = $-$2$m$','Y = $-$3$m$','Y = $-
$4$m$','Interpreter','latex')
hold off
savefig([num2str(name) '_NegYslice1m']);

figure(42)
hold on
plot(xN, Mflux_4m_y0)
plot(xN, Mflux_4m_y1)
plot(xN, Mflux_4m_y2)
plot(xN, Mflux_4m_y3)
plot(xN, Mflux_4m_y4)
title('Mean Particle Flux 4$m$ Below Nozzle','Interpreter','latex')
xlabel('X position ($m$)','Interpreter','latex')
ylabel('Mean Particle Flux ($kg/m^2s$)','Interpreter','latex')
legend('Y = 0$m$','Y = $-$1$m$','Y = $-$2$m$','Y = $-$3$m$','Y = $-
$4$m$','Interpreter','latex')
hold off
savefig([num2str(name) '_NegYslice4m']);

figure(43)
hold on
plot(xN, Mflux_7m_y0)
plot(xN, Mflux_7m_y1)
plot(xN, Mflux_7m_y2)
plot(xN, Mflux_7m_y3)
plot(xN, Mflux_7m_y4)
title('Mean Particle Flux 7$m$ Below Nozzle','Interpreter','latex')
xlabel('X position ($m$)','Interpreter','latex')
ylabel('Mean Particle Flux ($kg/m^2s$)','Interpreter','latex')
legend('Y = 0$m$','Y = $-$1$m$','Y = $-$2$m$','Y = $-$3$m$','Y = $-
$4$m$','Interpreter','latex')
hold off
savefig([num2str(name) '_NegYslice7m']);

figure(44)
hold on
plot(xN, Mflux_1m_y0)
plot(xN, Mflux_1m_yn1)
plot(xN, Mflux_1m_yn2)
plot(xN, Mflux_1m_yn3)
plot(xN, Mflux_1m_yn4)
```

```
title('Mean Particle Flux 1$m$ Below Nozzle','Interpreter','latex')
xlabel('X position ($m$)','Interpreter','latex')
ylabel('Mean Particle Flux ($kg/m^2s$)','Interpreter','latex')
legend('Y = 0$m$','Y = 1$m$','Y = 2$m$','Y = 3$m$','Y = 4$m$','Interpreter','latex')
hold off
savefig([num2str(name) '_PosYslice1m']);

figure(45)
hold on
plot(xN, Mflux_4m_y0)
plot(xN, Mflux_4m_yn1)
plot(xN, Mflux_4m_yn2)
plot(xN, Mflux_4m_yn3)
plot(xN, Mflux_4m_yn4)
title('Mean Particle Flux 4$m$ Below Nozzle','Interpreter','latex')
xlabel('X position ($m$)','Interpreter','latex')
ylabel('Mean Particle Flux ($kg/m^2s$)','Interpreter','latex')
legend('Y = 0$m$','Y = 1$m$','Y = 2$m$','Y = 3$m$','Y = 4$m$','Interpreter','latex')
hold off
savefig([num2str(name) '_PosYslice4m']);

figure(46)
hold on
plot(xN, Mflux_7m_y0)
plot(xN, Mflux_7m_yn1)
plot(xN, Mflux_7m_yn2)
plot(xN, Mflux_7m_yn3)
plot(xN, Mflux_7m_yn4)
title('Mean Particle Flux 7$m$ Below Nozzle','Interpreter','latex')
xlabel('X position ($m$)','Interpreter','latex')
ylabel('Mean Particle Flux ($kg/m^2s$)','Interpreter','latex')
legend('Y = 0$m$','Y = 1$m$','Y = 2$m$','Y = 3$m$','Y = 4$m$','Interpreter','latex')
hold off
savefig([num2str(name) '_PosYslice7m']);

%Radial Ave

figure(51)
hold on
plot(xM, RadialMflux1m(1:71))
plot(xM, RadialMflux4m(1:71))
plot(xM, RadialMflux7m(1:71))
title('Radial Average Particle Flux 1$m$ Below Nozzle','Interpreter','latex')
xlabel('X position ($m$)','Interpreter','latex')
ylabel('Mean Particle Flux ($kg/m^2s$)','Interpreter','latex')
legend('1$m$', '4$m$', '7$m$','Interpreter','latex')
hold off
savefig([num2str(name) '_Rad_ave']);

%Flux Check

FC = [1 2 3 4 5 6 7;fluxcheck1m fluxcheck2m fluxcheck3m fluxcheck4m fluxcheck5m
fluxcheck6m fluxcheck7m];
```

```
FCMax = max(FC(2,:));
FCMin = min(FC(2,:));
FCpercent = abs(FCMax-FCMin)/FCMax*100;

figure(50)
hold on
plot(FC(1,:),FC(2,:))
title( 'Flux Check - Percent Change', FCpercent)
xlabel('Distance below nozzle (m)')
ylabel('Flux (L/min)')

savefig('Fluxcheck');

hold off
```

Appendix F: Crossflow Y Slice Analysis, 4S vs Basic Nozzle

1 m/s, 4 m below nozzle

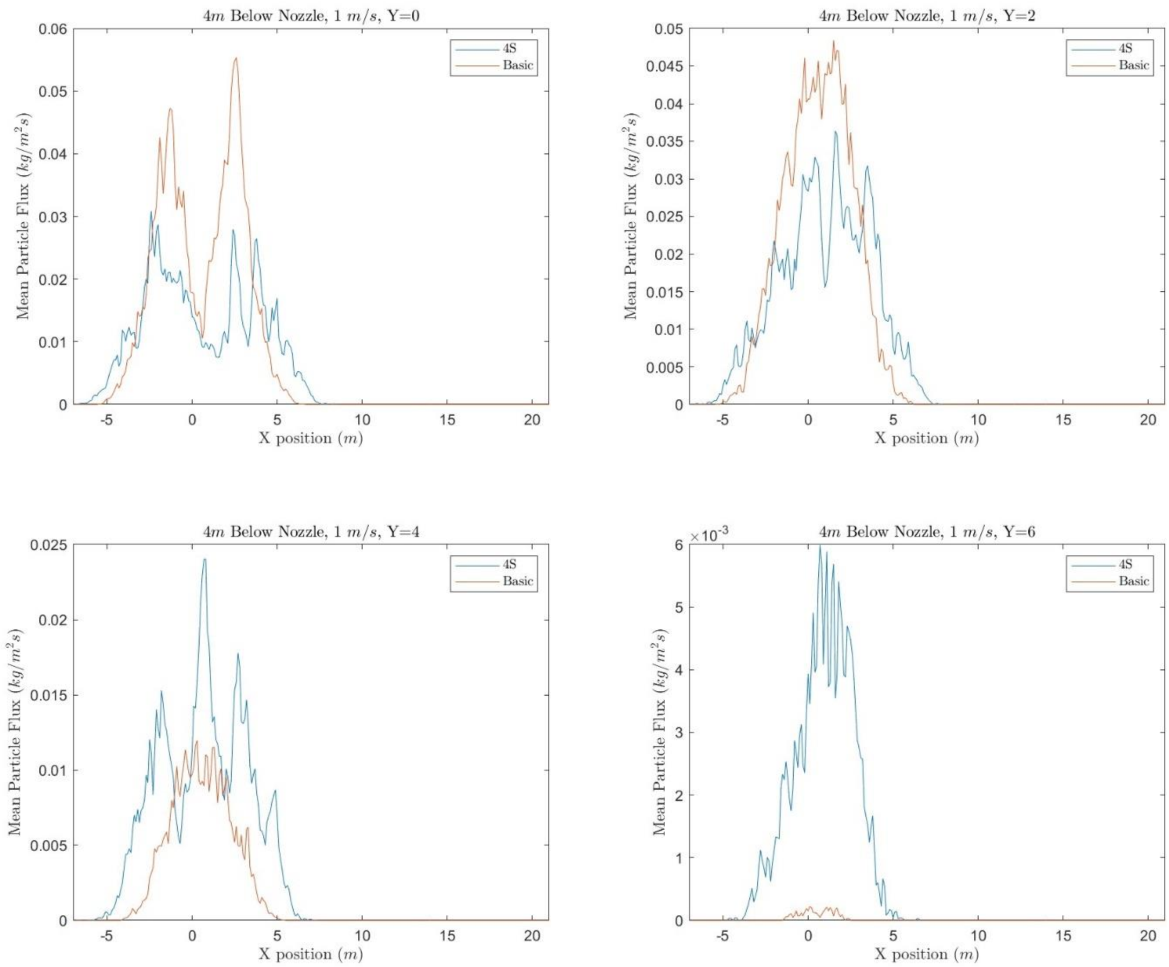

1 m/s, 7 m below nozzle

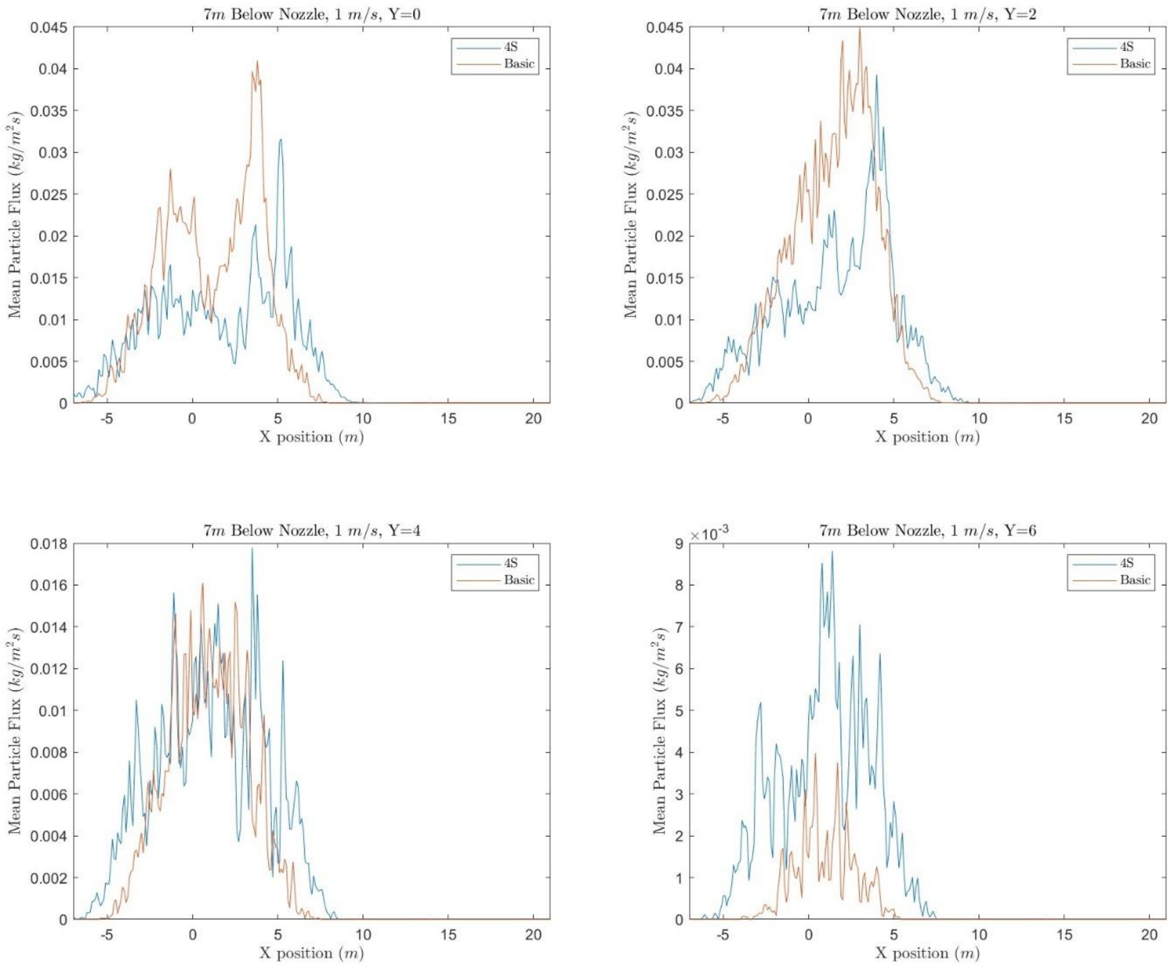

2 m/s, 4 m below nozzle

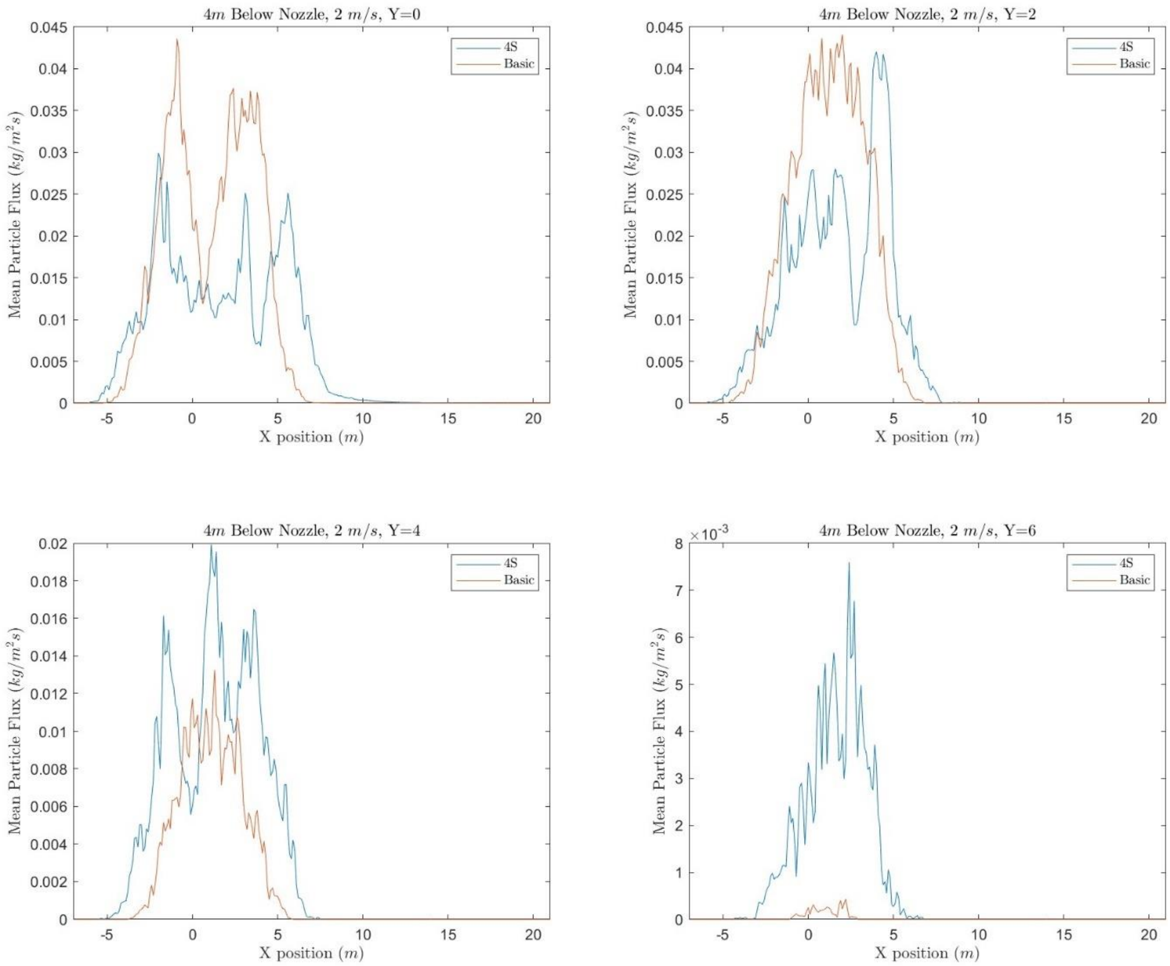

2 m/s, 7 m below nozzle

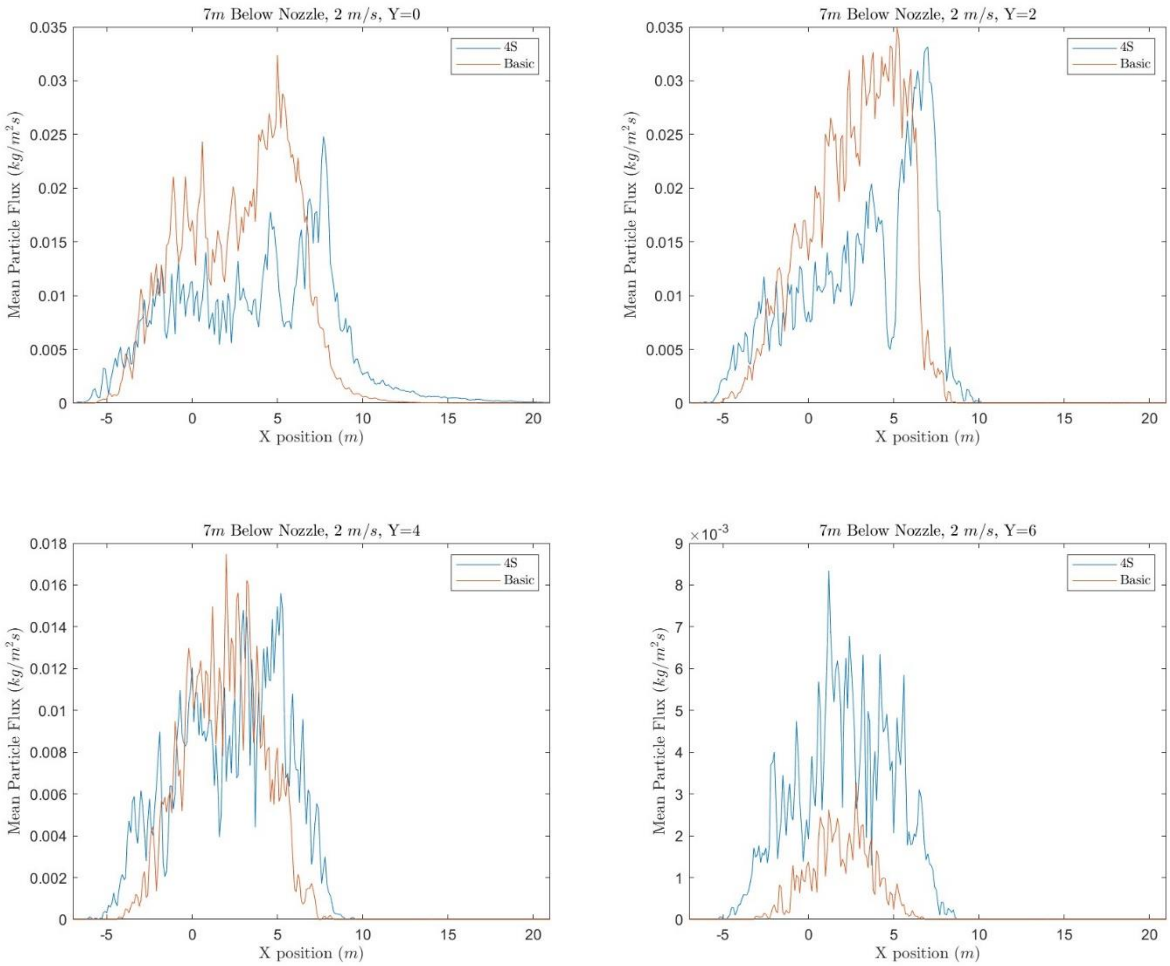

3 m/s, 4 m below nozzle

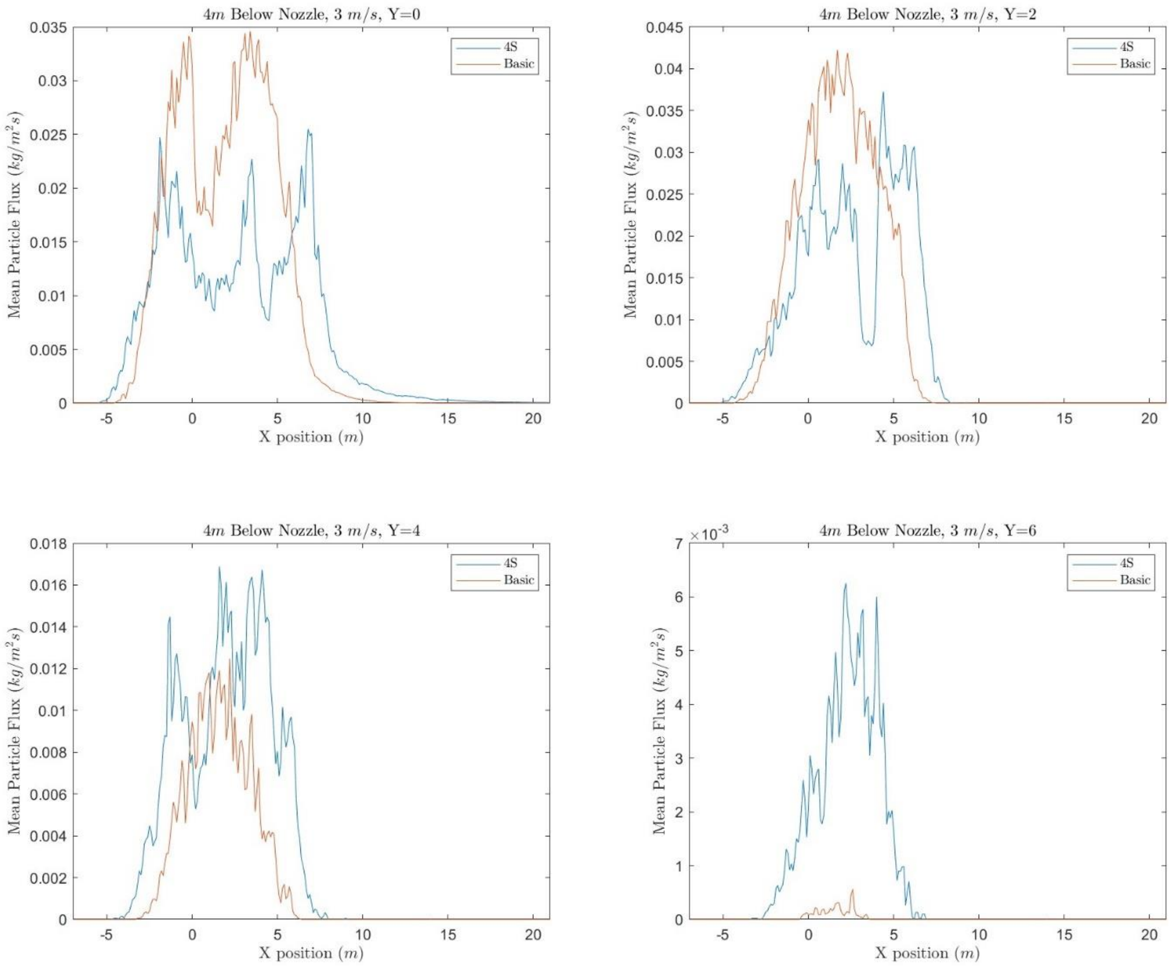

3 m/s, 7 m below nozzle

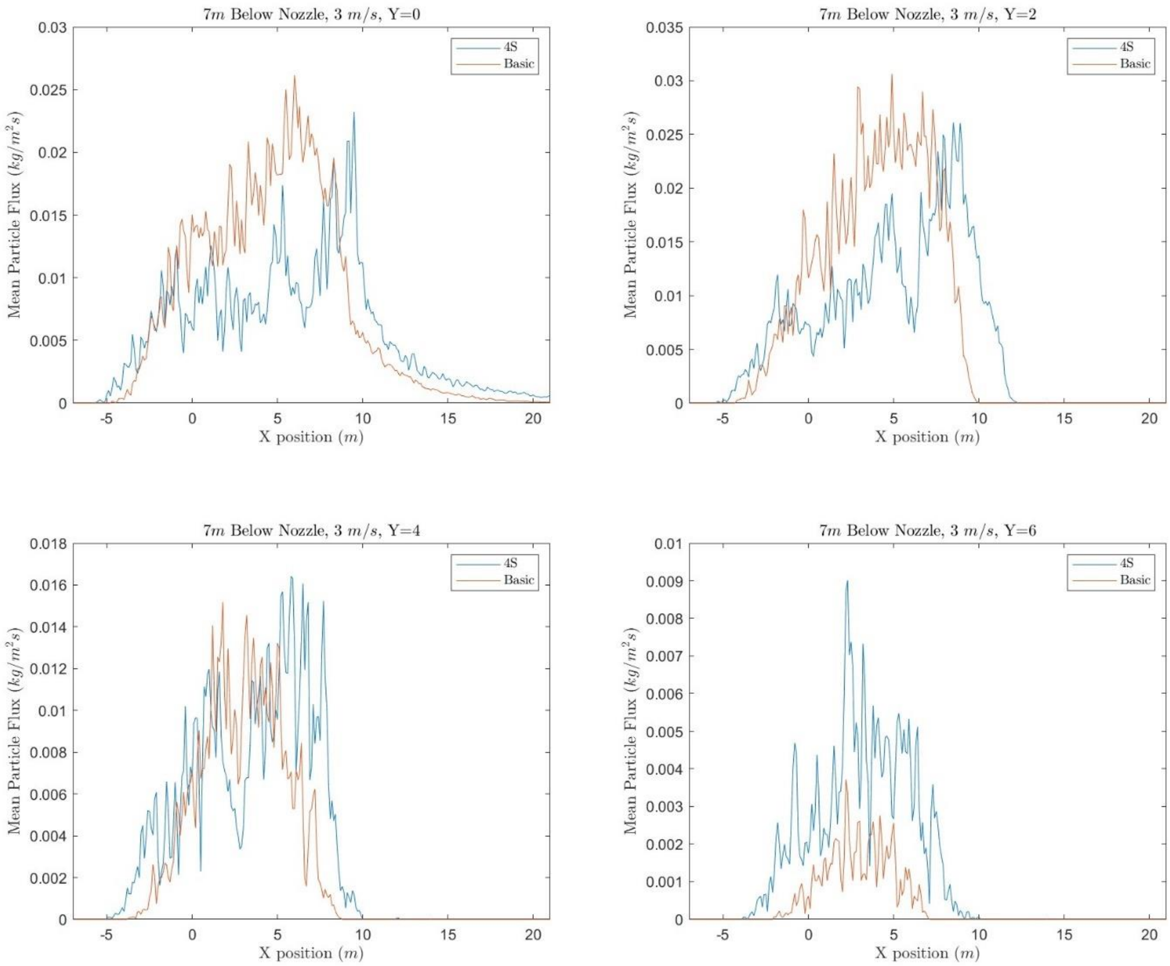

Appendix G: Enclosure Fire Analysis, 4S vs Basic Nozzle

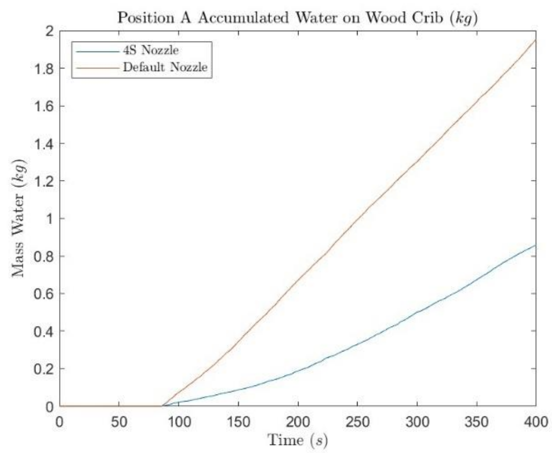

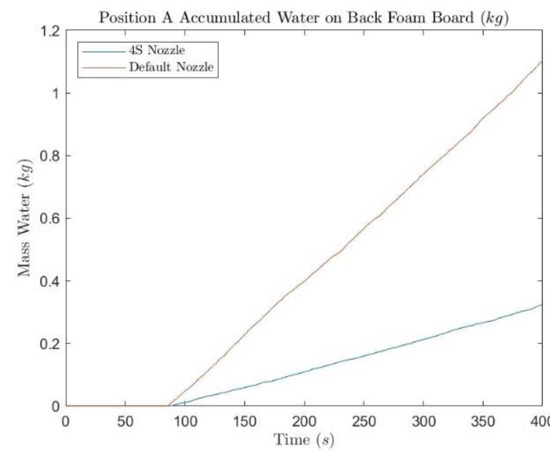

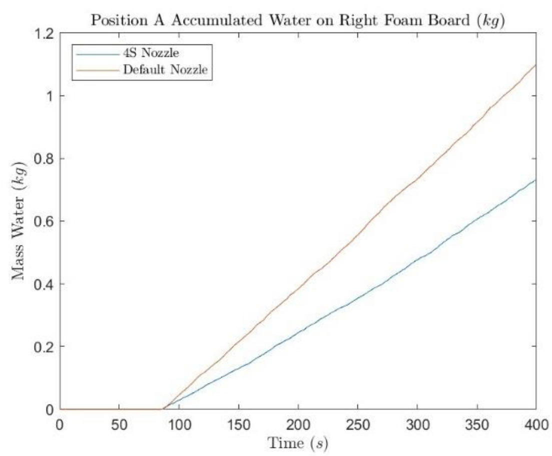

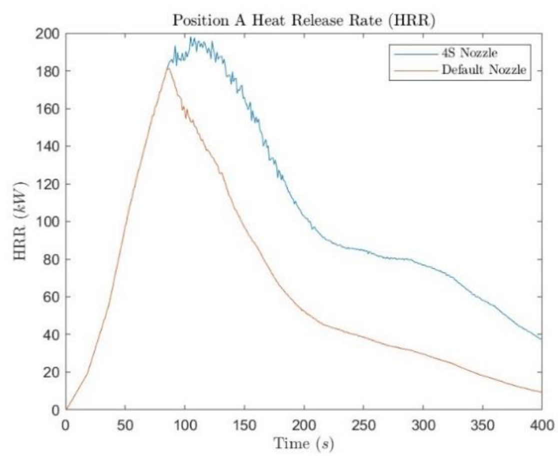

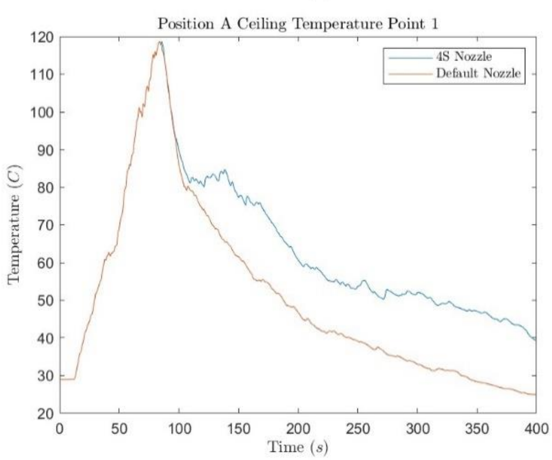

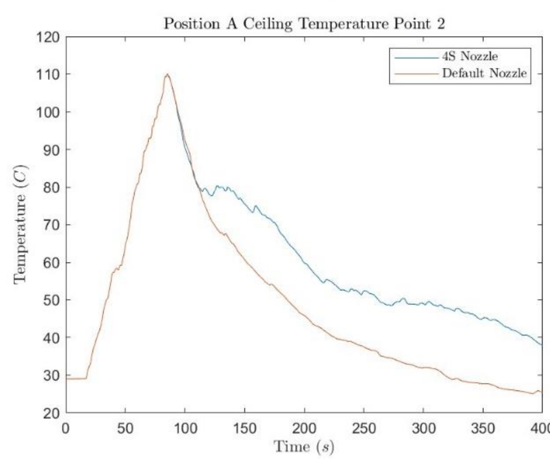

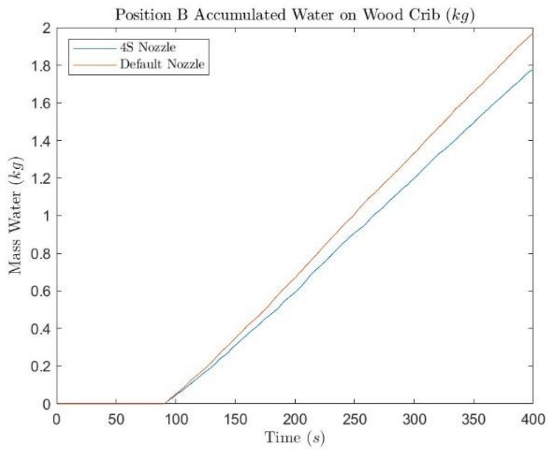
Position B Accumulated Water on Wood Crib (kg)
4S Nozzle
Default Nozzle
Mass Water (kg)
Time (s)

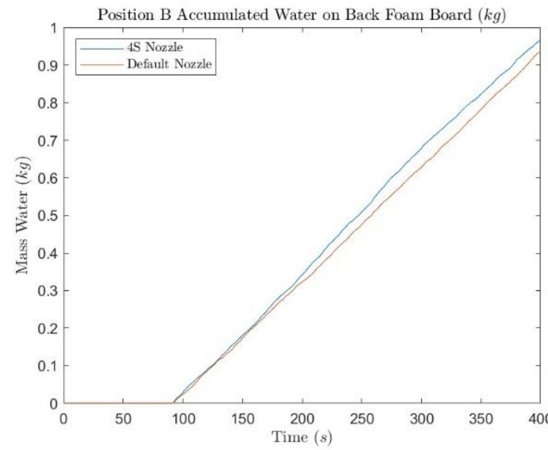
Position B Accumulated Water on Back Foam Board (kg)
4S Nozzle
Default Nozzle
Mass Water (kg)
Time (s)

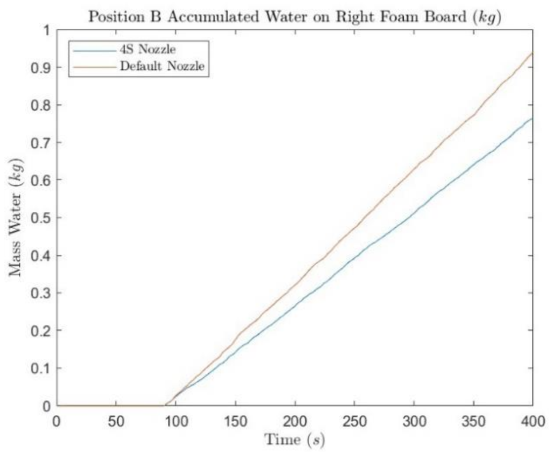
Position B Accumulated Water on Right Foam Board (kg)
4S Nozzle
Default Nozzle
Mass Water (kg)
Time (s)

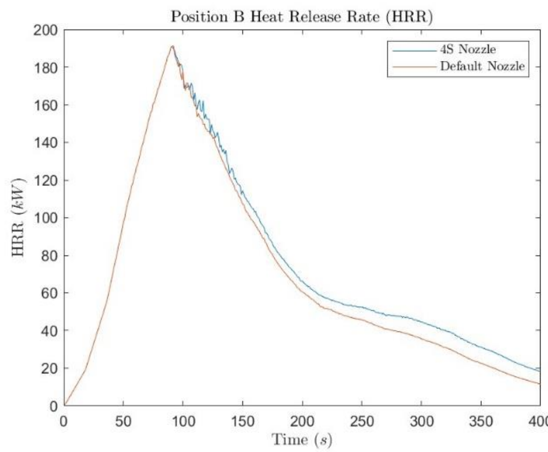
Position B Heat Release Rate (HRR)
4S Nozzle
Default Nozzle
HRR (kW)
Time (s)

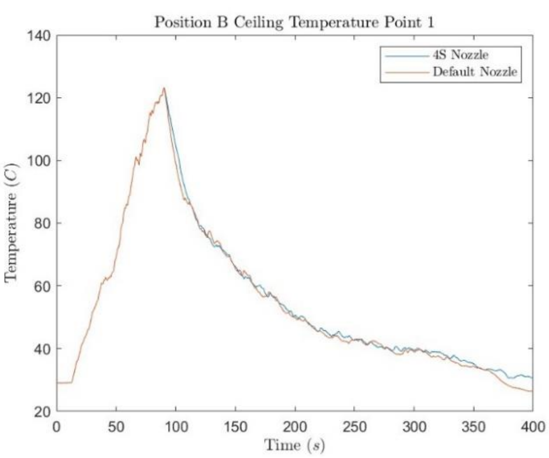
Position B Ceiling Temperature Point 1
4S Nozzle
Default Nozzle
Temperature (C)
Time (s)

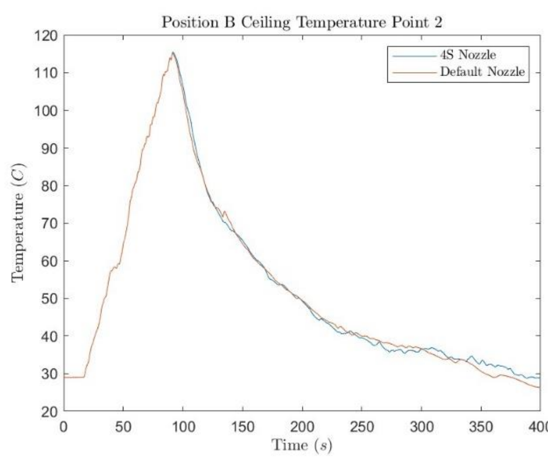
Position B Ceiling Temperature Point 2
4S Nozzle
Default Nozzle
Temperature (C)
Time (s)

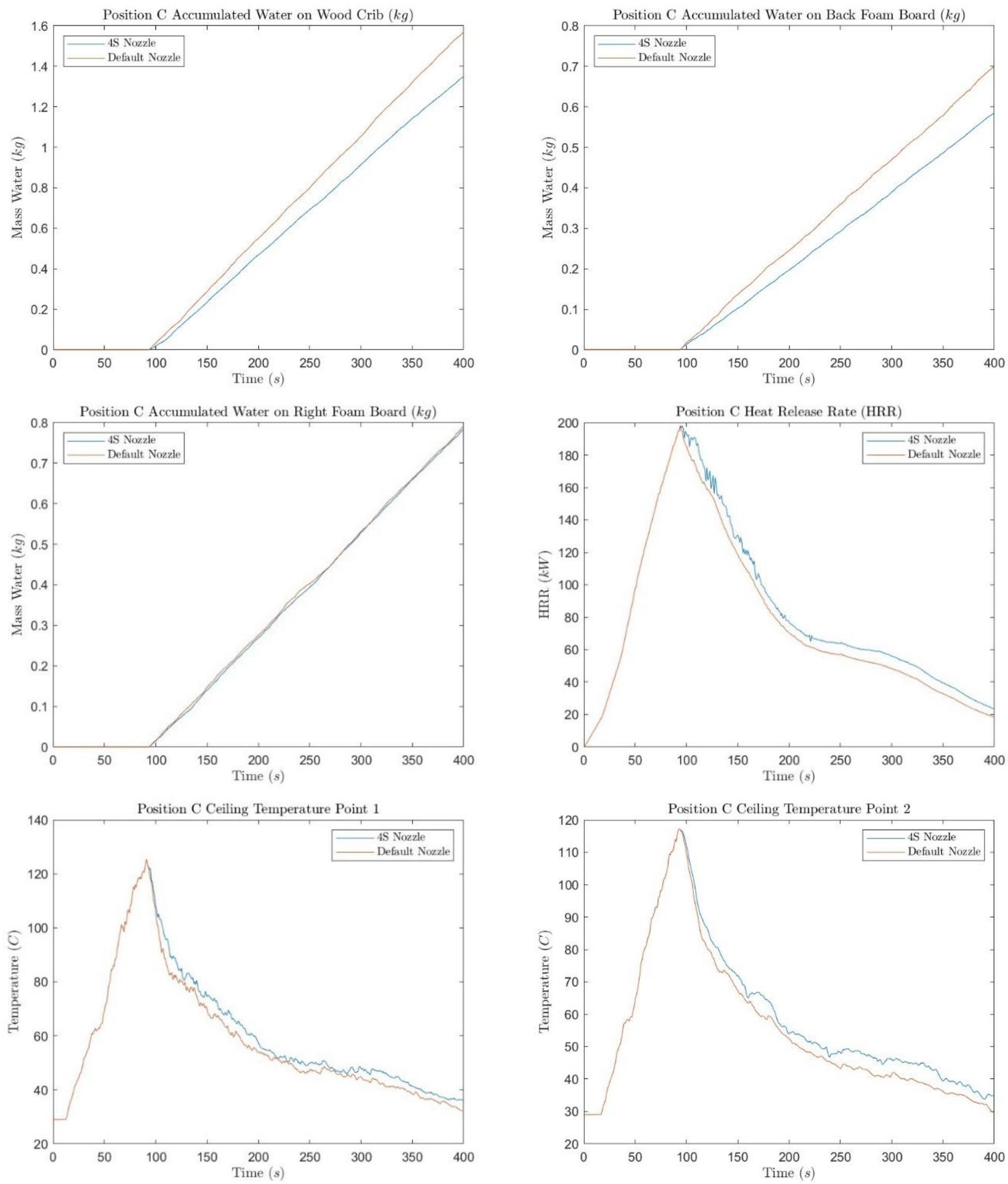
Position C Accumulated Water on Wood Crib (kg)
Mass Water (kg)
Time (s)
4S Nozzle
Default Nozzle
Position C Accumulated Water on Back Foam Board (kg)
Mass Water (kg)
Time (s)
4S Nozzle
Default Nozzle
Position C Accumulated Water on Right Foam Board (kg)
Mass Water (kg)
Time (s)
4S Nozzle
Default Nozzle
Position C Heat Release Rate (HRR)
HRR (kW)
Time (s)
4S Nozzle
Default Nozzle
Position C Ceiling Temperature Point 1
Temperature (C)
Time (s)
4S Nozzle
Default Nozzle
Position C Ceiling Temperature Point 2
Temperature (C)
Time (s)
4S Nozzle
Default Nozzle

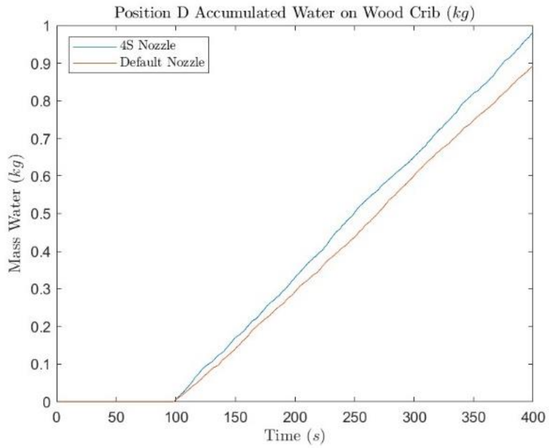
Position D Accumulated Water on Wood Crib (kg)
4S Nozzle
Default Nozzle
Mass Water (kg)
Time (s)

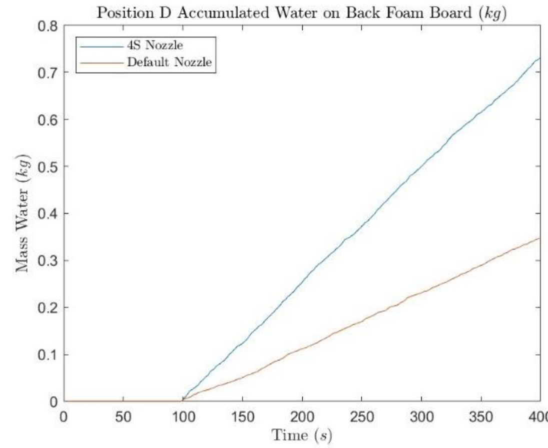
Position D Accumulated Water on Back Foam Board (kg)
4S Nozzle
Default Nozzle
Mass Water (kg)
Time (s)

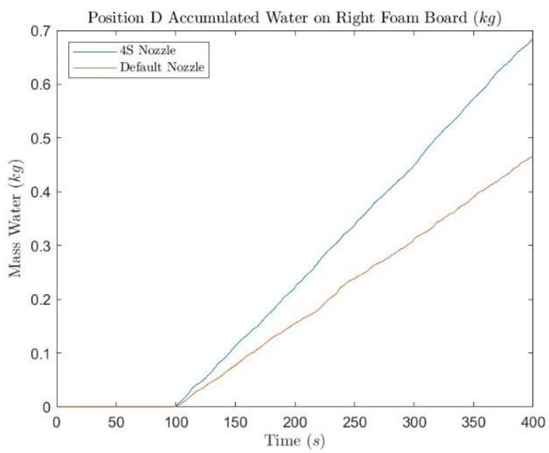
Position D Accumulated Water on Right Foam Board (kg)
4S Nozzle
Default Nozzle
Mass Water (kg)
Time (s)

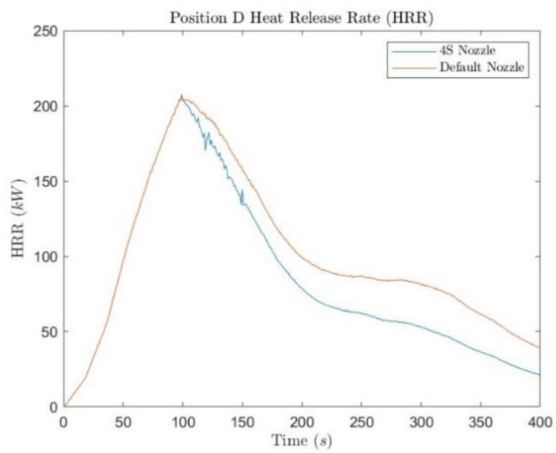
Position D Heat Release Rate (HRR)
4S Nozzle
Default Nozzle
HRR (kW)
Time (s)

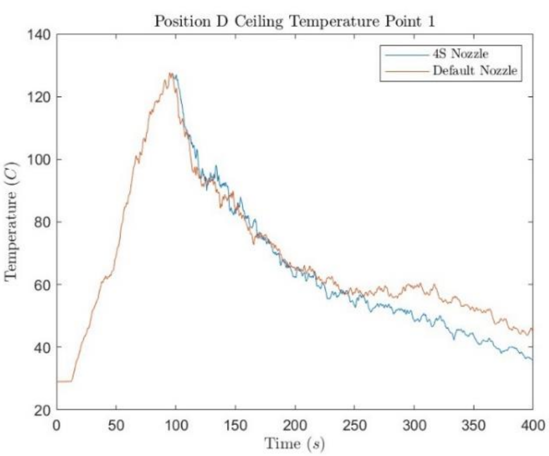
Position D Ceiling Temperature Point 1
4S Nozzle
Default Nozzle
Temperature (C)
Time (s)

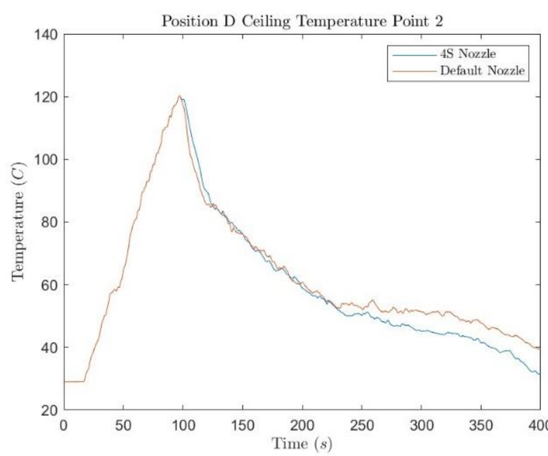
Position D Ceiling Temperature Point 2
4S Nozzle
Default Nozzle
Temperature (C)
Time (s)

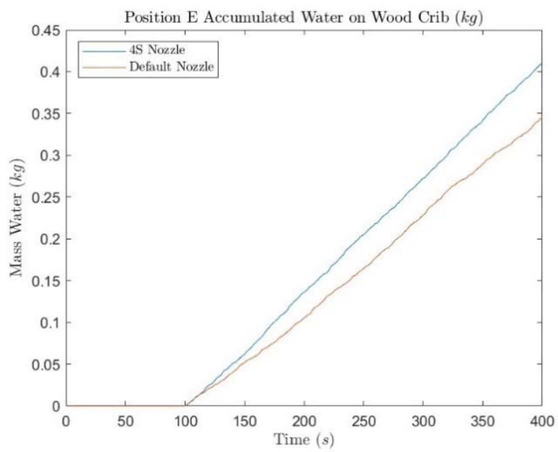
Position E Accumulated Water on Wood Crib (kg)
4S Nozzle
Default Nozzle
Mass Water (kg)
Time (s)

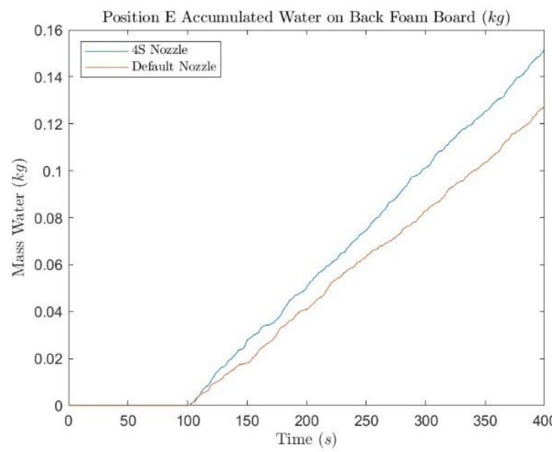
Position E Accumulated Water on Back Foam Board (kg)
4S Nozzle
Default Nozzle
Mass Water (kg)
Time (s)

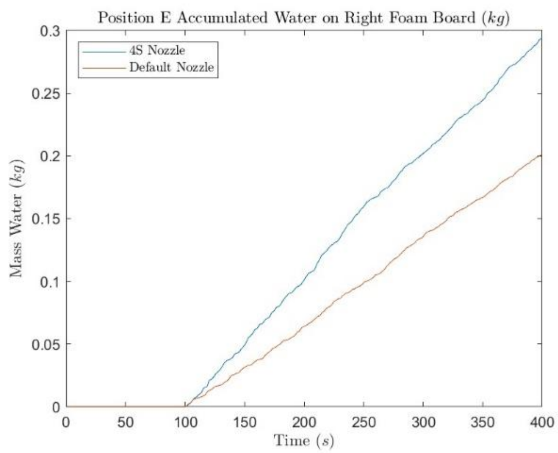
Position E Accumulated Water on Right Foam Board (kg)
4S Nozzle
Default Nozzle
Mass Water (kg)
Time (s)

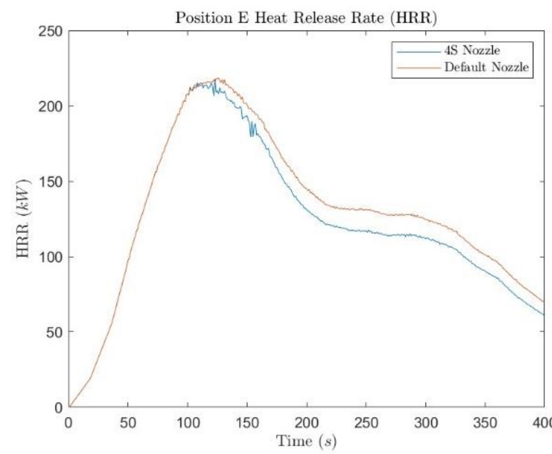
Position E Heat Release Rate (HRR)
4S Nozzle
Default Nozzle
HRR (kW)
Time (s)

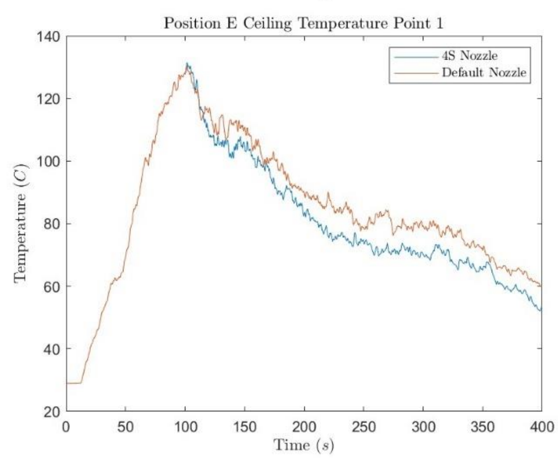
Position E Ceiling Temperature Point 1
4S Nozzle
Default Nozzle
Temperature (C)
Time (s)

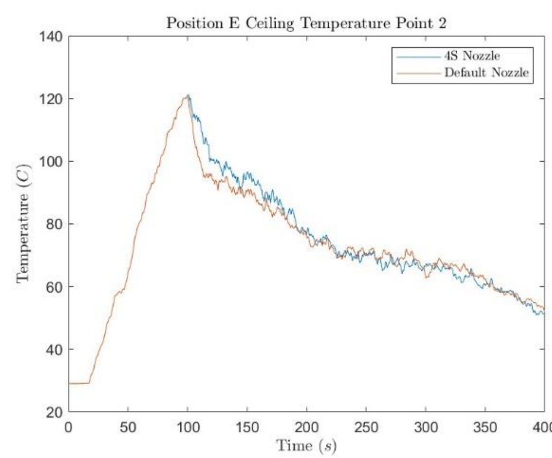
Position E Ceiling Temperature Point 2
4S Nozzle
Default Nozzle
Temperature (C)
Time (s)

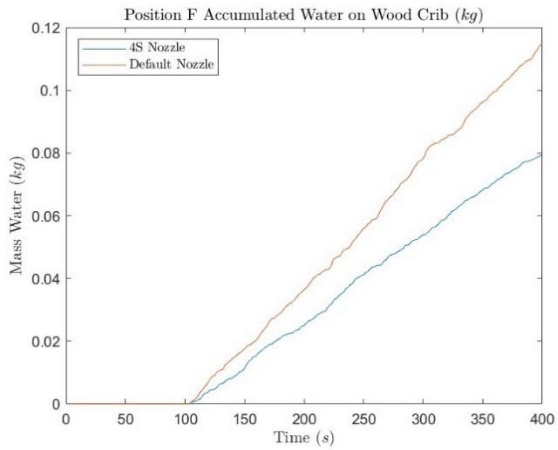
Position F Accumulated Water on Wood Crib (kg)
4S Nozzle
Default Nozzle
Mass Water (kg)
Time (s)

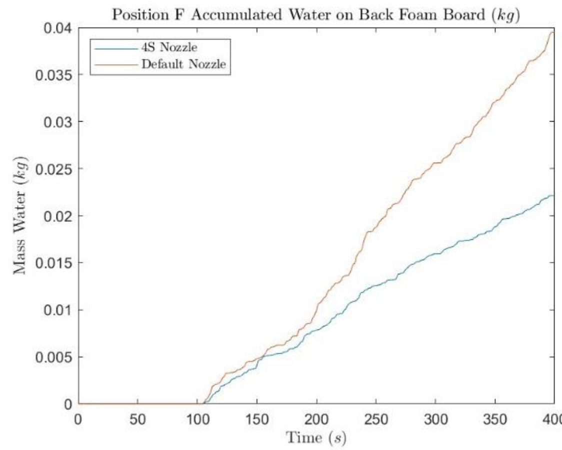
Position F Accumulated Water on Back Foam Board (kg)
4S Nozzle
Default Nozzle
Mass Water (kg)
Time (s)

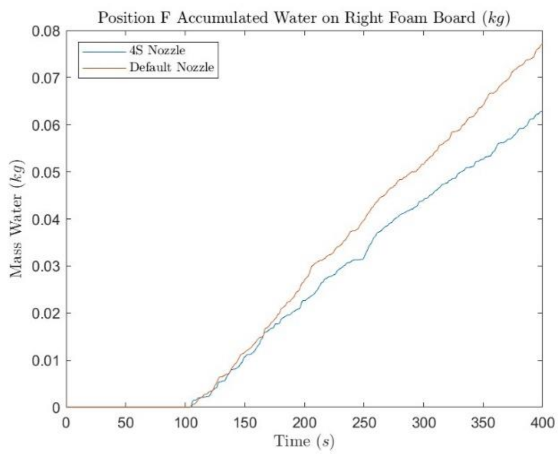
Position F Accumulated Water on Right Foam Board (kg)
4S Nozzle
Default Nozzle
Mass Water (kg)
Time (s)

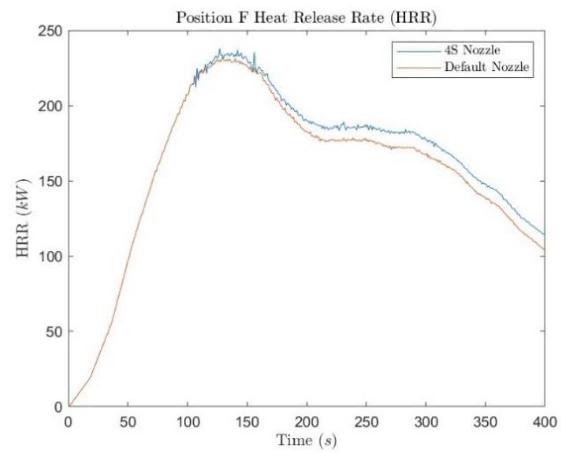
Position F Heat Release Rate (HRR)
4S Nozzle
Default Nozzle
HRR (kW)
Time (s)

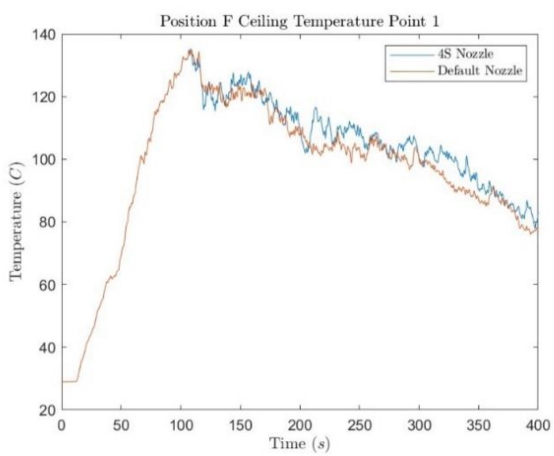
Position F Ceiling Temperature Point 1
4S Nozzle
Default Nozzle
Temperature (C)
Time (s)

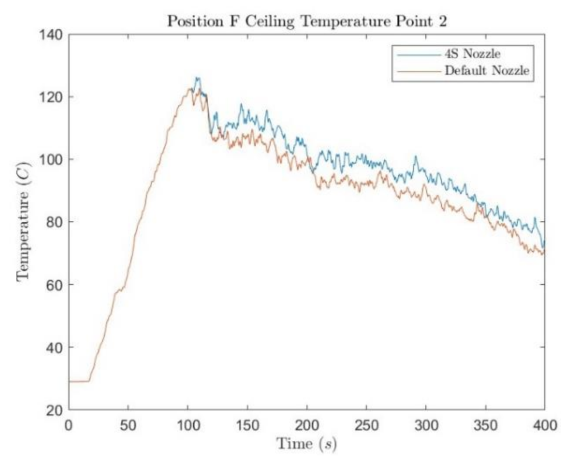
Position F Ceiling Temperature Point 2
4S Nozzle
Default Nozzle
Temperature (C)
Time (s)

Appendix H: Enclosure Fire Analysis, 4S Nozzle w/ & w/o Fire

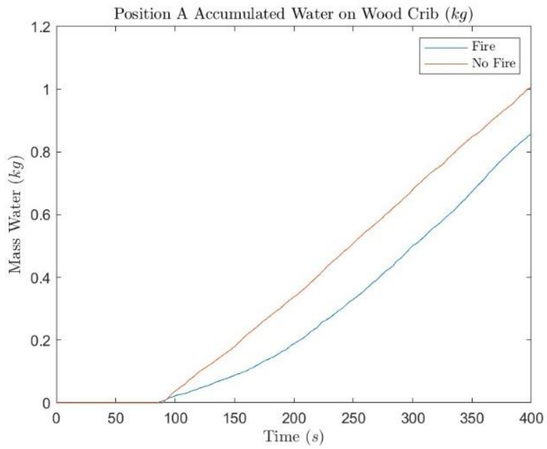

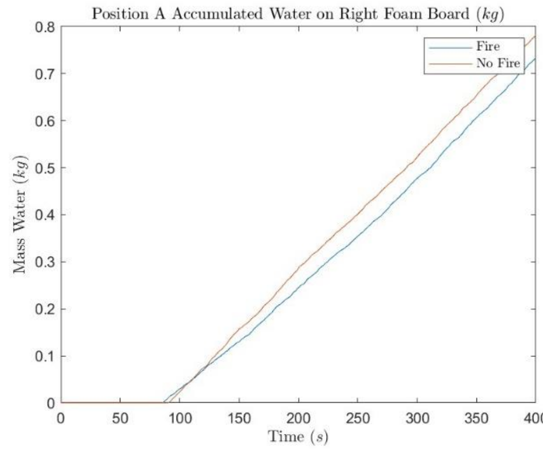

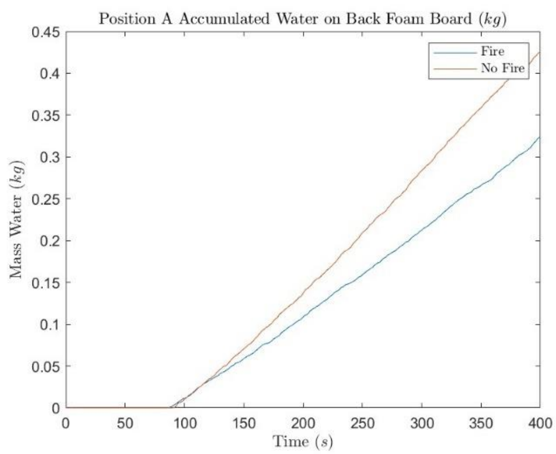

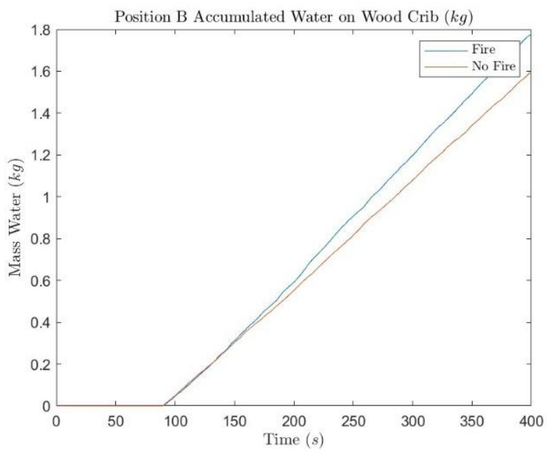
Position B Accumulated Water on Wood Crib (kg)
Fire
No Fire
Mass Water (kg)
Time (s)

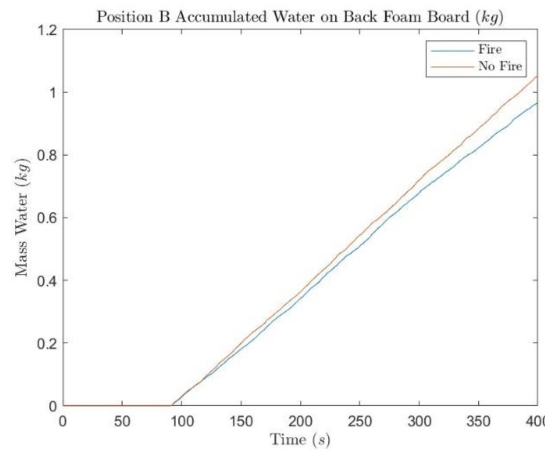
Position B Accumulated Water on Back Foam Board (kg)
Fire
No Fire
Mass Water (kg)
Time (s)

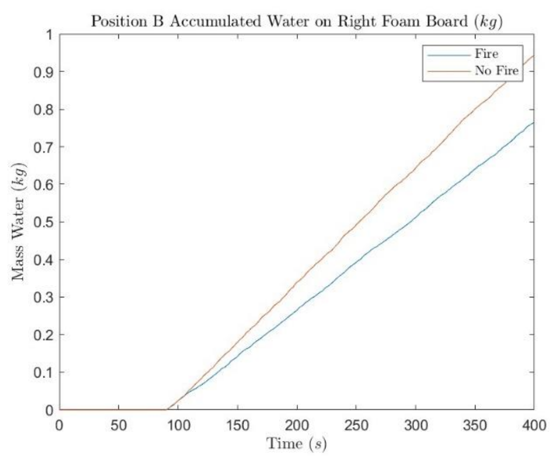
Position B Accumulated Water on Right Foam Board (kg)
Fire
No Fire
Mass Water (kg)
Time (s)

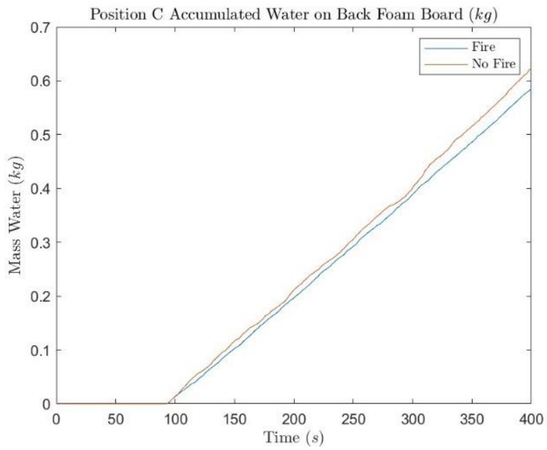
Position C Accumulated Water on Back Foam Board (kg)
Fire
No Fire
Mass Water (kg)
Time (s)
0
0.1
0.2
0.3
0.4
0.5
0.6
0.7
0
50
100
150
200
250
300
350
400

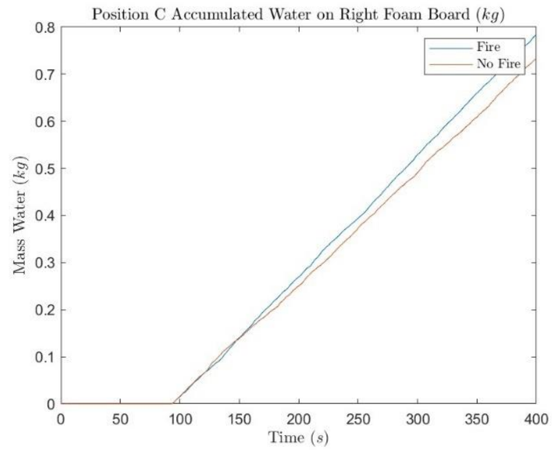
Position C Accumulated Water on Right Foam Board (kg)
Fire
No Fire
Mass Water (kg)
Time (s)
0
0.1
0.2
0.3
0.4
0.5
0.6
0.7
0.8
0
50
100
150
200
250
300
350
400

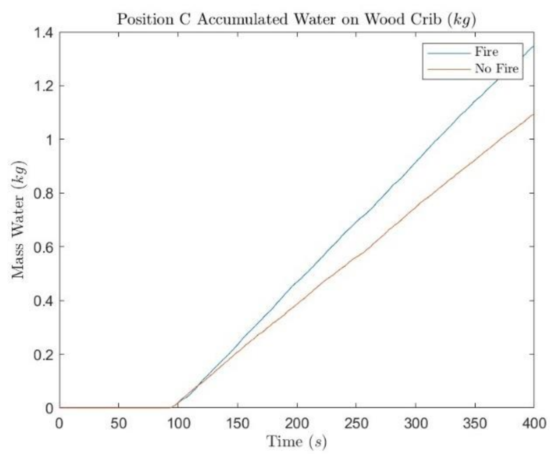
Position C Accumulated Water on Wood Crib (kg)
Fire
No Fire
Mass Water (kg)
Time (s)
0
0.2
0.4
0.6
0.8
1
1.2
1.4
0
50
100
150
200
250
300
350
400

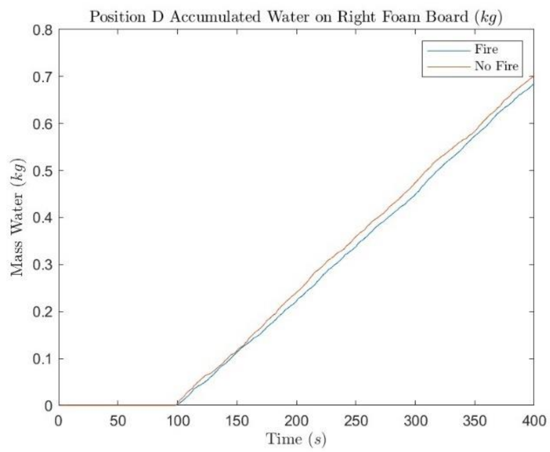
Position D Accumulated Water on Right Foam Board (kg)
Fire
No Fire
Mass Water (kg)
Time (s)

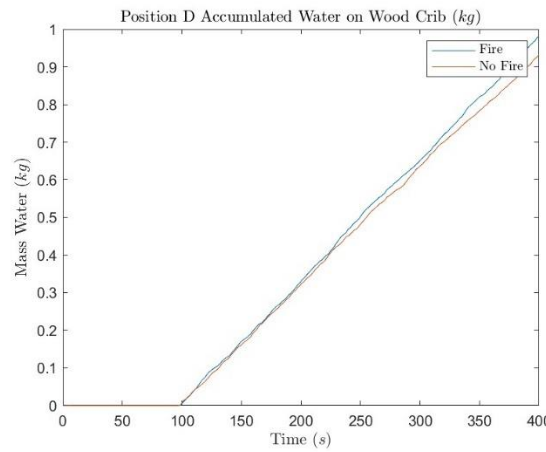
Position D Accumulated Water on Wood Crib (kg)
Fire
No Fire
Mass Water (kg)
Time (s)

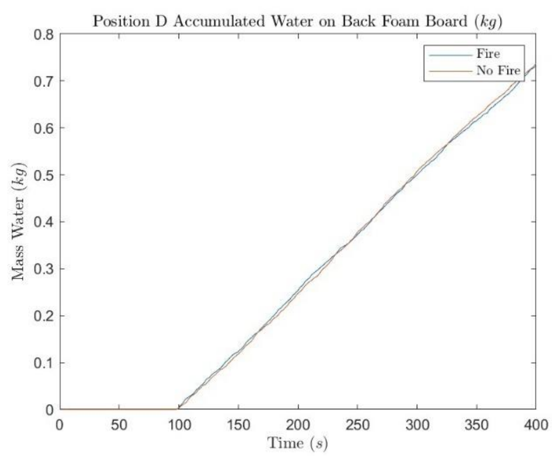
Position D Accumulated Water on Back Foam Board (kg)
Fire
No Fire
Mass Water (kg)
Time (s)

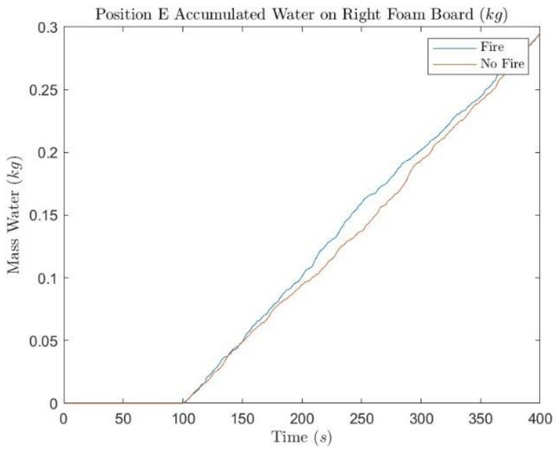
Position E Accumulated Water on Right Foam Board (kg)
Fire
No Fire
Mass Water (kg)
Time (s)

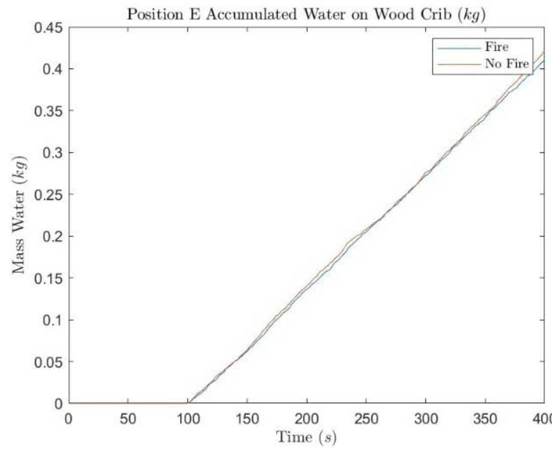
Position E Accumulated Water on Wood Crib (kg)
Fire
No Fire
Mass Water (kg)
Time (s)

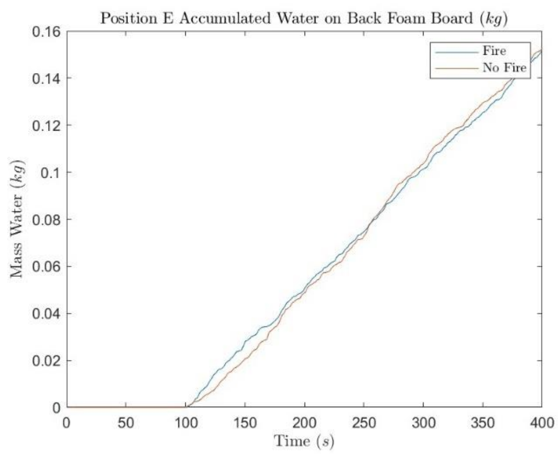
Position E Accumulated Water on Back Foam Board (kg)
Fire
No Fire
Mass Water (kg)
Time (s)

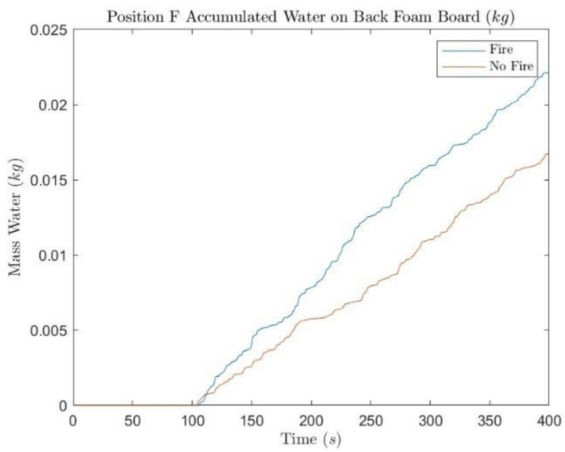

Position F Accumulated Water on Back Foam Board (kg)
Fire
No Fire
Mass Water (kg)
Time (s)

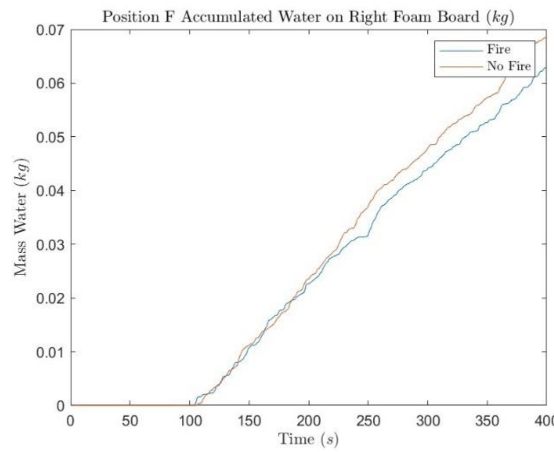

Position F Accumulated Water on Right Foam Board (kg)
Fire
No Fire
Mass Water (kg)
Time (s)

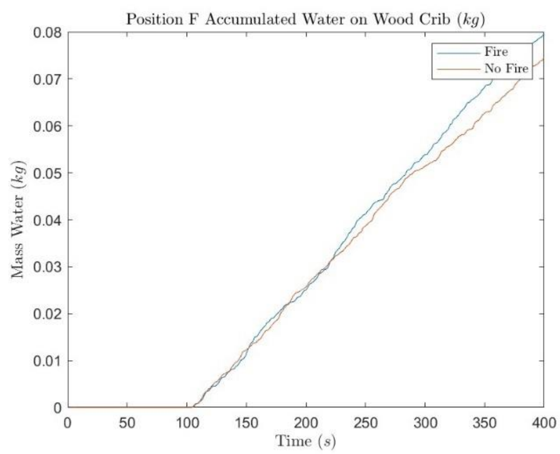

Position F Accumulated Water on Wood Crib (kg)
Fire
No Fire
Mass Water (kg)
Time (s)

Appendix I: Enclosure Fire Analysis, 4S Nozzle Rotation

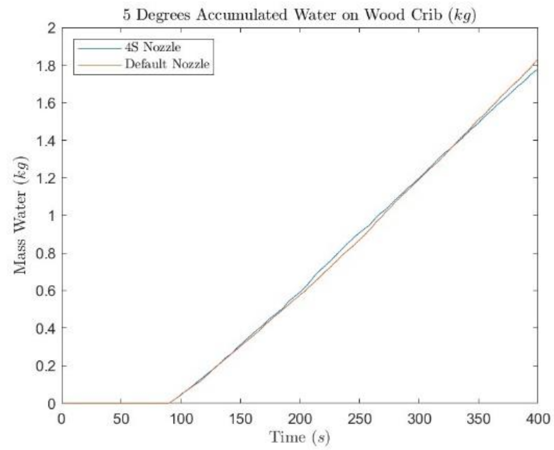

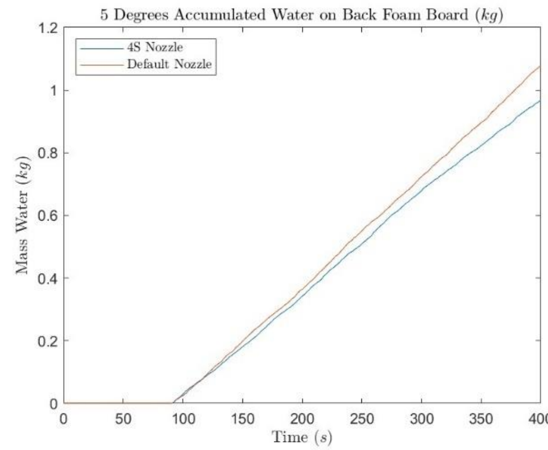

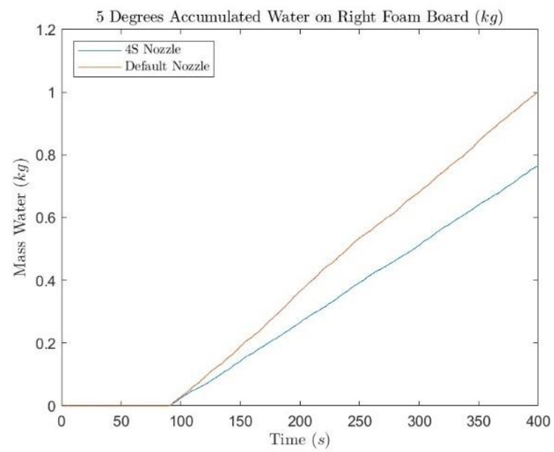

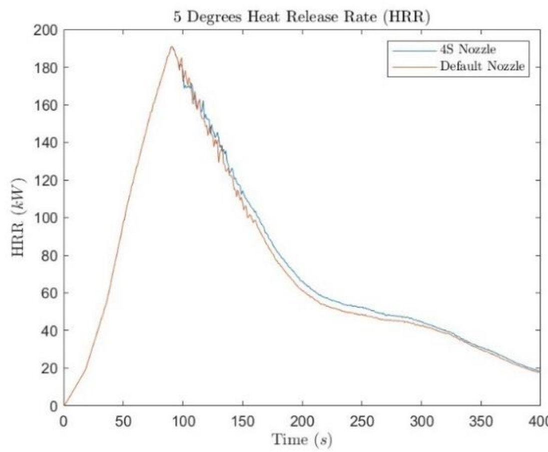

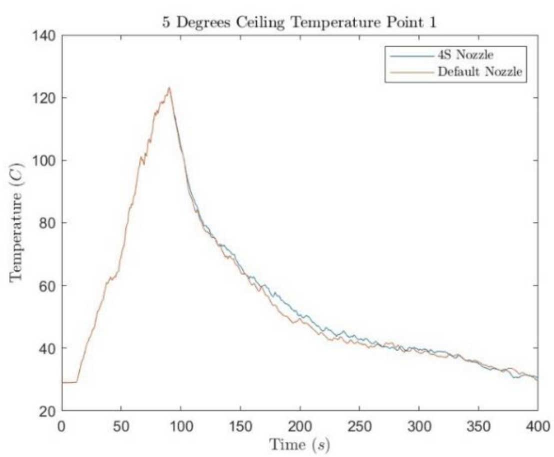

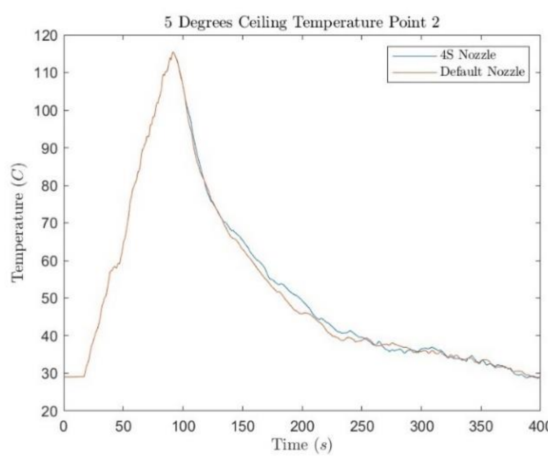

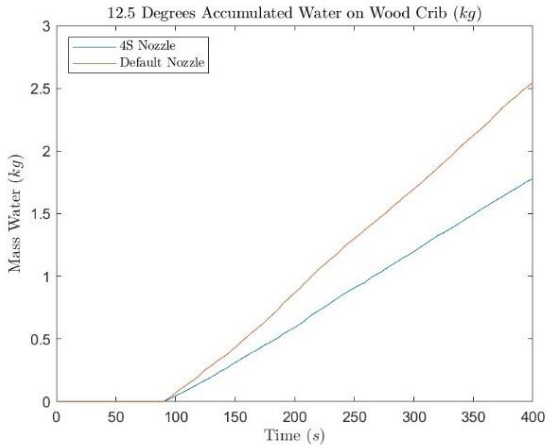
12.5 Degrees Accumulated Water on Wood Crib (kg)
Mass Water (kg)
Time (s)
4S Nozzle
Default Nozzle

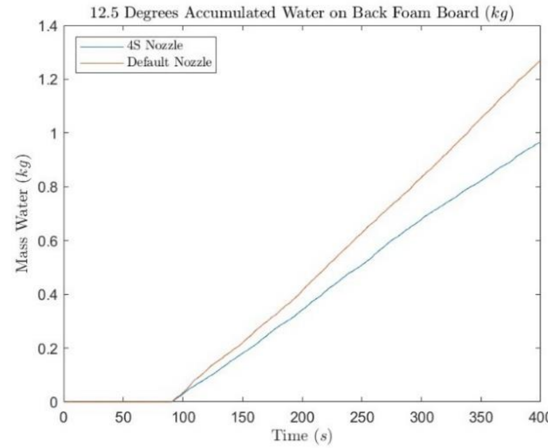
12.5 Degrees Accumulated Water on Back Foam Board (kg)
Mass Water (kg)
Time (s)
4S Nozzle
Default Nozzle

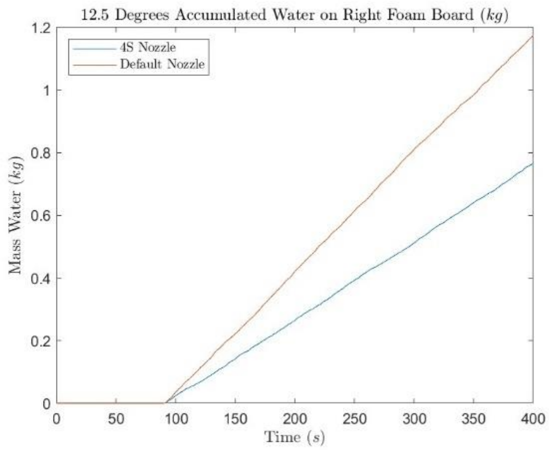
12.5 Degrees Accumulated Water on Right Foam Board (kg)
Mass Water (kg)
Time (s)
4S Nozzle
Default Nozzle

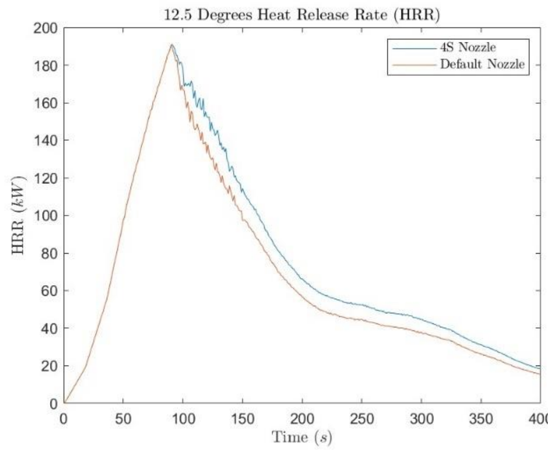
12.5 Degrees Heat Release Rate (HRR)
HRR (kW)
Time (s)
4S Nozzle
Default Nozzle

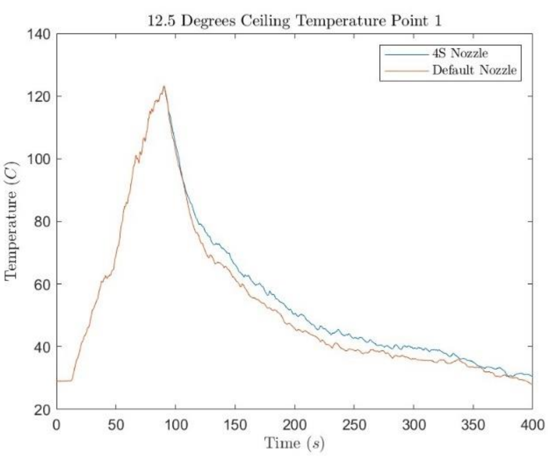
12.5 Degrees Ceiling Temperature Point 1
Temperature (C)
Time (s)
4S Nozzle
Default Nozzle

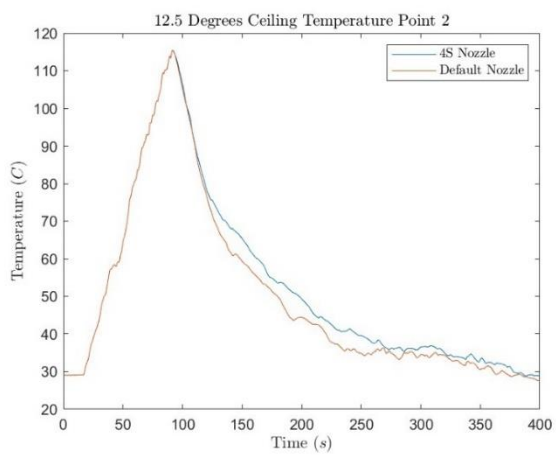
12.5 Degrees Ceiling Temperature Point 2
Temperature (C)
Time (s)
4S Nozzle
Default Nozzle

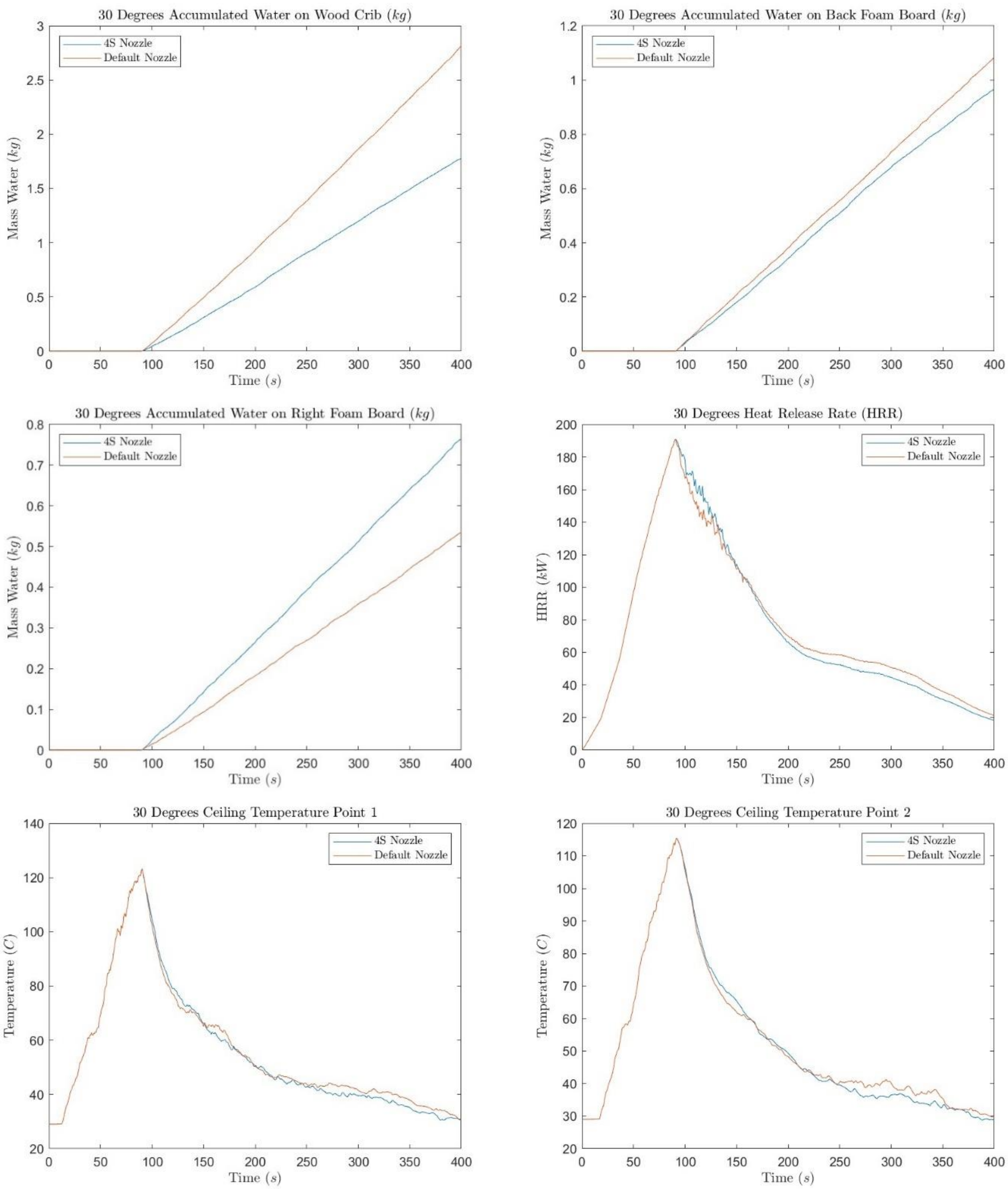
30 Degrees Accumulated Water on Wood Crib (kg)
Mass Water (kg)
Time (s)
4S Nozzle
Default Nozzle
30 Degrees Accumulated Water on Back Foam Board (kg)
Mass Water (kg)
Time (s)
4S Nozzle
Default Nozzle
30 Degrees Accumulated Water on Right Foam Board (kg)
Mass Water (kg)
Time (s)
4S Nozzle
Default Nozzle
30 Degrees Heat Release Rate (HRR)
HRR (kW)
Time (s)
4S Nozzle
Default Nozzle
30 Degrees Ceiling Temperature Point 1
Temperature (C)
Time (s)
4S Nozzle
Default Nozzle
30 Degrees Ceiling Temperature Point 2
Temperature (C)
Time (s)
4S Nozzle
Default Nozzle

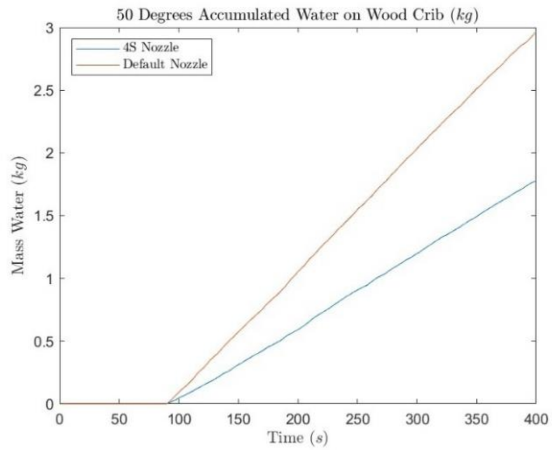
50 Degrees Accumulated Water on Wood Crib (kg)
Mass Water (kg)
Time (s)
4S Nozzle
Default Nozzle

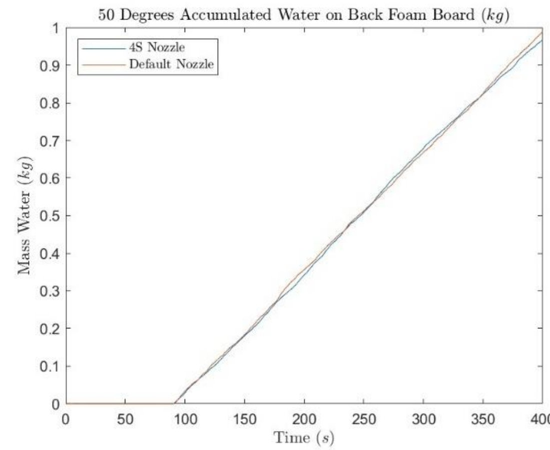
50 Degrees Accumulated Water on Back Foam Board (kg)
Mass Water (kg)
Time (s)
4S Nozzle
Default Nozzle

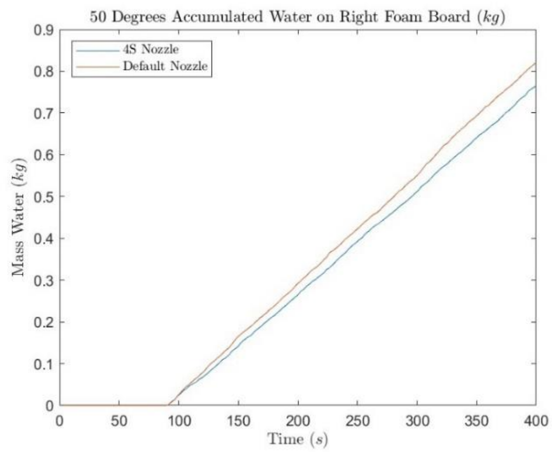
50 Degrees Accumulated Water on Right Foam Board (kg)
Mass Water (kg)
Time (s)
4S Nozzle
Default Nozzle

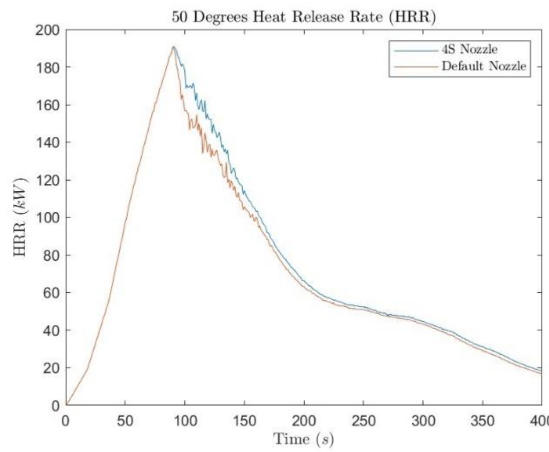
50 Degrees Heat Release Rate (HRR)
HRR (kW)
Time (s)
4S Nozzle
Default Nozzle

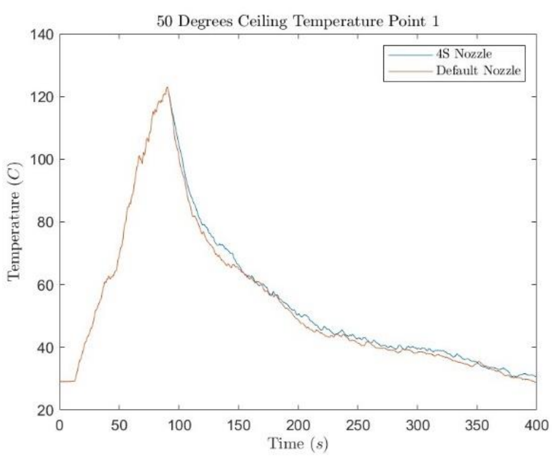
50 Degrees Ceiling Temperature Point 1
Temperature (C)
Time (s)
4S Nozzle
Default Nozzle

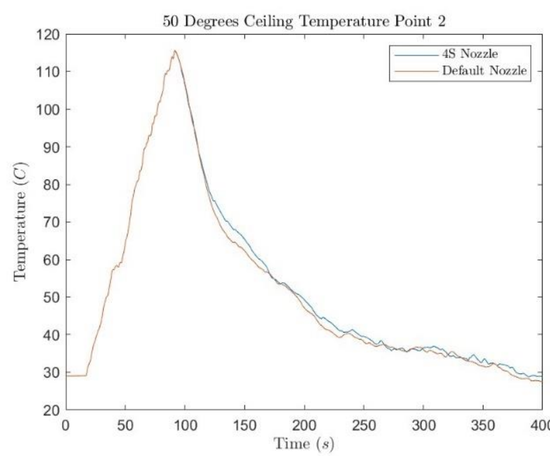
50 Degrees Ceiling Temperature Point 2
Temperature (C)
Time (s)
4S Nozzle
Default Nozzle

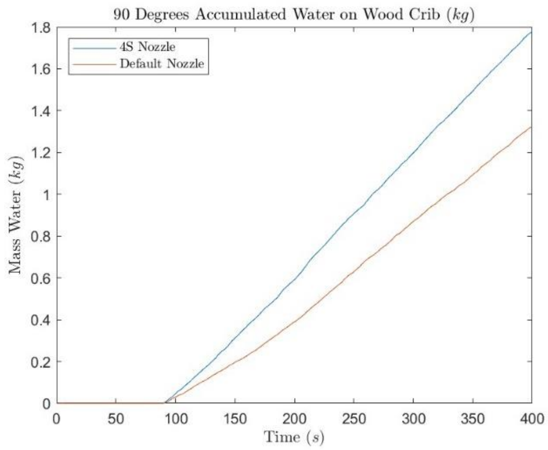
90 Degrees Accumulated Water on Wood Crib (kg)
4S Nozzle
Default Nozzle
Mass Water (kg)
Time (s)

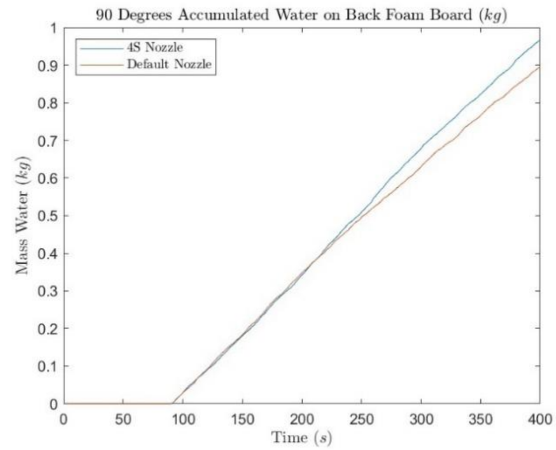
90 Degrees Accumulated Water on Back Foam Board (kg)
4S Nozzle
Default Nozzle
Mass Water (kg)
Time (s)

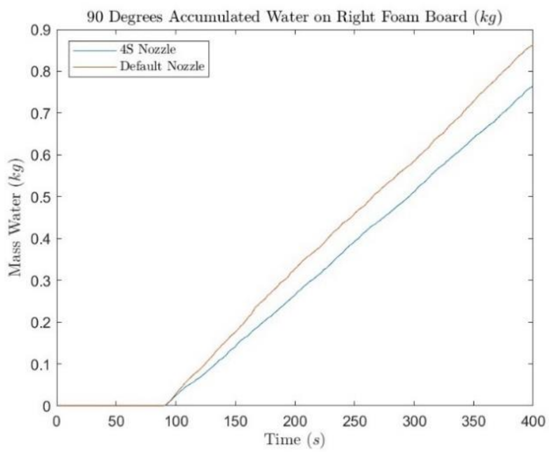
90 Degrees Accumulated Water on Right Foam Board (kg)
4S Nozzle
Default Nozzle
Mass Water (kg)
Time (s)

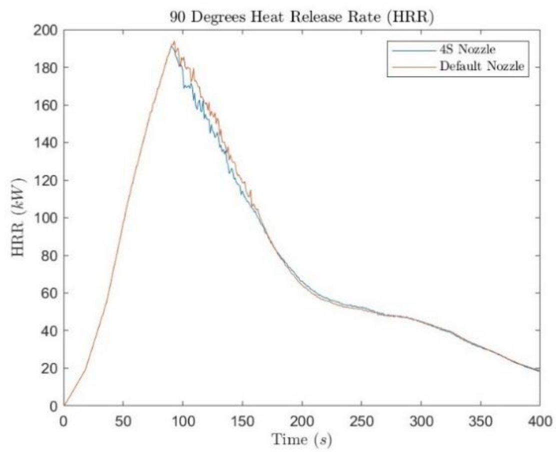
90 Degrees Heat Release Rate (HRR)
4S Nozzle
Default Nozzle
HRR (kW)
Time (s)

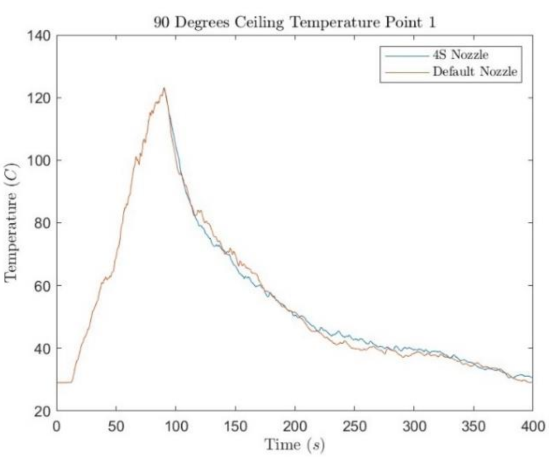
90 Degrees Ceiling Temperature Point 1
4S Nozzle
Default Nozzle
Temperature (C)
Time (s)

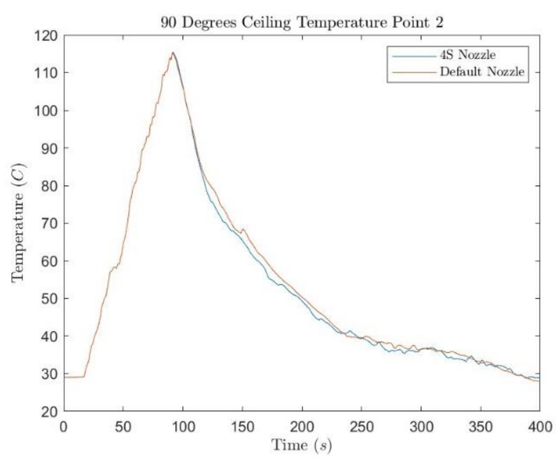
90 Degrees Ceiling Temperature Point 2
4S Nozzle
Default Nozzle
Temperature (C)
Time (s)

References

[1] Fleming, R. P. (2016). Automatic sprinkler system calculations. In M. Hurley (Ed.), SFPE Handbook of Fire Protection Engineering (5th ed., pp. 1423-1449). Springer.

[2] Grant, C. C. (n.d.). History of NFPA. National Fire Protection Association. http://www.nfpa.org/About-NFPA/NFPA-overview/History-of-NFPA

[3] Sheppard, D. T. (2002). Spray characteristics of fire sprinklers. National Institute of Standards and Technology.

[4] Jordan, S. J. (2017). Development of a spatially-resolved spray scanning system (Master's thesis). University of Maryland, College Park.

[5] Hadjisophocleous, G. V., Cao, S., & Kim, A. K. (1996). Modeling the interaction between fine water sprays and a fire plume. In Proceedings of the 4th International Conference on Advanced Computational Methods in Heat Transfer (pp. 853-862).

[6] Hadjisophocleous, G. V., & Knill, K. (2010). CFD modeling of liquid pool fire suppression using fine water sprays. Annual Conference on Fire.

[7] Mahmud, H. M. I., Moinuddin, K. A. M., & Thorpe, G. R. (2016). Experimental and numerical study of high-pressure water-mist nozzle sprays. Fire Safety Journal, 81, 109-117. https://doi.org/10.1016/j.firesaf.2016.01.015

[8] Trelles, J., & Mawhinney, J. R. (2010). CFD investigation of large scale pallet stack fires in tunnel protected by water mist systems. Journal of Fire Protection Engineering, 20(3), 149-199. https://doi.org/10.1177/1042391510362273

[9] National Institute of Standards and Technology. (2022). Fire Dynamics Simulator (Version 6.7.9) [Computer software]. GitHub. https://github.com/firemodels/fds/releases/

[10] National Institute of Standards and Technology. (2022). Smokeview (Version 6.7.22) [Computer software]. GitHub. https://github.com/firemodels/fds/releases/

[11] University of Maryland. (2022). Zaratan, High-Performance Computing Cluster, University of Maryland. https://hpcc.umd.edu/hpcc/zaratan.html

[12] McGrattan, K., Hostikka, S., Floyd, J., McDermott, R., & Vanella, M. (2022). Fire dynamics simulator user’s guide (Tech. Rep.). GitHub. https://github.com/firemodels/fds/tree/master/Manuals

[13] McGrattan, K., Hostikka, S., Floyd, J., McDermott, R., & Vanella, M. (2012). Fire Dynamics Simulator: Technical Reference Guide. GitHub. https://github.com/firemodels/fds/tree/master/Manuals

[14] McGrattan, K., Hostikka, S., Floyd, J., McDermott, R., & Vanella, M. (2012). Fire Dynamics Simulator: Technical Reference Guide Volume 3. Validation. GitHub. https://github.com/firemodels/fds/tree/master/Manuals

[15] The MathWorks, Inc. (2022). MATLAB R2022a. Natick, Massachusetts.

[16] Hostikka, S. (2008). slread.m [Matlab script]. GitHub. https://github.com/firemodels/fds/blob/master/Utilities/Matlab/scripts/slread.m.

[17] McDermott, R. (2010). radial_profile.m [Matlab script]. GitHub. https://github.com/firemodels/fds/blob/master/Utilities/Matlab/scripts/radial_profile.m.

[18] Yu, H.-Z. (1986). Invesitgation of spray patterns of selected sprinklers with the FMRC drop size measuring system. Fire Safety Science, 1, 1165–1176.

[19] Chan, T. S. (1994). Measurements of water density and drop size distributions of selected ESFR sprinklers. Journal of Fire Protection Engineering, 6(2), 79-97.

[20] Heskestad, G. (2016). Fire plumes, flame height, and air entrainment. In M. Hurley (Ed.), SFPE Handbook of Fire Protection Engineering (5th ed., pp. 373-395). Springer.

[21] Khoat, H. T., Kim, J. T., Quoc, T. D., Kwark, J. H., & Ryou, H. S. (2020). A numerical analysis of the fire characteristics after sprinkler activation in the compartment fire. Energies, 13(12), 3099. https://doi.org/10.3390/en13123099